Faculdade de Engenharia da Universidade do Porto

Exploring biomaterials and new energy sources to develop self-powered electronic medical devices

Joana Raquel Oliveira Gomes

MASTER DISSERTATION

Master in Bioengineering
Branch of Biomedical Engineering

Supervisor: Andreia T. Pereira (i3S/INEB)
Co-supervisors: Inês C. Gonçalves (i3S/INEB) and André M. Pereira (FCUP/IFIMUP)

July 2022

The work described in this master thesis was conducted at:

i3S – Instituto de Investigação e Inovação em Saúde, Universidade do Porto / INEB – Instituto de Engenharia Biomédica

FCUP – Faculdade de Ciências da Universidade do Porto / IFIMUP - Instituto de Física de Materiais Avançados, Nanotecnologia e Fotónica, Universidade do Porto

Other institutions involved in this master thesis:

Funding:

“ O que dá verdadeiro sentido ao encontro é a busca,
e é preciso andar muito para se alcançar o que está perto.”
José Saramago

Resumo

Doenças cardiovasculares (DCVs) são uma das razões proeminentes de morte ao nível mundial. Apesar dos notáveis benefícios de dispositivos cardíacos eletrónicos (DCEs) para o seu tratamento, estes apresentam várias limitações, nomeadamente o uso de baterias volumosas e com um tempo de vida limitado para a sua alimentação, estando ainda associadas a um elevado risco de libertação do seu conteúdo. A recolha de energia de fontes biomecânicas surge como uma tecnologia promissora para superar estas limitações, no sentido de alcançar DCEs autoalimentados, de menor volume e mais leves. Nanogeradores triboelétricos (TENG) conseguem fazer a recolha de energia elétrica a partir da energia cinética de movimentos corporais através do movimento relativo entre dois materiais de tribopolaridade oposta, gerando-se cargas na superfície de ambos e uma diferença de potencial nos elétrodos que lhes estão associados. Nanogeneradores triboelétricos fluídos (Flu-TENG) consistem numa abordagem recente alternativa aos TENGs mais tradicionais de contacto sólido-sólido, na qual um dos materiais é um fluído (fase-fluída) e o outro é um sólido (fase-sólida), sendo o elétrodo colocado sobre a sua superfície externa. Flu-TENGs apresentam a vantagem de um desgaste mecânico reduzido e contacto entre as duas camadas triboelétricas melhorado, o que permite um melhor resultado elétrico.

O objetivo final deste trabalho pioneiro é usar o fluxo sanguíneo através de vasos nativos e/ou enxertos vasculares para desenvolver um Flu-TENG que gera energia elétrica, em direção à alimentação de dispositivos eletrónicos médicos e sensores, e para usar como sensor de estreitamento/oclusão auto-alimentado. Flu-TENGs foram desenvolvidos recorrendo a enxertos vasculares sintéticos como fase-sólida, em particular ePTFE, um biomaterial comercialmente disponível, e pHEMA/GO, produzido no laboratório, bem como artérias nativas. Para a fase-fluída, diferentes fluídos foram testados, nomeadamente PBS, plasma e sangue. Uma bomba peristáltica foi utilizada para simular o fluxo pulsátil do sangue em circulação. Como elétrodos usaram-se tintas condutoras de prata, carbono e PEDOT:PSS e fita de cobre, para serem testados relativamente à sua estabilidade na fase-sólida (testes de

lavagem e SEM), eficiência (*outputs* elétricos) e biocompatibilidade (relativamente a fibroblastos (HFF-1)).

Uma aplicação estável das tintas condutoras em ePTFE foi conseguida, através de pintura com pincel, e sem se verificar infiltração para o interior do enxerto vascular. Prata mostrou-se o elétrodo mais estável quando aplicado no pHEMA/GO e nas artérias, ao contrário do carbono e PEDOT:PSS, para os quais foi observado um revestimento menos consistente e com infiltração para a superfície luminal. A fita de cobre levou ao estrangulamento das fases-sólidas, impedindo o fluxo normal da fase-fluída. Para a comparação do desempenho dos Flu-TENGs, foi avaliada a saturação de condensadores de 1 e 100 nF carregados. *Outputs* mais elevados foram alcançados recorrendo ao plasma como fase-fluída (23.6 V), comparativamente ao PBS (17.3 V), com o qual se conseguiram resultados mais próximos dos obtidos utilizando sangue (14.2 V). Estes *outputs* são ainda dependentes da taxa de fluxo, já que um aumento em 100 mL/min levou a um *output* 10 V mais alto. Para além disso, a energia elétrica gerada é altamente dependente do elétrodo utilizado e o seu *design*. Os elétrodos testados permitiram a aquisição de energia. Contudo, apresentam diferente eficiência, sendo que 17.3 V foram alcançados com prata, 12.9 V com carbono e 10.4 V com PEDOT:PSS. Este *output* é linearmente dependente do comprimento do elétrodo, tendo-se obtido um aumento em cerca de 30 V passando de 0.5 para 10 cm de um elétrodo de prata. Contudo, o respetivo posicionamento na fase-sólida é também importante, sendo que o *output* reduz à medida que aumenta a distância ao terminal proximal. Quanto à biocompatibilidade, prata e cobre foram determinados como elétrodos citotóxicos enquanto se concluiu que o carbono e PEDOT:PSS são citocompatíveis. As diferentes fases-sólidas mostraram propriedades triboelétricas, obtendo-se 10.5 V com o enxerto vascular de ePTFE e 14.5 V com o pHEMA/GO, e 8 V com a artéria. Estes resultados são ainda influenciados pela espessura de parede do material, cujo aumento reduz o *output*, tal como o seu diâmetro interno. Finalmente, mostrou-se a potencialidade de uso do Flu-TENG como um sensor de estreitamento, tendo-se verificado que um estreitamento induzido em 30% de um enxerto vascular de ePTFE leva a uma perturbação de 8 V no *output* elétrico. Assim, alterações no sinal elétrico podem ser associadas aos níveis de estreitamento, para a sua deteção.

De um modo geral, este trabalho foi pioneiro na demonstração do potencial do uso do fluxo de fluidos corporais em vasos nativos e (bio)materiais, em particular sangue em artérias e enxertos vasculares, para gerar energia elétrica a partir de fontes do corpo humano. Sendo assim, é proposta uma nova fonte de energia com a finalidade de alimentação de dispositivos eletrónicos médicos e sensores, que irão permitir a superação de limitações das baterias atuais. Além do mais, esta tecnologia pode ser ainda aplicada para desenvolver sensores autoalimentados, melhorando a monitorização e tratamento de DCVs. As conclusões alcançadas indicam que os *outputs* dos Flu-TENGs propostos podem ainda ser otimizados e que esta tecnologia pode ser estendida para várias outras aplicações semelhantes.

Abstract

Cardiovascular diseases (CVDs) are one of the prominent causes of death worldwide. Despite the remarkable benefits of cardiac electronic devices (CEDs) for their management, they have several limitations, namely the use of bulky batteries with a limited lifetime to power supply them, being also associated with a high risk of content leakage. Energy harvesting from biomechanical sources emerges as a promising technology to overcome these limitations towards self-powered, smaller and lighter CEDs. Triboelectric nanogenerators (TENG) can harvest electric energy from kinetic energy of human body motion through the relative movement between two materials with opposite tribopolarities, generating charges at both their surfaces, and a potential difference at the associated electrodes. Fluid triboelectric nanogenerators (Flu-TENG) are a recent approach to the most traditional solid-solid contact TENGs, where one material is a fluid (fluid-phase) and the other a solid (solid-phase), with the electrode being assembled on its outer surface. Flu-TENGs have the advantage of reduced mechanical wear and improved triboelectric layers' contact, which provides better electric outputs.

The ultimate goal of this pioneering work is to use blood flow through native vessels and/or vascular grafts to develop a Flu-TENG that generates electrical energy, towards powering of electronic medical devices and sensors, and that can be used as a self-powered narrowing/blocking sensor. Flu-TENGs were developed resorting to synthetic vascular grafts as solid-phases, in particular ePTFE, commercially available, and pHEMA/GO, produced in the lab, as well as native arteries. For fluid-phase, different fluids were tested, namely PBS, plasma and blood. A set-up with a peristaltic pump was assembled to simulate the pulsatile flow of blood circulation. As electrodes, silver, carbon and PEDOT:PSS conductive inks and copper tape were tested regarding their stability in the solid-phase (washing tests and SEM), efficiency (electrical outputs) and biocompatibility (towards fibroblast cells (HFF-1)).

Assembly of the conductive ink electrodes on ePTFE was successfully done by brush painting, as stable coatings were observed and there was no infiltration to the interior of the vascular grafts. Silver showed to be more stable for pHEMA/GO vascular graft and arteries, oppositely to carbon and PEDOT:PSS, for which less consistent coatings were achieved and

with some infiltration to the luminal surface. Copper tape electrode led to the strangling of solid-phases, hampering the normal flow of the fluid-phase. To compare Flu-TENGs' performance, the saturation of 1 and 100 nF charged capacitors was evaluated. Higher voltage outputs were achieved with plasma as fluid-phase (23.6 V), when compared to PBS (17.3 V), with which results were closer to using blood (14.2 V). Flu-TENG performance is also dependent on fluid's flow rate, as an increase of 100 mL/min led to a 10 V higher output. Besides, electrical energy generation is highly dependent on the electrode and its design. All electrodes tested allowed for energy acquisition. However, they showed different efficiency, as 17.3 V were achieved with silver, 12.9 V with carbon and 10.4 V with PEDOT:PSS. This output is linearly dependent on electrodes length, having increased it in almost 30 V passing from 0.5 to 10 cm of a silver electrode. The electrode's placement on solid-phase is also important as the output decreases as the distance to the proximal end increases. Regarding biocompatibility, silver and copper showed to be cytotoxic whereas carbon and PEDOT:PSS are concluded to be cytocompatible electrodes. The different solid-phases analyzed showed triboelectric properties, having obtained at least 10.5 V with ePTFE and 14.5 V with pHEMA/GO vascular grafts, and 8 V with the artery. These results are influenced by the material's wall thickness, whose increase decreases the output, as does its inner diameter. Finally, it was shown the Flu-TENGs potential as a narrowing sensor, as perturbation of flow induced by 30% narrowing of an ePTFE vascular graft led to a perturbation in the electrical voltage output of 8 V. Therefore, changes in the electrical signal could be associated with narrowing levels, for their detection.

Overall, this work was pioneer in demonstrating the potential of using the flow of body fluids in native vessels and (bio)materials, in particular blood in arteries and vascular grafts, to generate electrical energy from a human body source. Therefore, it is proposed a new energy source for powering of electronic medical devices and sensors, that will allow to overcome current battery limitations. Moreover, this technology can be applied to develop a self-powered sensor, improving CVDs management. The stated findings indicate that the proposed Flu-TENG's outputs could be further optimized and this technology extended to many other similar applications.

Agradecimentos

Em primeiro lugar, queria deixar um agradecimento especial à minha orientadora, Andreia Pereira, por todo o acompanhamento ao longo dos últimos meses, desde académico a pessoal, por todos os ensinamentos, pelo encorajamento diário e pelo à vontade e tranquilidade transmitidos deste o primeiro dia. À Inês Gonçalves, minha coorientadora, obrigada pela oportunidade, por todos os conselhos e conhecimentos transmitidos e todas as palavras de incentivo. Um agradecimento ainda ao meu coorientador, André Pereira, por toda a liberdade demonstrada para que pudesse explorar uma área que me era completamente nova, e por todos os conhecimentos, essenciais para a minha aprendizagem e desenvolvimento desta tese. Obrigada a todos pela confiança em dar início a este trabalho.

Ao meu grupo do i3S, Advanced Graphene Biomaterials, à Ana, ao Duarte, à Helena, à Margarida e à Patrícia, um enorme agradecimento pela disponibilidade constante para ajudar, por todos os conhecimentos passados e pela excelente companhia que foram ao longo dos últimos meses. Obrigada por tornarem tão mais fácil vir trabalhar todos os dias. Gostaria ainda de agradecer aos técnicos do i3S por toda a ajuda ao longo do trabalho, em particular à Dalila e ao Ricardo. Ao grupo do IFIMUP, um agradecimento por me ter recebido e por toda a ajuda e acesso a tudo o que precisei para desenvolver este trabalho da melhor forma. Em especial, quero agradecer à Carolina pela ajuda incansável durante estes meses, por estar sempre disponível a tirar todas as minhas dúvidas e por todas as sugestões, que foram uma contribuição essencial para o meu trabalho.

A todos os meus amigos, os que sempre me acompanharam e os que vieram só nos anos de faculdade, um obrigado por tornarem tudo mais fácil. Às minhas amigas mais antigas, Ana Rita, Cat, Gela e Lisa, obrigada pela amizade genuína e por partilharem comigo todos os bons e maus momentos, longe ou perto. À Margarida, a minha amiga recente, mas que parece que esteve cá a vida toda, um agradecimento por estes últimos 5 anos e por ser a companheira de todas as ocasiões.

Queria deixar ainda o meu agradecimento à minha família, que sempre acreditou em mim e no meu valor. E por último, mas sem dúvida não menos importante, o maior agradecimento vai para os meus pais, Delfina e Vitor, e o meu irmão, Vitor Hugo, pelo apoio e amor incondicionais durante toda a minha vida. Por me darem sempre tudo aquilo que eu preciso, por estarem presentes em todos os momentos, por aturarem todo o stress e tornarem tudo mais fácil. Sem vocês nada seria possível. Sou muito grata por me ter saído esta família.

Joana Gomes

Table of Contents

Figures List

Tables List

Abbreviations and Symbols

AC	Alternating current
APS	Ammonium persulfate
ATCC	American Type Culture Collection
C	Chitosan
CE	Contact electrification
CED	Cardiac electronic device
CRT	Cardiac resynchronization therapy
CVD	Cardiovascular disease
DAPI	4′,6-diamidino-2-phenylindole
DC	Direct current
DMEM	Dulbecco's modified Eagle medium
EDL	Electric double layer
EO	Ethylene oxide
EVA	Ethylene vinyl acetate
ePTFE	Expanded polytetrafluoroethylene
FBS	Fetal bovine serum
FDA	Food and Drug Administration
Flu-TENG	Fluid triboelectric nanogenerator
GO	Graphene oxide
HEMA	Hydroxyethylmethacrylate
HFF-1	Human foreskin fibroblasts
ICD	Implantable cardiac defibrillator
ID	Inner diameter
IoMT	Internet of Medical Things
ISO	International Organization for Standardization
iTENG	Implantable triboelectric nanogenerator
LVDA	Left ventricular assist device
OD	Optical density
PBS	Phosphate-buffered saline
PDMS	Polydimethylsiloxane

PEDOT:PSS	poly(3,4-ethylenedioxythiophene):polystyrene sulfonate
PENG	Piezoelectric nanogenerator
PET	Polyethylene terephthalate
PFA	Paraformaldehyde
pHEMA	Poly(2-hydroxyethyl methacrylate)
PLA	Polylactic acid
PMU	Power management unit
P/S	Penicillin/Streptomycin
PTFE	Polytetrafluoroethylene
PVDF	Polyvinylidene fluoride
PyENG	Pyroelectric nanogenerator
PZT	Lead zirconate titanate
RFU	Relative fluorescence unit
Rpm	Revolutions per minute
SD	Standard deviation
SEM	Scanning electron microscopy
SMB	Sodium metabisulfite
SPM	Symbiotic pacemaker
TC-PET	Tissue culture polyethylene terephthalate
TEGDMA	Tetraethylene glycol dimethacrylate
TENG	Triboelectric nanogenerator
TEG	Thermoelectric generator
WT	Wall thickness

Chapter 1: Motivation, Aims and Dissertation Outline

1.1. Motivation

Cardiovascular diseases (CVDs) are the prominent cause of death worldwide, with an estimation of 17.9 million yearly victims, which represents 32% of deaths, according with world health organization (WHO). Moreover, these diseases are responsible for 38% of premature deaths (people under the age of 70) [1]. CVDs are increasing all over the world due to sedentarism and aging, being now one of the leading causes of disability adjusted life years lost [2, 3]. Several conditions such as atrial fibrillation, congenital heart diseases, coronary heart disease, or cardiomyopathy require cardiac electronic devices (CEDs) to be treated, such as pacemakers, implantable cardioverter defibrillators (ICDs), cardiac resynchronization therapy (CRT) devices and left ventricular assist devices (LVDA). In approximately 85% of the overhaul procedures for these devices, which consist in the replacement of the whole device or the main device box (computer/electronics and battery), is caused by battery depletion [4]. Additionally, in the future, to satisfy all clinical requirements, CEDs will incorporate more functions, which will lead to powerful computing and remote communication, consequently requiring a higher energy consumption. Overhaul procedures involve a new surgical intervention in the patient, being in 1.5-2% of the cases associated to infection occurrence [5]. Other major complications that can occur include hematomas/blood clots [5, 6]. Minor complications consist of less serious hematoma, implant related pain, minor wounds, among others [7]. According to the Markov model developed by Schmier *et al.* [8], by extending 20% the battery life of an ICD, the need of overhaul reduces in 13.5%, when compared to legacy devices, reducing the risk for health complications and also long-term costs of therapy (~€5000 per patient). Moreover, increasing 80% the lifespan of CEDs' batteries leads to savings of ~34% (~€19000 per patient), for the avoidance of replacement procedures and reduced health complications [9]. In sum, studies for CEDs highlight that by extending batteries' longevity, overhaul procedures can be delayed or even completely avoided, which has a high impact on health and economy [7].

In the framework of current digital Era, the Internet of Medical Things (IoMTs), which aims to perform a continuous monitorization of patient and medical device conditions, appears as the next breakthrough in the medical field. IoMTs purposes the development of large-scale sensor networks and systems to provide an interaction between medical device/patient, sensors and actuators through the internet, with standardized and interoperable communication protocols [10]. Although the implementation of IoMTs has taken its first steps, with a market evaluated in 41.17B € (2020) [11], it is still far from its full potential use and development. In most cases, sensor nodes need to be distributed across a large area or even implanted inside the body being required to operate wirelessly and without centralized power sources, which is a driver that encourages studies towards self-powered sensors [12].

Despite the remarkable benefits and growing innovations associated with both CEDs and IoMTs, limitations mostly related to the devices' battery still need to be addressed [13]. The current electronic devices market is ruled by lithium-ion batteries, which have a limited lifetime, are bulky, difficult to recycle, and may leak their toxic content into the surrounding tissues [14]. Theoretically, a batteries' capacity can be made as high as needed but that will come at the cost of a larger sized device [15]. Therefore, there is a huge need for innovations towards miniaturized, endless and biologically safe sources of electrical energy. One strategy to overcome batteries drawbacks that has been extensively studied over the last few years is the harvesting of energy from biological sources (*e.g.*, muscle movement, biofluids, temperature) and from environment to obtain electric energy to power supply medical electronic devices [13].

1.2. Aims

The aim of this work is to study the use of an unexplored energy source, blood flow through vascular grafts or vessels, to power implantable cardiac electronic medical devices and/or wireless sensors. To achieve this, it was proposed the design of a triboelectric fluid-solid nanogenerator (Flu-TENG), which uses blood, as fluid-phase, and vascular grafts or native vessels, as solid-phase (Figure 1). Four specific goals were defined to design this novel Flu-TENG.

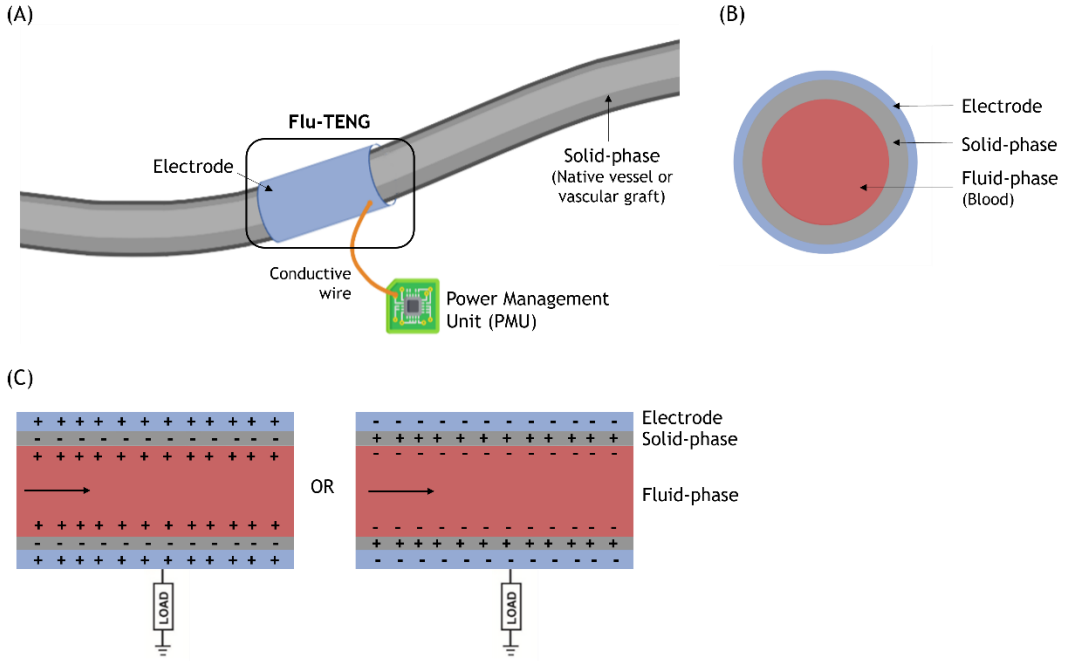

Figure 1. Flu-TENG proposed in this study to harvest energy from the relative motion of the blood (fluid-phase) flowing through the native vessels or vascular grafts (solid-phase). (A) Flu-TENG composition: fluid-phase (blood), solid-phase (native vessel or vascular graft) and an electrode around the solid-phase. The Flu-TENG will be connected to a Power Management Unit (PMU), through a conductive wire, for further powering of a device; (B) Transversal view of the Flu-TENG; (C) Two possible mechanism of charge generation in Flu-TENGs.

The first task is to set-up a perfusion system that mimics, *in vitro*, the physiological blood flow through vessels and vascular grafts. Second purpose is to evaluate the efficiency of Flu-TENGs, consisting of vascular grafts and native blood vessels as solid-phases. For this, the influence of different parameters associated with the main components of Flu-TENG in the generated electrical output was studied, namely fluid-phase (type and flow rate), electrode (stability, type and design) and solid material (wall thickness, inner diameter and type). Another focus is to evaluate the biocompatibility of the adopted electrodes as they will be the only foreign material, not approved by FDA, to be implanted, considering the future application of Flu-TENG in medical settings. Aligned with IoMTs implementation and envisioning the next generation of vascular grafts, the last goal is to study the potential of Flu-TENG as a self-powered sensor of narrowing/blockage of vascular grafts. Figure 2 summarizes studied parameters regarding each component of the Flu-TENG.

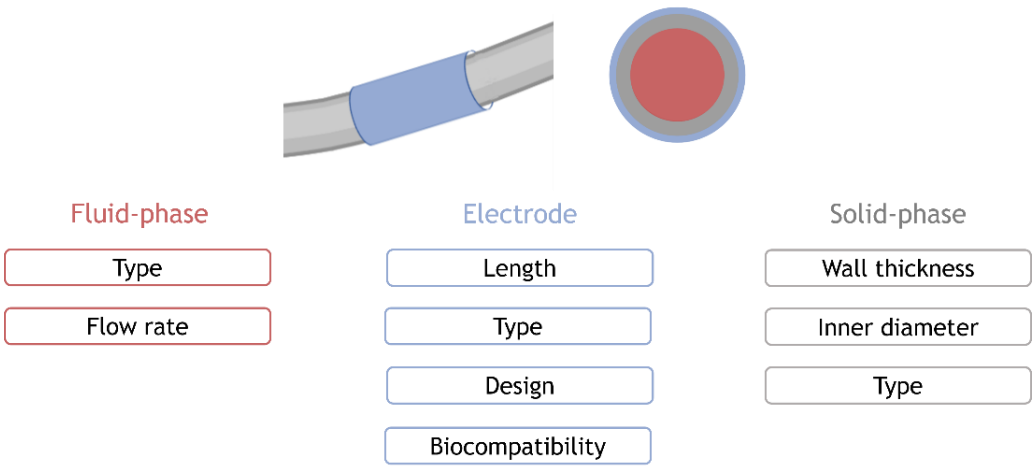

Figure 2. Summary of the Flu-TENG's parameters that will be evaluated in this dissertation.

1.3. Dissertation Outline

Chapter 1 presents the motivation, main objectives, and outline of this dissertation.

Chapter 2 comprises an extensive literature review on the main topics discussed in this dissertation. The first section describes the relevance and latest advances in energy harvesting, mentioning the working principle and main advantages and disadvantages of pyroelectric, thermoelectric, biofuel cells, piezoelectric and electromagnetic nanogenerators. The second section focuses on triboelectric nanogenerators, specifying the state-of-the-art for biomedical applications. This is followed by a review on fluid triboelectric nanogenerators, the approach explored in this dissertation. The last section focuses on the main aspects related to the use of blood flow for energy harvesting.

Chapter 3 focuses on the materials and methodology adopted for Flu-TENG assembly, triboelectric outputs measurement and *in vitro* cytocompatibility assessment.

Chapter 4 contains the results and further discussion regarding electrodes assembly and stability, triboelectric outputs, divided in influence of fluid, solid and electrode associated parameters, as well as application of Flu-TENG as sensor, and *in vitro* cytocompatibility of electrodes.

Chapter 5 summarizes the conclusions of this dissertation and future direction to further explore the Flu-TENG application in medical settings.

Chapter 2: Literature Review

2.1. Energy harvesting

Over the last few years, it has been clear the growth of implantable and wearable smart electronic devices. However, the growing concern of current battery limitations and their impracticality, as well as environmental issues related to the disposal of electronics, due to short replacement cycles, leads to a need for continuous, sustainable and biofriendly energy sources for these electronics [16, 17]. From this, energy harvesting emerges as the ideal answer, as it allows for the transformation into usable electric energy of various forms of energy, such as biological, chemical, thermal, mechanical and solar energy, already naturally available in the human body and our surrounding environment, that would otherwise be lost and wasted [18]. This is also driven by the emergence of nanomaterials and nanotechnology, that allows for the fulfillment of current powering requirements, through the production of nanogenerators [19]. Concerning biomedical applications, these technologies could be used 1) to power supply medical electronic devices and/or available sensors (*e.g.* temperature, pressure, flow) or 2) to be the sensor itself (active sensor), by directly converting biological/physiological signals into electricity that can be modulated to give information about patient status [13].

Among some of the most explored energy harvesting technologies are pyroelectric nanogenerators (PyENG), thermoelectric generators (TEG), biofuel cells, piezoelectric nanogenerators (PENG), electromagnetic generators and triboelectric nanogenerators (TENG). These have a vast range of emerging applications, one of them being the powering of medical devices. Figure 3 consists of a representation of the functioning of some energy harvesters and their application for self-powered CEDs and sensors.

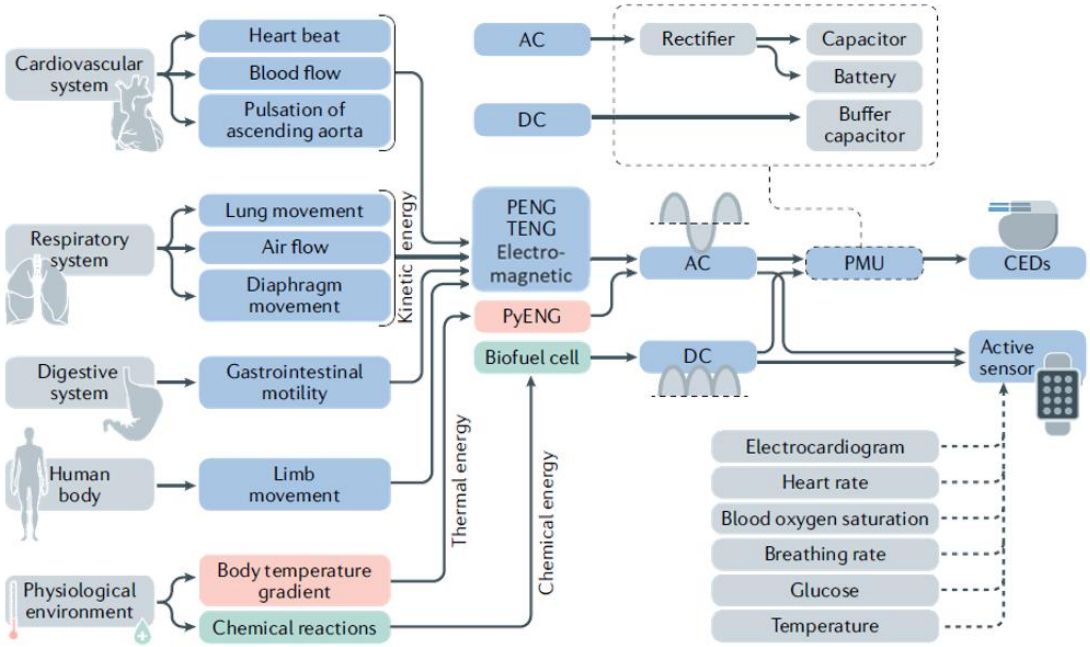

Figure 3. Pathway of energy harvesting systems based on human body motion, temperature or chemical reactions to power CEDs and sensors. Adapted with permission from ref. [13], copyright 2020, Springer Nature.

Pyroelectric nanogenerators are devices able to convert thermal into electric energy based on the pyroelectric effect, in which spontaneous polarization of crystals by temperature changes occurs. Maintaining a continuous heating and cooling cycle, an alternate current (AC) is generated (Figure 4 (A)). This is a highly sensitive technology of fast response rate that can easily be coupled to other types of energy harvesters to boost their performance [20, 21].

Thermoelectric generators are based on p-/n-type materials and can produce electricity from thermal energy but based on the Seebeck effect, in which electrons migrate from the hot to the cold side when there is a temperature gradient across the device, *i.e.* a temperature difference between the electrodes, generating a potential (Figure 4 (B)) [22, 23]. As a continuous electron flow occurs, direct current (DC) is produced [24]. Therefore, TEGs can be directly connected to an energy storage device. This consists of an advantage over PyENGs, as AC generators require a bridge rectifier for AC/DC conversion and further charging of capacitors/batteries [25].

PyENG and TEG have an unlimited lifetime as they can use body temperature as a heat-energy source, which itself is also unlimited. Nonetheless, body thermal fluctuations/gradients are somewhat small, due to the high regulation of body temperature, and so it is difficult to obtain great power outputs [13, 15].

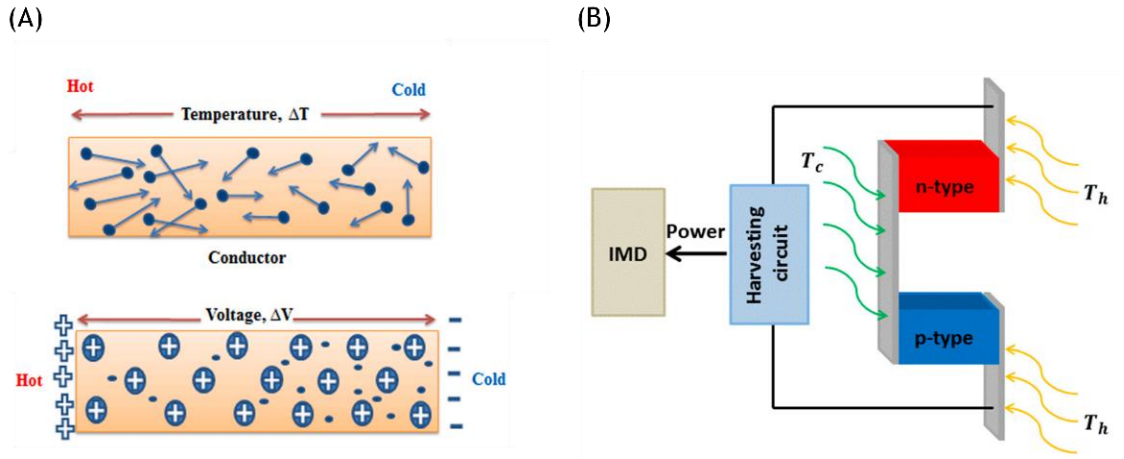

Figure 4. Working principle of thermal energy harvesters. (A) Pyroelectric nanogenerators. Adapted with permission from ref. [26], copyright 2021, Elsevier; (B) Thermoelectric nanogenerators [27].

Biofuel cells harvest biochemical energy from biofluids (biocatalysts) by reduction and oxidation reactions occurring at the cathode and anode, respectively. The electrons that are released from the anode travel to the cathode forming an electric current via an external circuit (Figure 5). Advantages of this approach are the possibility of use of recyclable nature materials, moderate operating conditions of temperature and pH for the reactions, and biocompatibility [28]. Disadvantages consist of the difficulty to maintain an added catalyst for a long period of time, since surgical interventions must be avoided, the production of μW level energy, which will not fit some applications, and also the inevitable biofouling [13, 15].

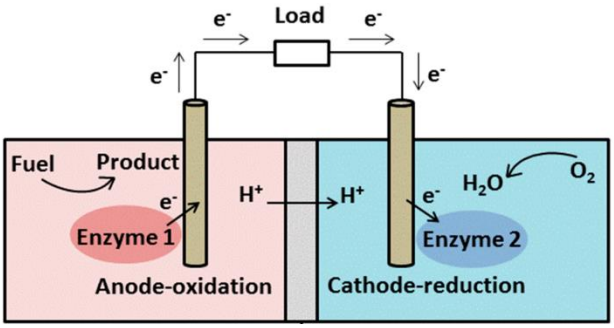

Figure 5. Working principle of biochemical energy harvester, biofuel cells [27].

Piezoelectric nanogenerators are based on piezoelectric materials (*e.g.*, zinc oxide, (ZnO), lead zirconate titanate (PZT) and polyvinylidene fluoride (PVDF)) that can produce electric energy from the kinetic energy of biomechanical sources through the piezoelectric effect. This is a phenomenon where an external force is applied to a crystal whose displacement of anions and cations produces an electric dipole moment and progressively generates a potential difference, accumulated all through the material in the direction of the applied tension (Figure 6 (A)) [13]. This leads to an AC output [25]. Therefore, this technology easily takes advantage of the mechanical energy produced by discontinuous body motion. However, this type of material will not be as adequate for the harvesting of energy

from continuous body motion, since they require movements of high frequency/force amplitude to generate a considerable amount of power, and so implantation locations are limited as they should be associated with significant body motions. Besides, costs per watt for low-frequency values (under 1 Hz) tend to be higher when compared to other harvesters [15, 29]. Current challenges in PENG application for biomedical settings are associated with their biocompatibility and large dimension, having a need for miniaturization [13].

Electromagnetic generators also harvest kinetic energy but based on the Faraday Neumann Lenz law. This law states that the relative motion between a conductor coil and a permanent magnet generates a time-variable magnetic flux and, as a consequence, a potential difference at the coil's ends (Figure 6 (B)). This approach can generate electric energy from low-frequency and irregular body movements. Although, these devices are the most efficient when operating at their resonant frequencies and body motion are mostly at a lower range frequency (1-10 Hz). Outputs of this technology tend to be of high current but low voltage. Current challenges include its size, mass, and inflexibility, which difficult integration and miniaturization [15, 16, 21].

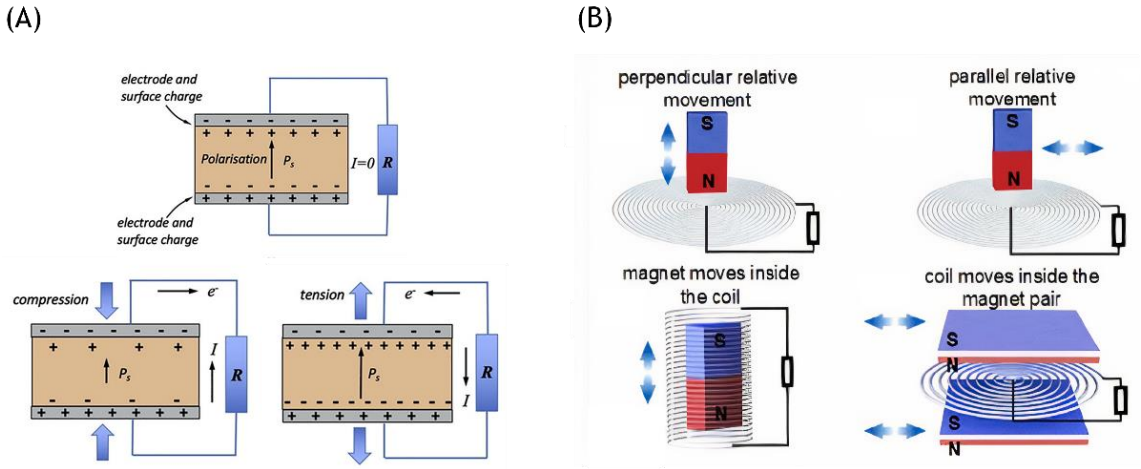

Figure 6. Working principle of kinetic energy harvesters. (A) Piezoelectric nanogenerators [30]; (B) Electromagnetic generators [31].

Lastly, triboelectric nanogenerators have emerged in 2012 as an alternative kinetic energy harvesting device with unique advantages.

Table 1 summarizes the main advantages and disadvantages of the reviewed energy harvesting technologies.

Table 1. Main advantages and disadvantages of the different energy harvesting technologies.

Energy harvester	Energy type	Advantages	Disadvantages
Pyroelectric	Thermal 	Unlimited lifetime; High sensitivity.	Small body thermal gradients/fluctuations leading to low power outputs.
Thermoelectric			
Biofuel cells	Chemical 	Recyclable nature materials; Biocompatibility.	Lifetime; μW level energy.
Piezoelectric	Kinetic 	Useful for discontinuous body motion.	Not as adequate for continuous body motion; Limited implantation sites; Biocompatibility issues; Low output and efficiency.
Electromagnetic	Kinetic 	Generation of energy from low-frequency irregular body movements; High current.	Larger size and mass; Complex fabrication; Low voltage.
Triboelectric	Kinetic 	High power outputs; Efficient for low frequency friction; Wide variety of material and design options; Cost-effective.	Long-term biocompatibility and biosafety; Infiltration of body fluids; Mechanical wear; Size.

2.2. Triboelectric Nanogenerators

Triboelectric nanogenerators are energy harvesters that work on the basis of the triboelectric effect. Triboelectric effect is the phenomenon where dielectric materials (electrical insulators that upon electrical stimulation can be polarized) and/or their surface become electrically charged when they contact with another material of opposite tribopolarity – contact electrification. Surface's tribopolarity is determined by the material's tendency to lose or gain electrons, leading to positive or negative charges, respectively. Due to external mechanical movements, the materials will move relatively to each other, and the oppositely charged surfaces will change periodically as charge transfer occurs, from the material with higher energy to the one with the lower energy of occupied surface state [32]. This induces a potential difference between the electrodes attached to the back of the materials and connected by an external circuit – electrostatic induction. Electrostatic equilibrium is maintained by having the free electrons move back and forth, which produces an AC output. Depending on the electrodes configuration and how the materials move in relation to each other, TENGs can work in four different modes - vertical contact-separation, lateral sliding, single-electrode and freestanding triboelectric-layer mode (Figure 7) [12, 33].

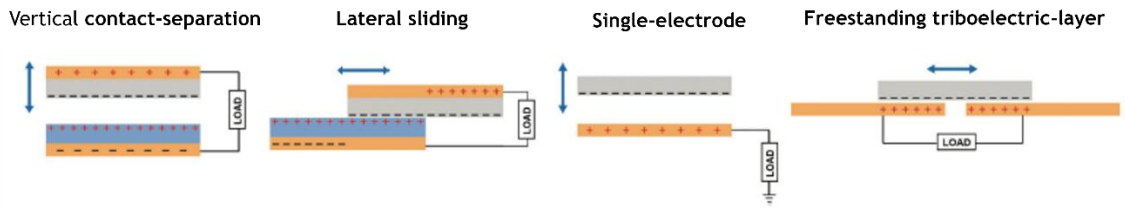

Figure 7. TENG's four working modes, varying in relative movement between the triboelectric layers (represented in gray and blue) and electrodes configuration (represented in orange) [10].

In vertical contact-separation mode, energy is harvested from the application of a mechanical force vertical to the triboelectric materials' surfaces [14]. At first, when there is no force applied, the two triboelectric layers are separated by a gap, leading to a potential drop. At this point, free electrons flow from one electrode to the other to balance the electrostatic field created. When the force is applied, the top layer approaches the bottom one and the materials come in vertical contact, leading to a reverse flow of the electrons, which results in a complete cycle for AC output as the potential disappears [10]. Thus, space gap determines the potential difference between the electrodes at the back of each triboelectric layer and, as this contact-separation process repeats, continuous AC is generated [13, 14]. This type of TENG device is simple and easy to fabricate, providing high outputs, but its packaging is difficult for its larger volume [34].

Lateral sliding mode generates electric energy by the relative sliding motion of the top layer over the bottom layer in a parallel motion. At a first instance, both layers are in full contact with each other and so have opposite charge density. As the top layer slides off of the bottom, contact area reduces and a potential difference is generated, with electrons flowing from the bottom to the top electrode until there is no contact between the layers. By reversing the sliding direction, electron flow is also reversed for electrostatic equilibrium [10]. In this case, the back and forth sliding cycles generate the AC output [13]. It shows lower structural performance than the previous mode but generates charges more efficiently [34].

As for a slightly different configuration, single-electrode mode uses only one electrode, opposed to the previous two modes where there are two electrodes. In this approach, a reference electrode is grounded and so there is only one triboelectric layer that can move freely, in relation to the reference electrode. As the material moves and the space between the layers varies, a potential difference is created due to the surface triboelectric charges. Current is then generated between the electrode and the ground. This mode is useful to reduce restrictions and collect energy from moving devices, but with a cost of reduced effectiveness [13]. The removal of one electrode from the structure limits charge transfer and, consequently, reduces power outputs [34].

Finally, freestanding triboelectric-layer mode consists of an optimized version of the single-electrode mode. Similarly, the top triboelectric layer does not need to be connected to an electrode and wires (freestanding), but as for the bottom layer, two symmetric

electrodes need to be placed alongside each other and with a small gap between them. The mechanism of generating electric energy is similar to the lateral sliding mode, as electrons flow from one electrode to the other to balance the difference in potential created by the movement of the freestanding layer [13, 14]. The freedom of movement while maintaining two static electrodes makes this mode the most efficient for energy harvesting [34].

TENG provides robust outputs (high power density) and great efficiency of energy conversion for low frequency frictions, unlike other technologies [35]. These have the unique advantages of being easy to fabricate with a wide variety of material options (lightweight and small volume, flexible and biocompatible) and device structural designs, being cost-effective and environment friendly [14]. Regarding the materials chosen for the production of these devices, the triboelectric layers' materials (dielectric materials) should be as far as possible from each other in the triboelectric series (Figure 8), to have opposite tribopolarities, but also have the appropriate characteristics to satisfy a specific application (*e.g.* wear resistance, flexibility, stretchability, biocompatibility) [35].

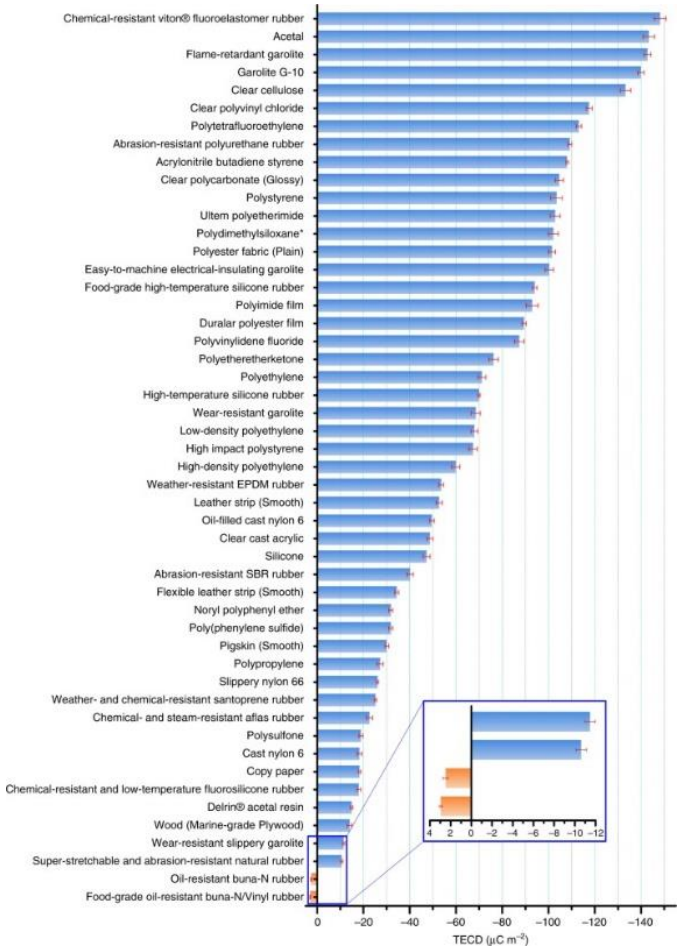

Figure 8. Triboelectric series for solid materials, according to their quantified triboelectric charge density (TECD), determined through the method proposed by Zou *et al.* for universal standardized evaluation [36].

One of the most reported materials for TENG is polytetrafluoroethylene (PTFE), for being highly tribonegative and for its high electron affinity, which improves the transfer

during the electrification process, due to the polymer's composition in fluorine atoms. Besides, it has low surface energy, making it hydrophobic [33, 37]. Expanded PTFE (ePTFE) can be obtained from PTFE films by a stretching process, having a distinctive microporous structure that greatly impacts its triboelectric performance, as the increased surface contact area improves surface charge density and charge transfer [37].

2.2.1. Self-powered cardiac electronic devices based on TENG

TENGs have been extensively studied to provide electric energy for a great number of biomedical applications such as cell modulation, nerve stimulation, wound/tissue repairing, gene delivery, power supply to electric devices, among others [14]. This section reviews the state-of-the-art applications currently being explored for the powering of electric devices, in particular the ones related to cardiovascular diseases. Figure 9 summarizes the timeline of the first TENGs and following applications for cardiac electronic devices.

The first TENG capable of harvesting mechanical energy to generate electricity was demonstrated in 2012 by Wang *et al*. [38], when it was proposed the stacking of the insulating polymers Kapton and Polyethylene terephthalate (PET), with a thin layer of Au on the top and bottom surfaces, as the electrodes (Figure 9 (A)). By applying external mechanical deformation cycles and promoting a relative sliding motion between the polymer layers, electric energy was generated with peak output voltage of 3.3 V and current of 0.6 μA, with a power density of 10.4 mW/cm^3.

In 2014, the first *in vivo* implant of TENG (iTENG) was performed. The iTENG was designed with a highly flexible thin triboelectric layer of pyramid nanopatterned PDMS on Kapton with Au electrode and one of Al foil, working as both the second triboelectric layer as well as the electrode. This iTENG was encapsulated with a thin polydimethylsiloxane (PDMS) layer to protect the whole structure from the biofluids of the surrounding environment (Figure 9 (B)). Thus, a robust, flexible, leak proof, biocompatible device capable to generate a voltage of 3.73 V and current of 0.14 μA from living rat's periodic breathing motion (expansion and contraction of the thorax) was achieved, through the contact-separation principle of TENG. This electric energy was stored in a capacitor and used to supply a pacemaker prototype. It was then verified that the stimulation pulses generated were able to regulate the rat's heart rate. However, an inflammatory response was observed, compromising long-term performance [39]. In small animals, pacemaker regulation of heartbeat requires much less electrical energy than in large animal models, which makes the results obtained with large animals more reliable to extend for applications in the human body. Thus, in 2019, it was evaluated the ability of an iTENG device to power a symbiotic pacemaker (SPM) on a large-scale animal, a porcine, using its cardiac motion. The simpler version of a pacemaker comprises a pulse generator, leads and a battery that is put inside a soft tissue pocket, and it can function in single (right ventricle passing, 1 lead) and dual-

chamber modes (right ventricle and atrium passing, 2 leads) [40]. The iTENG powered pacemaker is referred to as a symbiotic pacemaker as it consumes energy from the body, through the iTENG, and the body, in return, obtains electrical stimulation from the device. The whole system consisted of an iTENG, a power management unit (PMU), consisting of a microcontroller with power functions such as AC/DC conversion and storage, and a pacemaker (Figure 9 (D)) [41]. For the iTENG, one triboelectric layer comprised a nanostructured PTFE on Kapton with a titanium strip layer, for improved elasticity and strength for the relative movements, with Au electrode, and the other layer of Al, which also served as the second electrode. The entire device was encapsulated with Teflon and PDMS for stability enhancement and protection from biofluids. *In vivo*, it was achieved a maximum voltage of 65.2V with a corresponding short-circuit current of 0.5 μA. Moreover, 0.495 μJ of energy was harvested in each cardiac cycle and the threshold required for pacing is only 0.377 μJ, which highlights the efficiency to power this cardiac device. For the most part, the SPM was able to pace the heart correctly, but fast pacing led to failure. There are still some challenges that must be addressed in order to get the SPM to clinical applications, mostly related to the need for iTENGs to be smaller with high energy density, for a safer long-term fixation of the device to the tissues and a more efficient PMU [41].

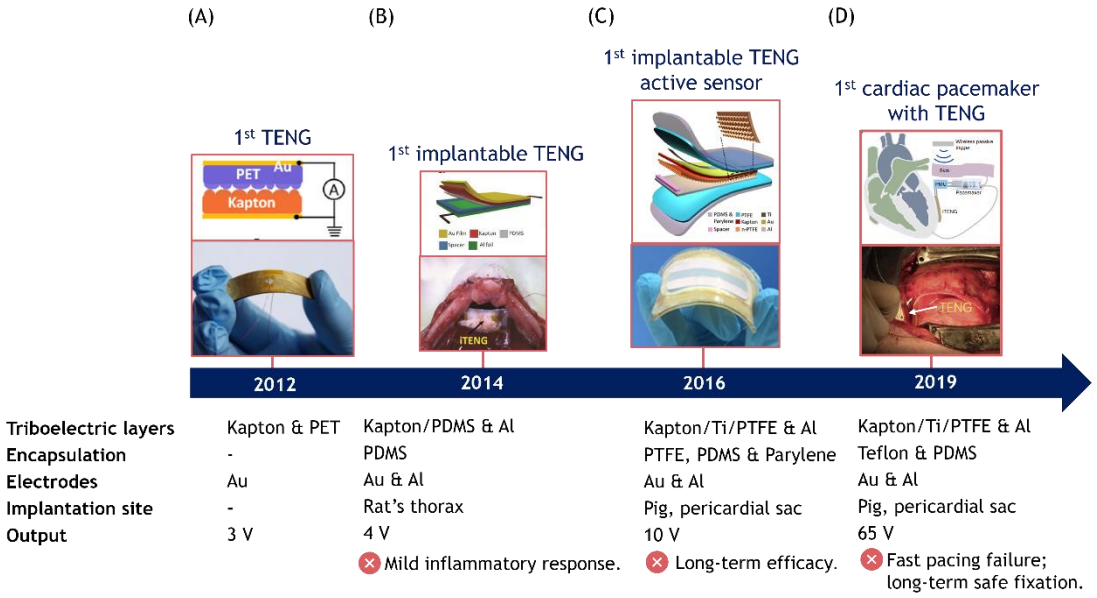

Figure 9. Timeline of TENG applications for cardiac electronic devices. (A) First TENG, discovered by Wang *et al*. Adapted with permission from ref. [38], copyright 2012, Elsevier; (B) First implantable TENG, developed by Zheng *et al*. Adapted with permission from ref. [39], copyright 2014, Wiley; (C) First implantable active sensor based on TENG for cardiac applications, developed by Ma *et al*. Adapted with permission from ref. [42], copyright 2016, American Chemical Society; (D) First symbiotic cardiac pacemaker powered by a TENG, developed by Ouyang *et al*. [41].

Regarding TENG applications for sensors powering, it was recently proposed an epicardial bioelectric patch that could work on the basis of the triboelectric effect to power itself for monitoring and treating of cardiovascular problems. This device, encapsulated by PDMS, contains an array of transistors to do a spatiotemporal mapping of biopotentials

(electrocardiogram) and pacing, a strain sensor, a thermal sensor/actuator to provide thermal ablation and, additionally, a TENG, for the harvesting of energy from heart beating, in vertical contact-separation mode (Figure 10 (A)). This patch is made of all soft rubbery materials that match heart tissue, being easily deformed with the beating motion. The TENG portion is based on the contact of two layers composed of Ag nanowires, embedded in PDMS for encapsulation, and provides a maximum 0.68-0.74 V and 8.01-13.39 nA output, which consists of an approximate output power of 5.45-9.91 nW. Despite relatively low outputs, these studies corroborate the possibility to further optimize this energy to power the patch. Besides, this is a temporary implant proposed for cardiac surgery support, and even though tests *in vivo* did not show damage to the heart, biocompatibility is yet to be address, so it is assumed that a long-term application would need further optimization to avoid an inflammatory reaction and fibrosis [43]. Another example of this functioning principle but for a wearable application was reported for a self-powered human heart-rate sensor. This system comprised a commercial heart-rate sensor, a signal processing unit, a Bluetooth module to send the processed cardiac signal to a smartphone, and finally a TENG, to the harvest the energy from the arm movement during walking, and a PMU, to manage it to power the system. To increase contact area and, consequently, the electrical output, a TENG with downy structure was developed, which consist in two basic functional units: 1) a multilayer structure with acrylic as supporting backbone, with anchored segmentally alternating films of Cu back coated PTFE and Cu with a free standing end; 2) an acrylic sheet segmentally adhered on the front and back surface by the copper-coated PTFE and copper thin films. The two layers are connected with a stretchable rubber (Figure 10 (B)). Thus, energy was generated from the contact of PTFE and Cu of each layer. It was possible to obtain a maximum of 2.28 mW [44].

As for active sensor applications of TENG, the first implantable sensor was proposed in 2016 by Ma *et al.* [42] to measure heart and respiratory rates, for the detection of arrythmia, by using the electrical outputs generated as consequence of the user's heartbeat and breathing motion. TENG was composed by a layer of nanostructured PTFE on Kapton/Ti and Au, and the other of Al film. For the encapsulation it used PTFE, PDMS and Parylene film (Figure 9 (C)). When implanted in a swine's pericardial sac, it was obtained a peak output of 10 V and 4 μA, with heart and respiratory rates being effectively and precisely monitored in real time. Moreover, Ouyang *et al.* [45] developed a wearable TENG active sensor which detects abnormalities associated with CVDs, based in person's pulse sensing. TENG consisted of a nanostructured Kapton triboelectric layer with a Cu electrode at its back side, and the other layer of nanostructured Cu, in this case also doubling as the second electrode, deposited on Kapton film, with a PDMS encapsulation (Figure 10 (C)). Placing the sensor over the radial artery, it was achieved an output of 1.52 V and 5.4 nA. Furthermore, voltage signal

was acquired, and by Bluetooth, the data transmitted and displayed in a smartphone or computer.

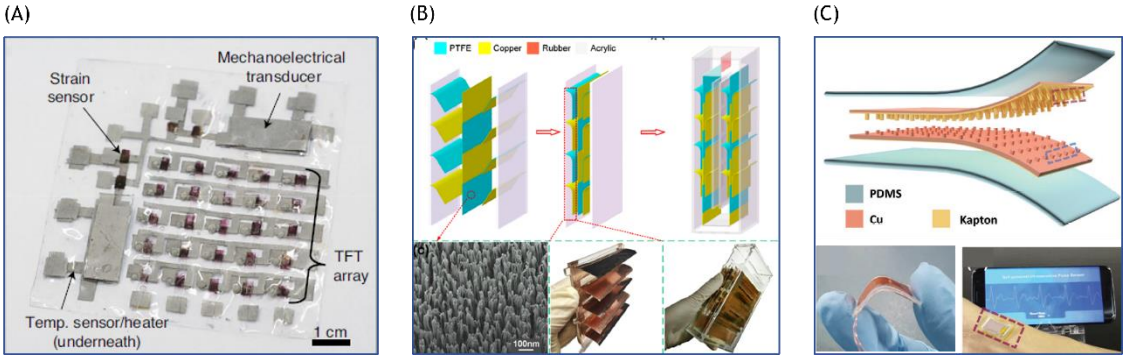

Figure 10. TENG designs for self-powered cardiac sensor applications. (A) Implantable epicardial bioelectric patch, powered by incorporated TENG (mechanoelectrical transducer), for spatiotemporal mapping of electrophysiological activity, developed by Sim *et al*. Reprinted with permission from ref. [43], copyright 2020, Springer Nature; (B) Downy-structured TENG for powering a wearable heart-rate sensor, developed by Lin *et al*. Reprinted with permission from ref. [44], copyright 2017, American Chemical Society; (C) Wearable active sensor for pulse signal monitoring, developed by Ouyang *et al*. Adapted with permission from ref. [45], copyright 2017, Wiley.

2.2.2. Current limitations of TENG

In summary, despite the large number of reports on TENG's potential to power CEDs and other medical electronic devices, there are still several limitations that must be addressed to introduce this technology in clinical practice. Not only for medical applications, TENG's performance, as well as other energy harvesting systems, should be improved to meet the electronic requirements of currently available devices. Considering that TENG outputs are highly dependent on the chosen materials to integrate the triboelectric layers, pairs of materials with opposite tribopolarities, as well as different designs (with increased contact area), should be explored to develop more efficient devices [35]. Moreover, all components must be reliable and durable to achieve longevity for the devices [10]. Specifically for biomedical settings, higher levels of complexity are required in TENG's development, namely regarding their biocompatibility, as they should be non-cytotoxic and non-immunogenic, their size, that should be as small as possible to integrate complex systems, and flexibility, to be adaptable to all sites of human body [46]. Moreover, for implantable TENGs, there is the added concern of infiltration of biofluids that will compromise the devices performance and so must be avoided [39].

Besides the optimization of TENG devices, there is a need to improve the PMUs in order to take full advantage of all harvested electric energy and also optimize its storage [10].

2.3. Fluid Triboelectric Nanogenerators

Recently, a liquid-solid approach for TENG has been explored, the so-called Fluid triboelectric nanogenerators (Flu-TENGs). As the name suggests, this TENG variation consists of the use of a fluid and a solid as the two materials for the triboelectric layers. Similarly to the most traditional solid-solid contact TENG, mentioned previously, as the liquid moves over the solid surfaces, opposite charges are generated in both materials and there is charge transfer across the interface, as a result of the interaction between the molecules and ions of the fluid and the solid surface [33]. The identification of the charge carriers involved in the fluid-solid contact electrification (CE) process is still a topic of discussion, as there are not many in depth studies on the matter. CE is usually associated with ion transfer merely due to the common ion composition of fluids [47]. However, this process can now be explained by the studies of Wang *et al*. [48] and Lin *et al*. [47], that are based on CE being a result of both electron transfer derived from electron clouds overlapping and the formation of an electric double layer (EDL) from ion transfer. Therefore, a two-step model is proposed for a better understanding of these fluid-solid interface interactions [33]. In the first step, according to this theory, a virgin solid surface contacts with a fluid as a result of induced external mechanical forces, and the molecules and ions in the fluid interact with the atoms of the solid surface (Figure 11 (A) i-iii). This interaction leads to an overlap of the electron clouds that culminates in electron transfer to charge the neutral atoms (Figure 11 (A) iv) owing to the reduction in interatomic potential barrier, in its case caused by the reduced interatomic distance of the two rubbing materials (solid and fluid). The second step consists of the formation of the EDL and it is suggested that it is driven by the electron transfer that occurs in the first step (Figure 11 (A) v) [32, 48]. Ions are atoms with extra or a lack of electrons, therefore ionization occurs at the surface when the atoms of the solid become charged [47]. The first layer of the EDL is composed of the ions resulting from chemical reactions that stay absorbed to the solid surface - stern layer - whereas the second one consists of oppositely charged ions that move freely on the fluid and are attracted to the surface charges on the basis of Coulomb forces – diffuse layer (Figure 11 (B)) [47, 48].

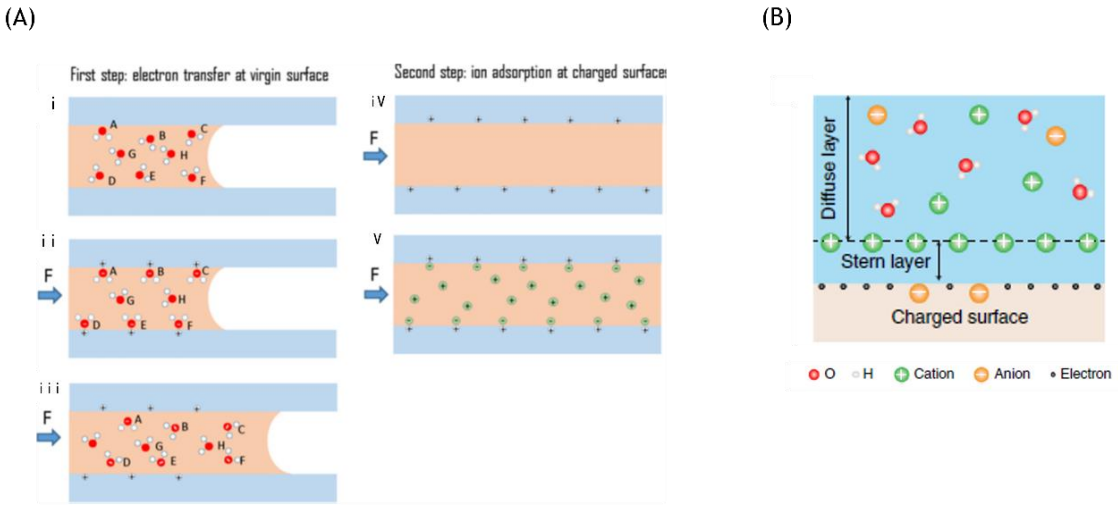

Figure 11. Fluid-solid contact electrification mechanism. (A) Two-step process consisting of the electron transfer, in the first step, and ion transfer, in the second step, proposed by Wang *et al.* (i) The fluid and the virgin solid surface come in contact; (ii)(iii) Interactions between the molecules of the fluid and atoms of the solid surface during fluid flow resulting in (iv) a charged surface; (v) Formation of the electric double layer. Adapted with permission from ref. [48], copyright 2019, Elsevier; (B) Final step, consisting of the formation of the electric double layer, composed of the stern and the diffuse layers, described by Lin *et al.* [47].

It is also important to mention that the polarity of the surface after CE depends on both ionic and electronic charge density [33]. Moreover, Lin *et al.* found that CE involving hydrophilic surfaces is dominated by ion transfer, whilst electron transfer is the prominent phenomenon when it comes to hydrophobic solid materials [47].

This Flu-TENG technique has relevant advantages over solid TENGs, such as reduction of mechanical wear, since the latter's durability is highly affected by wear abrasion, compromising long-term performance and sensing stability. Besides, solid TENGs can be influenced by different external factors and, sometimes, it is difficult to assure the proper contact between the triboelectric layers' materials, which does not happen for fluid nanogenerators because of the fluid's capability of adjusting its shape, so there is a complete contact with the solid surface, leading to better electric outputs [33, 49]. The first TENG based on fluid-solid contact was developed in 2014 [50] by Su *et al.* [51]. In their studies, it was developed a Flu-TENG for the harvesting of the energy generated from water waves, capable of obtaining both the electric energy resulting from the liquid-solid contact of the water and a solid material and also from the mechanical energy associated with the impact of waves, a hybridization technique that allowed for the full use of water motion related energies.

Concerning the fluid nanogenerator's fluid-solid interface interacting modes, there are three main ones that can be identified, varying in the fluid's behavior, which are the droplet, wave and flow mode Flu-TENGs [33]. Flow mode is of utmost interest for the herein present work and, in general, for many future biomedical applications, as the resulting energy from streaming flow in conduits can be easily accessed from not only environmental sources but also from the human body, as is the case of the blood flowing in our circulatory

system [52]. In 2018, Cui *et al*. [53] first reported a flow mode approach for Flu-TENG, based on the use of water flowing along a PTFE tube for the production of a self-powered sensor for the detection of the water flow rate, location and blockage (Figure 12 (A)). Its function was successfully observed as voltage peaks were obtained as the water moved passed each Cu electrode of the linear array placed around the outside of the PTFE pipe, and so those could be assigned to certain time points and positions of the water flow along the tube. For the enhancement of the output, besides the hydrophobicity of the material, a micro-structured surface was used to provide a larger active surface area, thus, higher charge density. Changes on the acquired voltage were observed as the electrodes' length, inner diameter and slant angle of the tube, flow rate and external load resistance were varied. This Flu-TENG was able to generate a maximum output of 40 V and 0.4 μA under a 200 mL/min flow rate. Optimum results were obtained for 7 cm of inner diameter, 90º of slant angle, 3 cm of length and 80 MΩ resistance.

Furthermore, electric output of Flu-TENG is highly impacted by the type of flow, steady or unsteady [33]. A steady flow is characterized by a constant flow rate over time whereas the unsteady flow has a varying one. In spite of the known importance of these flow dynamics, the use of an unsteady flow for energy harvesting is still poorly explored. In 2019, Cheedarala *et al*. [52] reported the first energy harvester based on Flu-TENG with unsteady flow, resorting to a peristaltic pump to create a pulsatile unsteady water flow across a micro porous PVDF hydrophobic membrane placed inside an elastomeric tube (Figure 12 (B)). Under 140 revolutions per minute (rpm), with deionized water, was obtained a peak-to-peak voltage of 7 V, and of 11.06 V with tap water, a difference justified by the latter's mineral content that seems to increase the conductive properties of water. Later the same year, Ahn *et al*. [54], by experimenting with unsteady water flow driven across a polymeric pipe, have demonstrated that it could be achieved an electric output up to 70 times higher than the one resulting from the use of steady flow (70 nA versus 1 nA peak to peak output), highlighting how promising having this type of fluid motion can be for the generation of energy from various sources. Nam *et al*. [50] have added the technique of an automatic ON-OFF control of a peristaltic pump to promote a highly unsteady flow, in order to take advantage of what had been found before on the effect of this type of flow's dynamics and achieve even greater outputs. This way, approximately 46.1 V and 5.03 μA (peak module values for open circuit voltage and short circuit current, respectively, resorting to water flow) were able to be generated. Besides, in this study it was explored an alternative to the most common approach of indirect charge transfer, in which during the electrostatic induction process of TENGs, the generated charges move from the solid surface to the electrode. In the proposed direct charge transfer TENG, after the fluid is in contact with the solid dielectric material and charges are generated in its surface, on the basis of the triboelectric effect, it is put in direct contact with the electrodes thus a potential difference is efficiently generated in them

as a result of flow electrification (Figure 12 (C)). Here, the main focus are not only the properties of the solid material of the Flu-TENG (*e.g.*, thickness and hydrophobicity) but also of the fluid alone.

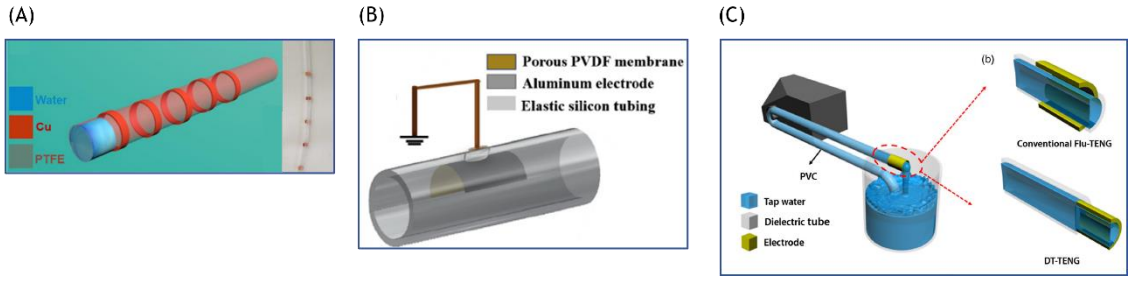

Figure 12. Flu-TENG designs for energy harvesting applications. (A) First flow mode approach of Flu-TENG for detection of water flow rate, location and blockage, developed by Cui *et al*. Adapted with permission from ref. [53], copyright 2018, Elsevier; (B) Flu-TENG design for the first unsteady flow approach for fluid-phase, developed by Cheedarala *et al*. Reprinted with permission from ref. [52], copyright 2019, Elsevier; (C) Comparison of conventional Flu-TENG and the direct charge transfer approach, developed by Nam *et al*. [50].

As the liquid is one of the main components that influence the performance of Flu-TENGs, it is important to note the influence of its intrinsic properties on the electric output. Firstly, the ion activity will have a significant influence on the contact electrification process [33] since it was demonstrated that for the case of ionic fluids (*e.g.*, NaCl and $CuSO_4$) charge transfer is mostly dominated by ion transfer. As ion concentration increases, at first the charges transferred also increase but then it starts to decrease, reaching zero as a result of the accumulation of ions at the fluid-solid interface, hindering the electron transfer process [55]. Additionally, more studies have corroborated that the increase in the fluid's ion concentration reduces the power output of Flu-TENGs.

Regarding the solid material of fluid nanogenerators, its hydrophobicity and high surface charge density are highlighted as the most crucial properties for favorable triboelectric outputs, independently of the corresponding fluid-phase. Surface morphology and composition are a very important factor to take into consideration because it will influence the contact interface, and it can be modified to enhance the materials' triboelectric properties. For instance, surfaces can be made to be superhydrophobic to reduce friction, and also designed for patterns which increase the surface volume to ratio and, consequently, the charges generated at the interface [33]. A common problem for Flu-TENGs is the difficulty of complete removal of reminiscent liquid on the solid layer after contact, which reduces further electrical outputs. Therefore, superhydrophobic surfaces (contact angle above 150º and sliding angle below 10º) are considered to be the most efficient solid-phase materials for Flu-TENGs [56]. Moreover, surface modification can be done either chemically or by pre-charging of the solid surfaces. Chemical modification allows for the selection of functional groups that will either be electron-donating or withdrawing, tuning the surface charge density by altering the sites tendency to gain or lose electrons, respectively. Besides, functionalization can be also done to modify the surfaces wettability,

which is an important property that will influence the performance of the TENG, as previously mentioned. Concerning pre-charging techniques, these consist on the introduction of electrical charges, even before the contact electrification process to facilitate it and improve the electric outputs that can be achieved [33].

2.4. Blood flow for energy harvesting

From the study of the different existing energy harvesting technologies, it can be perceived that the transformation of body motion associated with the flow of biofluids, like blood, into electrical energy is an emerging interest for many biomedical applications, such as to address cardiovascular health issues.

Recently, Cu *et al.* [49] proposed a biomedical droplet sensor for monitoring the drainage of bottles in medical settings. This sensor uses the triboelectrification resulting from the contact between droplets over a PTFE superhydrophobic solid surface, which generates opposite charges on their surfaces leading to pulse current peaks (Figure 13 (A)). The analysis of these peaks provides information on how many droplets rolled over the electrodes of the sensor as well as speed. The importance of having hydrophobic materials derives from not having residual (bio)fluids on the surfaces after flow, which would reduce efficacy in energy conversion. Furthermore, for biomedical applications, this type of surface is essential to minimize the possibility of thrombus formation, hemolysis and adsorption of biomolecules. Most studies on the applications of fluid nanogenerators for energy harvesting focus on the use of water as the fluid triboelectric layer, but in this study [49] were first introduced experiments with other types of fluids, namely PBS (neutral), HCl (acid), NaOH (alkaline) and the biofluids urine and blood (Figure 13 (A)). Regarding the generation of triboelectric outputs, all fluids originated pulsed current peaks as droplets rolled over the solid material, with blood having the most charges generated due to its higher weight and, consequently, larger area for contact electrification. Additionally, it was demonstrated the gradual reduction in current output as blood flow rate across the sensor developed reduces, emphasizing not only the efficacy in response of the sensor but also the ability of the blood to generate higher electric outputs with significant flow rates in TENGs. Therefore, even though the use of streaming blood flow along polymeric materials or even vessels as Flu-TENG's, for energy harvesting from a human body source, was never attempted before, from the analysis of literature, it is concluded that it shows promising results.

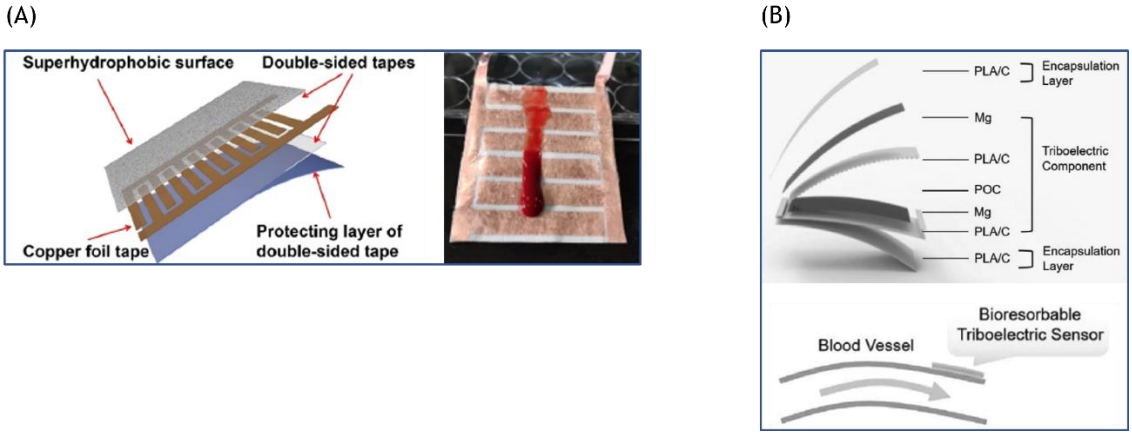

Figure 13. Energy harvesting applications resorting to blood-related motions. (A) Flu-TENG design for droplet sensor for monitoring of bottles' drainage in medical settings, with real representation of tests using blood drops, developed by Cu *et al*. Adapted with permission from ref. [49], copyright 2020, American Chemical Society; (B) First bioresorbable solid-solid TENG designed for occlusion sensor, based on variation of biomechanical movements as a consequence of hampered blood flow, developed by Ouyang *et al*. [57].

More recently, in 2021, it was demonstrated that blood flow causes a relative movement, thus friction, between blood constituents (plasma, blood cells and salts) on the vessel walls or vascular grafts (upon patient implantation), and that this leads to triboelectrification of all the involved components. In particular, red blood cell's (erythrocytes) membrane has unique characteristics that could allow the generation of high levels of triboelectricity. In contrast, in white blood cells (leukocytes), weaker charges are generated because of their soft nature and surface's wrinkles and folds as well as inferior floating speed [58]. Additionally, as the outcome of Flu-TENGs is highly dependent on fluids characteristics and its flow type/rate, the difference between fluids rheological properties should be taken into consideration. Blood behaves as a non-Newtonian fluid, meaning that its viscosity varies with shear rate, and that is mainly due to the interaction of blood cells. As a result, blood's viscosity increases when the flow is slower during diastole, whereas in systole it becomes thinner, as velocity increases. Blood's viscosity also varies with location as there is a difference in diameter between vessels and, consequently, in shear rate [59]. Plasma is the main constituent of blood and is mostly composed of water (approximately 92%) along with proteins, minerals, hormones and glucose. Oppositely to blood, for its different composition, plasma is believed to be a Newtonian fluid, even though more recent studies have been raising the possibility of some viscoelastic behavior [60, 61].

Other energy harvesting systems based on blood have been developed, and at this point, it is also relevant to mention the importance of these technologies for sensing applications, concerning blood flow. One of the most common causes of vascular grafts failure is the formation of thrombus, that can be caused by a variety of reasons [62]. A hemodynamically failing graft undergoes stenosis, which consists on the reduction of its diameter, and is at an high risk of occlusion within about a year if not properly treated, therefore it is of utmost importance to detect this pathology before this occurs [63]. Neville

et al. [64] reported a preliminary self-monitoring prosthetic bypass graft based on energy harvesting technologies. For this, an ePTFE graft was assembled with PVDF piezoelectric microsensors wrapped around its outer surface and integrating battery/processing related microelectronics. To mimic a pathological situation, the flow was varied, and different levels of stenosis were tested by gradually reducing the diameter of the tubing through which a fluid flows to the graft. The signals acquired, resulting from the application of varying external forces from the movement of the graft on the sensors, were processed for the establishment of a relationship with the flow variation and respective level of stenosis, for failure detection. This demonstrated the potential of using failure associated blood flow perturbations for the production of self-powered sensors, that could have a huge impact on early detection and treatment of an occluded vascular graft. For a similar application, but resorting to the solid-solid contact TENG principle, Ouyang *et al*. [57] developed the first bioresorbable self-powered sensor, with demonstrated *in vivo* efficacy on detection of abnormal vascular occlusion events in a post operation situation. For the triboelectric layers it was used the biomaterials film poly(lactic acid)/chitosan (PLA/C) with Mg electrode, capable of degrading only after the normal postoperative period. The solid-solid TENG is placed on the outside wall of a vessel and, through abnormal variations in blood pressure caused by occlusion, biomechanical movements of the vessel originated from consequent hampered blood flow are converted into electrical signals, that are then associated to the occurrence of such events (Figure 13 (B)). For *in vivo* performance demonstration, a balloon was implanted on a large animal's vessel and, when inflated, mimicking occlusion, it led to an abrupt pressure drop. After deflating, blood pressure was repaired. These events could be detected with a sensitivity of 11 mV/mmHg. With this, great advances on postoperative care were shown, proving yet again the potential of the use of blood flow with energy harvesting techniques for sensing applications.

Chapter 3: Materials and Methods

3.1. Solid-phase preparation

3.1.1. Synthetic vascular grafts

3.1.1.1. ePTFE

Commercially available expanded polytetrafluoroethylene (ePTFE) vascular grafts used in clinic for peripheral bypass surgery and vascular access were kindly provided by Zeus Industrial Products, Inc. Vascular grafts varying in inner diameter (ID) and wall thickness (WT), namely with 1.5 mm ID and 100 μm WT, 4 mm ID and 500 μm WT, 4.5 ID mm and 75 μm WT and 6 ID mm and 152 μm WT, were used to study the influence of ID and WT in the achieved triboelectric outputs.

3.1.1.2. pHEMA/GO

A prototype with 4 mm ID and 1 mm WT of a vascular graft under development in our lab was used to evaluate its triboelectric properties. This vascular graft is made of poly(2-hydroxyethyl methacrylate), a FDA approved hydrogel, and graphene oxide (pHEMA/GO) [65].

Briefly, 2-hydroxyethyl methacrylate (HEMA) monomers were polymerized *in* situ by adding 1.5% (v/v) of a 1:1 mixture of 40% ammonium persulfate (APS) and 15% sodium metabisulfite (SMB), in the presence of 1% (m/v) of GO (prepared by oxidation graphite by modified Hummer's method) and 3% (v/v) of crosslinking agent tetraethylene glycol dimethacrylate (TEGDMA). 3D tubes were produced resorting to a plastic tube mold and inner glass rod of 6 and 4 mm diameter, respectively. The hydrogels were then removed from the molds, after an overnight resting, and rinsed with distilled water.

3.1.2. Native vessels

To mimic native coronary arteries present in the heart, arteries were isolated from umbilical cords of cesarean births, provided by Centro Hospitalar de S. João, Porto, Portugal, with the approval of the ethical committee (334-16) and informed consent of the donors.

The two umbilical cord arteries of each umbilical cord were isolated from Wharton's jelly and the vein using surgical tweezers (Figure 14) [66]. Then, to remove residual blood and clots present inside of the arteries, they were connected to 14GA and 16GA Venflon™ using surgical threads, and were flushed inside with PBS.

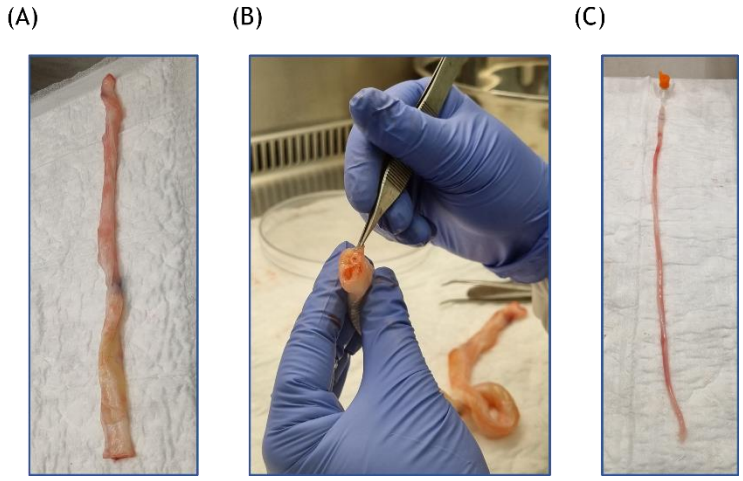

Figure 14. Isolation process of umbilical cord arteries. (A) Umbilical cord; (B) Isolation of the arteries; (C) Isolated artery.

3.2. Electrode preparation

3.2.1. Electrode assembly

Different conductive inks, namely silver (VFP ink technologies, SE-001), carbon (Elantas, Bectron® GP 9553) and poly(3,4-ethylenedioxythiophene):polystyrene sulfonate (PEDOT:PSS, Heraeus, Clevios ™ S V4 STAB, 81098168) were tested to be used as the Flu-TENG electrode. For reference, electrical conductivity of silver is 6.30×10^7 S/m, 10^6-10^7 S/m for carbon nanotubes [67] and 20 S/m for PEDOT:PSS films [68]. They were assembled in the three different solid-phases by brush painting. A copper wire was attached to all conductive inks to allow the connection to the acquisition set up. In the case of synthetic vascular graft, the inks were cured for 10 minutes under 130 ºC to achieve maximum conductivity, as recommended by the inks' suppliers, while for native vessels, to avoid vessel damaging due to the high temperature, they were left drying at room temperature for 30 minutes.

Besides conductive inks, copper tape was also tested as electrode. Copper tape was wrapped in the different solid-phases.

For silver conductive ink, it was tested the influence of different electrode lengths (0.5, 1, 2, 4, 6, 8 and 10 cm) and designs in the achieved triboelectric outputs.

3.2.2. Electrode stability

The stability of the assembled inks in the three different solid-phases was assessed by washing test, as previously described [69]. 1 cm length pieces of ePTFE (1.5 mm ID and 100 µm WT), pHEMA/GO (4 mm ID and 1 mm WT), and native vessels, assembled with the electrodes, were immersed in 1 mL of PBS, on a 2 mL Eppendorf® tube, and subjected to vortexing for 5 seconds at maximum speed, 3 times. Leachables were visually examined to detect the presence of the ink, that may have detached from the solid-phase during washing test. As all the used inks are colored, absorbance of the leachables was measure for the visible light wavelength range (400 to 700 nm) in microplate reader (Synergy ™ Mx, BioTek Instruments®) to further detect their presence (Figure 15).

Solid-phases assembled with conductive inks were evaluated before and after the washing test by scanning electron microscopy (SEM) using a desktop SEM (Phenom XL, Phenom World), to evaluate its detachment from the solid-phases outer surface and ink penetration to the inner surface. Solid-phases were cut longitudinally to expose the lumen. For synthetic vascular grafts, samples submitted to the washing tests were dried at room temperature overnight. In the case of native vessels, they were fixed and dehydrated before SEM visualization, as previously described [66]. Samples were fixed with a 1.5% glutaraldehyde (Sigma-Aldrich ®, ref: G005) in 0.14 M sodium cacodylate (Fisher Chemical ™, ref: 10627232) buffer solution for 30 minutes at room temperature, followed by water rinsing. Then, dehydration was achieved by immersing the samples in a growing ethanol/water gradient (60, 70, 80, 90, 99 % (v/v)), each solution for 10 minutes. Lastly, hexamethyldisilazane (Sigma-Aldrich ®, ref: H4875) was added to each sample, which were left to evaporate overnight in the hotte. Synthetic vascular grafts and native vessels were mounted on SEM pin stubs using a conductive carbon tape and sputtered with gold to improve their conductivity and, consequently, image quality.

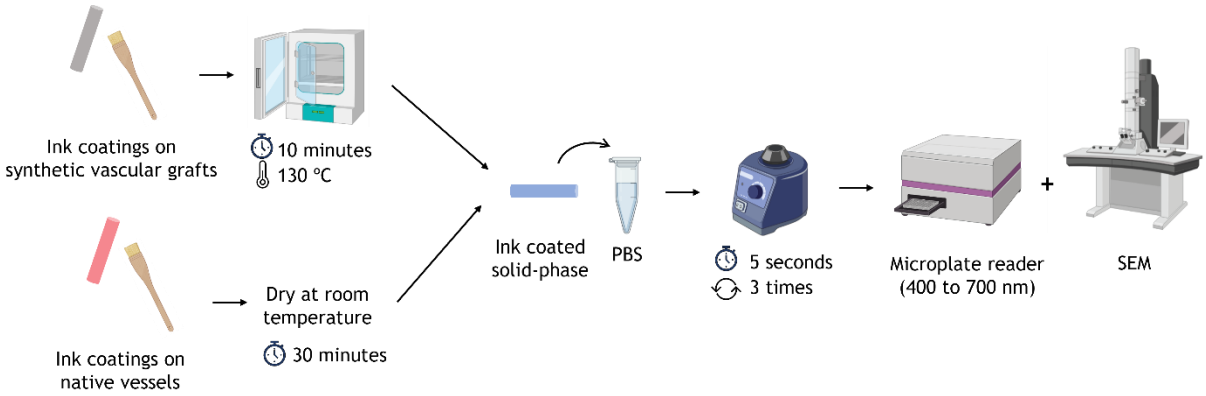

Figure 15. Schematics of electrode stability assessment.

3.3. Fluid-phase preparation

Three different fluids, PBS, plasma and whole-blood were adopted as fluid-phases. Plasma and whole-blood were obtained from Centro Hospitalar de S. João, Porto, Portugal, with the approval of the ethical committee (90/19) and informed consent of the donors. To mimic the normal recirculating pulsatile flow of blood in vasculature, a LongerPump® BT100-1L peristaltic pump was used. The different fluids circulate through silicon tubes from a reservoir, passing through the solid-phase and back to the reservoir. Depending on their inner diameter, solid-phases were connected to 14GA and 16GA Venflon™ or Luer Lock adapters, by surgical threads, to allow the assemble to the peristaltic system (Figure 16). The influence of flow rate in triboelectric outputs was studied, simulating physiological conditions, namely using two different angular velocities, 60 rpm and 100 rpm, which are the lower and upper limit of normal resting heart rate.

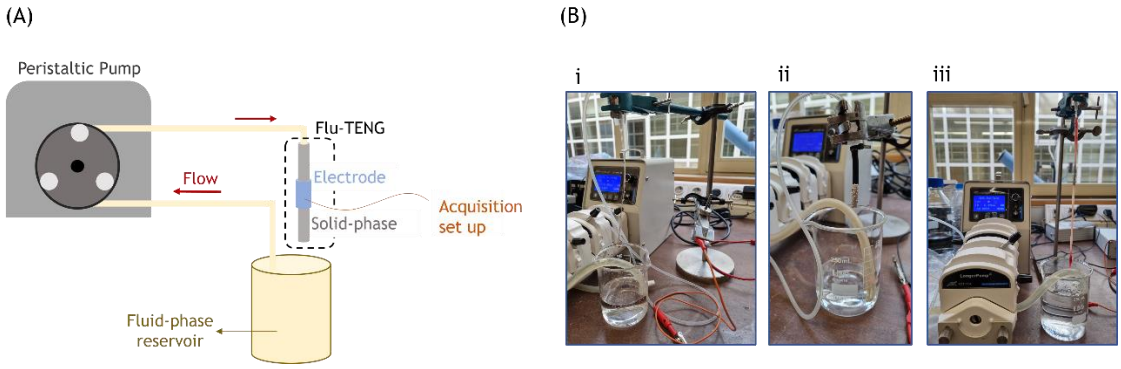

Figure 16. Peristaltic system for fluid-phase preparation and whole Flu-TENG assemble. (A) Representation of the assembled Flu-TENG, resorting to a peristaltic pump to simulate the unsteady pulsatile flow of the fluid-phase through the solid-phase; (B) Real Flu-TENGs assembled, with the different solid-phases: (i) ePTFE vascular graft, (ii) pHEMA/GO vascular graft and (iii) umbilical cord artery.

3.4. Electrical measurements of Flu-TENG

A Keithley™ 6514 system electrometer was employed for the measurement of voltage and current outputs, as previously described [70]. The assembled set up is represented in Figure 17 (A). A full characterization of the Flu-TENGs, with varying influencing parameters, was performed by varying external resistance between 10^3 and 10^9 Ω and capacitance from 10^{-11} to 10^{-4} F, and acquiring both voltage and current output electrical signals, for 30 seconds, resorting to the electric circuits represented in Figure 17 (B). Moreover, 1 and 100 nF capacitors were charged with the Flu-TENG's output for 10 minutes, using the circuit in Figure 17 (C).

The raw voltage and current output data was visualized and acquired through a National Instruments LabVIEW™ software, further interpreted by a process of peak detection and integration in OriginPro® software, being represented the mean of peaks for each

resistance and capacitance value along with the respective standard deviation (SD). Furthermore, power density was calculated, for each resistance and capacitance value, by multiplying the respective voltage and current mean values (power), and then normalizing by the electrode's area.

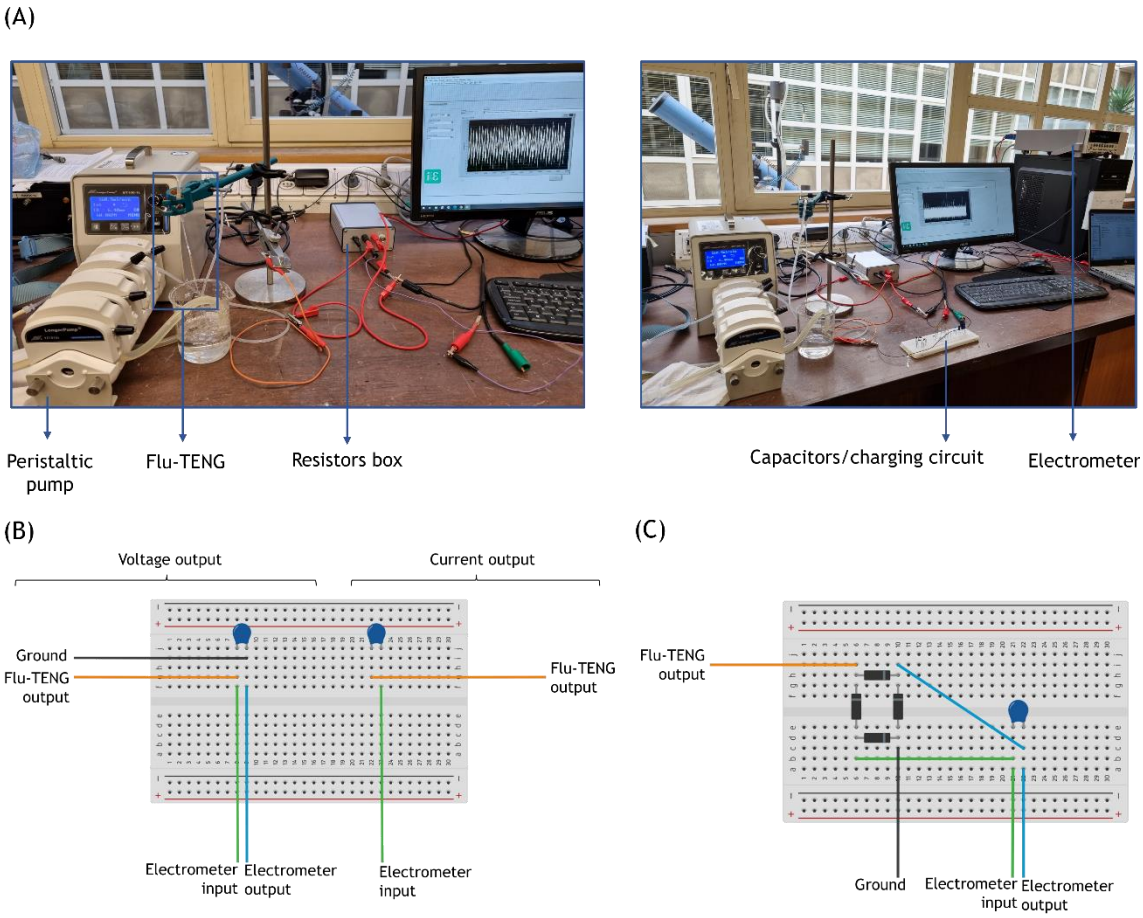

Figure 17. Set up assembled for the acquisition of the triboelectric outputs. (A) Flu-TENG connected to the resistors box and capacitors circuit, for varying external resistor and capacitor, respectively, for voltage and current outputs acquisition, and for charging capacitors. Measurements done with an electrometer, associated with a LabVIEW software for output observation and data acquisition; (B) Representative circuits of voltage and current output acquisition, for which the varying external component (resistor or capacitor, here represented a capacitor) is in parallel or in series with the electrometer, respectively; (C) Circuit composed of a bridge rectifier for charging of capacitors.

For triboelectric outputs acquisition, different parameters were varied. For the fluid-phase, PBS, plasma and blood were used with varying flow rates of 60 rpm (161 mL/min) and 100 rpm (268 mL/min). Concerning the electrode, it was varied its type, length and design, as previously mentioned. Lasty, regarding the solid-phase, different types were used, namely vascular grafts and native vessels, and it was varied the wall thickness (75 and 500 µm) and inner diameter (1.5 and 6 mm). Table 2 summarizes the parameters studied, along with their specification.

Moreover, triboelectric measurements were done after narrowing of the vascular graft, using a plastic clamp placed around the solid phase, resulting in a 30% narrowing.

Table 2. Summary of the Flu-TENGs' parameters varied for evaluation of triboelectric performance.

Flu-TENG component	Parameter	Specification
Fluid	Type	PBS, plasma and blood
	Flow rate	60 and 100 rpm
Electrode	Length	0.5, 1, 2, 4, 6, 8 and 10 cm
	Type	Silver, carbon and PEDOT:PSS conductive inks
	Design	Position on solid-phase and segmentation
Solid	Wall thickness	75 and 500 µm
	Inner diameter	1.5 and 6 mm
	Type	ePTFE and pHEMA/GO vascular grafts and umbilical cord artery

3.5. *In vitro* cytocompatibility assessment

In vitro cytocompatibility of silver, carbon and PEDOT:PSS conductive inks and copper tape was assessed towards human foreskin fibroblast cell line (HFF-1). HFF-1 was used in these cytocompatibility assays since fibroblasts are the cells present in tunica externa, the outer surface of the arteries, which will be in contact with electrodes, in the case of synthetic and native vessels. All tests were performed according to the ISO 10993, defined for the biological evaluation of medical devices, namely the samples preparation and reference materials (part 12) and *in vitro* cytotoxicity evaluation (part 5).

3.5.1. HFF-1 culture

HFF-1 were grown on Dulbecco's modified Eagle medium (DMEM, gibco® by life thechnologies™, ref: 21885-025) supplemented with 10% (v/v) fetal bovine serum (FBS, gibco®, ref: 10270-106) and 1% (v/v) Penicillin/Streptomycin (P/S) (complete growth medium) at 37 ºC, in a humidified atmosphere with 5% CO_2, in T75-flasks. Media were replaced every two days.

Once cells reached 90% confluence, cell passages were done by discarding the culture medium and rinsing with 5 mL of PBS, followed by the addition of 2 mL of trypsin and a 5 minute incubation at 37 ºC, to detach cells from the T75-flask. After centrifugation (1200 rpm, 5 minutes) and resuspension of the pellet, cell density was determined through counting on the Neubauer chamber, and the grown cells were then resuspended and seeded in new cell culture flasks with a density of 0.8×10^4 cells/cm^2, as recommended by the American Type Culture Collection (ATCC).

3.5.2. Extracts assay

ePTFE solid-phases coated with the different electrodes were sterilized with ethylene oxide (EO Gas Series 3+) at Centro Hospitalar de S. João. Samples' extracts were prepared by incubating the materials with the appropriate volume of cell culture medium, considering their area (6 cm^2 per mL of extract), according to ISO 10993-12, at 37 ºC with agitation (120 rpm) for 24 hours. Extracts of uncoated ePTFE and TC-PET coverslips were used as positive controls of cytocompatibility, and 1 mM of H_2O_2 as negative control. After the incubation, samples were removed from the medium, being obtained the extract (Figure 18 (A)).

HFF-1 were seeded in 96-well tissue culture plate with cell density of 10^4 cells/well. The cells were incubated for 24 hours at 37 ºC and 5% CO_2 humidified atmosphere. After the 24 hours, medium was removed and the extracts added, followed by another 24 hour incubation (Figure 18 (B)). After this, cell metabolic activity was evaluated by resazurin assay and cells morphology visualized by microscopy.

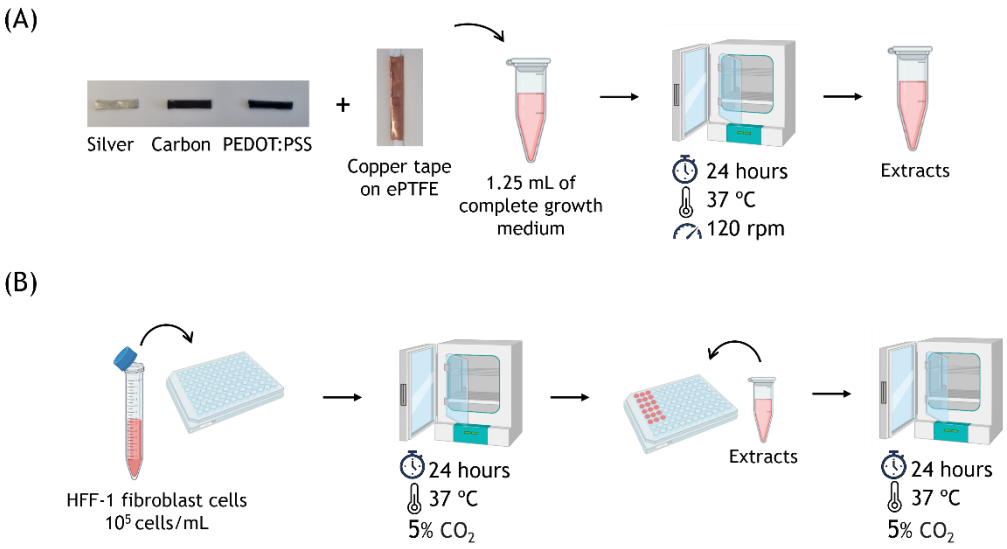

Figure 18. Schematics of extracts cytocompatibility assay. Extracts (A) preparation and (B) incubation with cells.

3.5.3. Direct contact assay

To evaluate the cytocompatibility of electrodes by direct contact, conductive inks were brush painted in glass coverslips and then dried for 10 minutes under 130 ºC, and copper tape was cut and glued to glass coverslips (Figure 19 (A)). All samples were sterilized with ethylene oxide (EO Gas Series 3+) at Centro Hospitalar de S. João.

For following cell seeding, samples were placed in 24-well suspension plates and HFF-1 seeded in density of $4.15x10^4$ cells/well (400 µL cell suspension/well), as recommended by ISO 10993-12, considering samples' area. TC-PET coverslips were used as positive controls and 1mM H_2O_2 as negative control. Electrode coated coverslips with just complete growth medium (without cells) were used as blanks, to evaluate its sterilization. Plates were then incubated

for 24 hours and 7 days, at 37 ºC and 5% CO_2 humidified atmosphere, during which the media was replace every two days, to allow for normal cell growth (Figure 19 (B)). After this, cell metabolic activity was evaluated by resazurin assay and cells morphology visualized by microscopy.

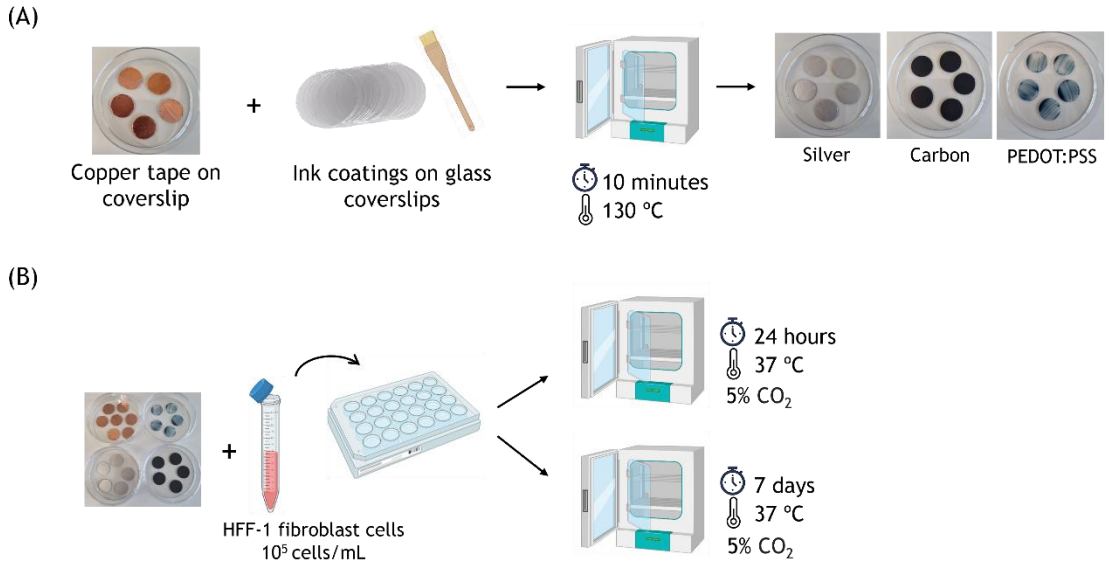

Figure 19. Schematics of direct contact cytocompatibility assay. (A) Sample preparation; (B) cell seeding.

3.5.4. Metabolic activity assessment

Cells' metabolic activity was evaluated by incubating them in 20% (v/v) resazurin in complete cell culture medium, for 4 hours at 37 ºC. The resulting solutions were transferred to a 96-well black/clear bottom plate (150 µL) to measure fluorescence (λ_{ex}: 530 nm and λ_{em}: 590 nm), resorting to Synergy ™ Mx (BioTek Instruments ®) microplate reader, and assess viable cells' metabolic activity in the presence of the testing samples comparing to positive control. Results are represented in (mean ± SD) relative fluorescence units (RFUs). Statistical analysis was done in GraphPad Prism software.

3.5.5. Cells morphology visualization

After metabolic activity assessment, the plate wells were rinsed with PBS and then cells were fixed with paraformaldehyde 4% (w/v) (PFA) for 20 minutes at room temperature. After this, PFA was removed, and the wells were washed. Fixed cells were permeabilized with Triton x-100 0.1 wt%, for 5 minutes, and incubated in the dark with Phalloidin (Alexa Fluor ™ 488, Invitrogen by Thermo Fisher Scientific ™, ref: A12379) 1:100, for 30 minutes, for fibroblasts' cytoskeletal actin staining, and then with 3 µg/mL 4',6-diamidino-2-phenylindole (DAPI, Merck, ref: 10236276001), a marker for nucleic acids in the nuclei, for 15 minutes.

After staining, the samples were observed in the inverted fluorescence microscope (Zeiss Axiovert 200M). Acquired images were processed using ImageJ (Fiji) software.

Chapter 4: Results and Discussion

4.1. Electrode assembly and stability

The potential use of three different conductive inks (silver, carbon and PEDOT:PSS) as electrodes of the Flu-TENG was assessed by assembling them by brush painting in the three solid phases (ePTFE and pHEMA/GO vascular grafts and umbilical cord artery). Furthermore, copper tape was also tested. Figure 20 shows the different solid-phase materials uncoated and coated with conductive inks.

Figure 20. Solid-phases (ePTFE and pHEMA/GO vascular grafts and umbilical cord artery) uncoated and portions coated with silver (grey ink), carbon (black ink) and PEDOT:PSS (dark blue ink) electrodes (from left to right).

Overall, it was achieved an effective coating of all solid-phases with the tested conductive inks, with exception of carbon ink in pHEMA/GO, that seems to be detaching from the surface. Furthermore, copper tape was also tested as electrode. However, its application onto the solid-phases resulted in its strangling, hampering the normal flow of the fluid inside, consequently affecting the Flu-TENG's proper functioning (Figure A1 Annexes).

Considering that when implanted in the body these electrodes will be in contact with body fluids, their stability in the presence of PBS was assessed. The leachables obtained from the washing test of ink coated ePTFE, pHEMA/GO and artery, and their respective optical density spectrum, are represented in Figure 21.

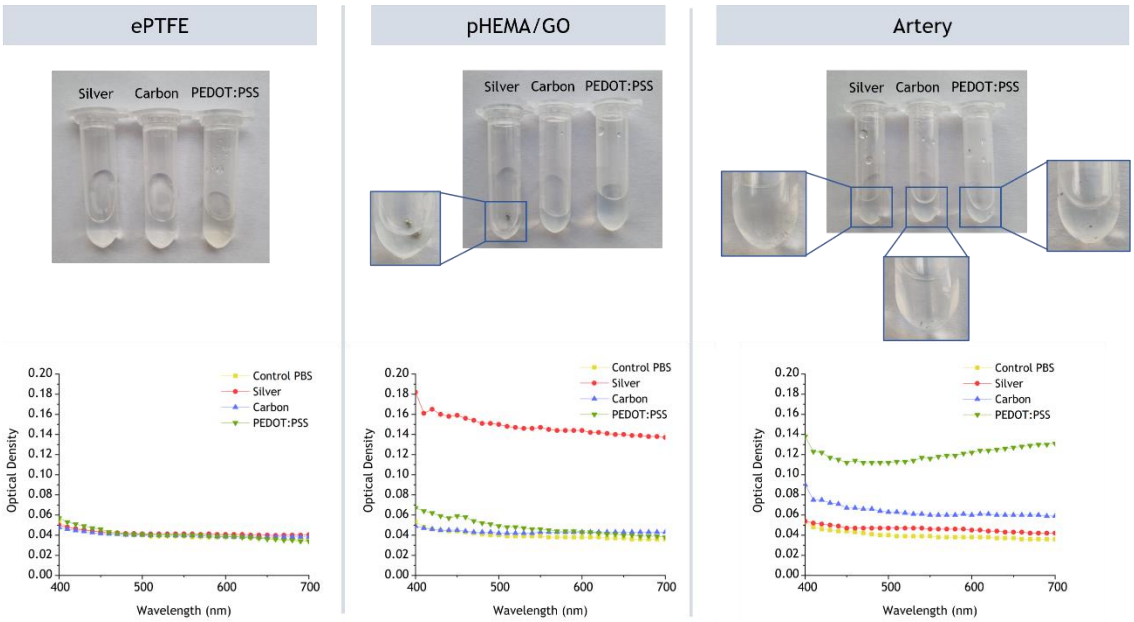

Figure 21. Photography and optical density spectra of leachables resulting from washing test of ePTFE, pHEMA/GO and artery coated with silver, carbon and PEDOT:PSS inks. PBS spectrum was used as control.

From the visual inspection of the resulting leachables of ePTFE coated samples, no aggregates of the inks were identified. Additionally, similar leachable optical density spectra were obtained for silver, carbon and PEDOT:PSS coatings when compared to control PBS, confirming that there was no release of these ink's particles into the PBS solution during the washing test. Regarding the stability on pHEMA/GO, there were no significant visible changes in the PBS washing solution for the case of carbon and PEDOT:PSS coated samples. However, it is possible to see an aggregate of silver ink, meaning that a there was some release of the coating into the washing solution. This is corroborated by the optical density spectrum obtained for the leachable of the silver coated sample, which is significantly different from the others, most importantly from the control PBS. Lastly, concerning the artery solid-phase, small particles can be visualized in the leachables. Optical density spectra of the leachables confirm the release of a part of the coating into the washing solution, altering its optical properties. Although, it must be emphasized that arteries cannot be submitted to the 130 ºC, otherwise they would dry out and become unusable, and that is a very important step for the drying of the inks and improvement of their stability.

Moreover, to further analyze the assembly and stability of the inks' coatings on the solid-phases, SEM images of the coated samples were collected before and after washing for the vascular graft solid-phases. For the case of the artery, as it is known that coating stability is compromised, the topography was observed only before performance of any washing tests to the samples. SEM images are represented in Figure 22.

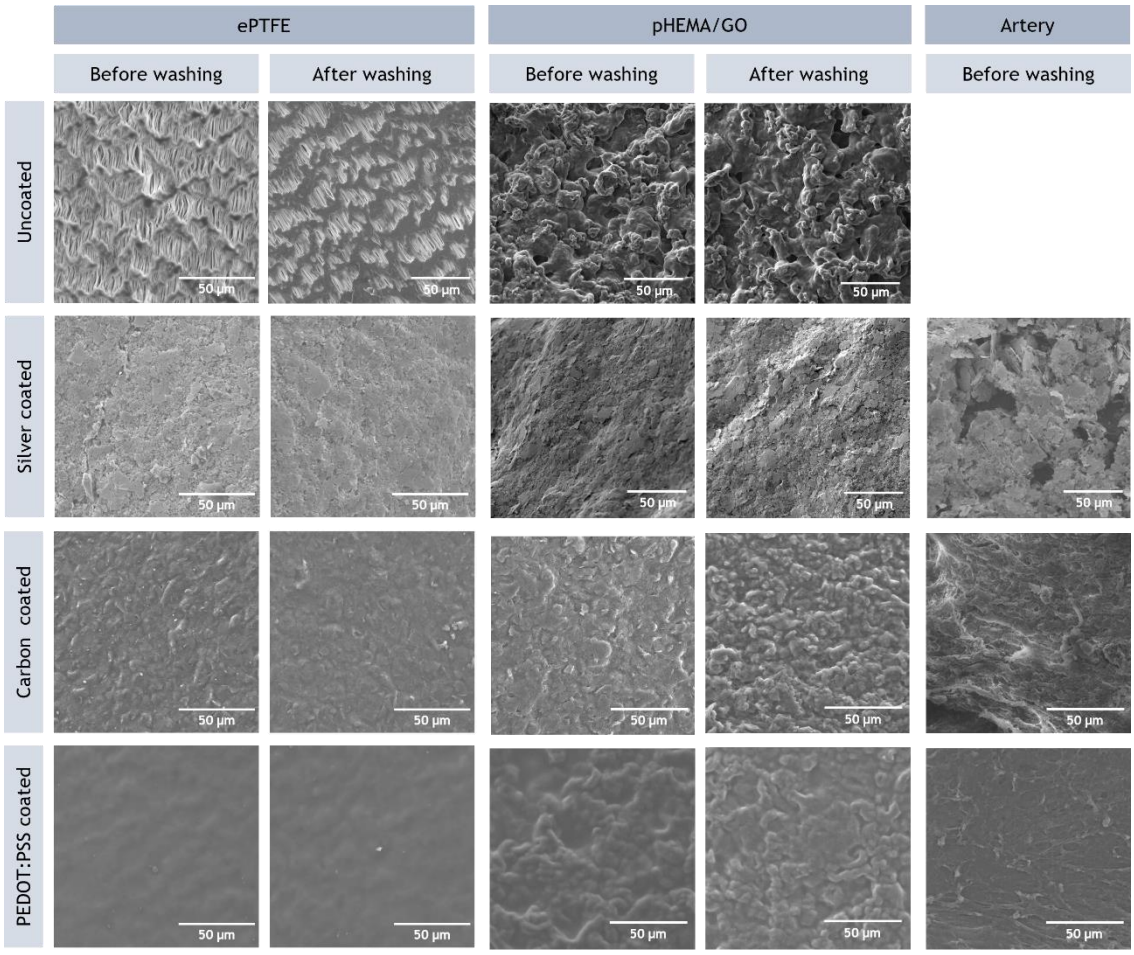

Figure 22. SEM analysis of the outer surfaces of the coated and uncoated ePTFE and pHEMA/GO vascular grafts samples before and after the washing tests, and of coated artery samples before washing tests. Each row represents a different conductive ink coating. Scale bar: 50 µm. Magnification 2000x.

Comparing the topography of the outer surface of the uncoated and coated ePTFE samples, it is possible to see that there was an adherence of the inks since the topography changed and is different for the three inks. Moreover, after washing, all samples preserved that coating, as no changes are observed. This confirms the stability of the inks assemble on the ePTFE solid-phase.

Analyzing the images obtained for pHEMA/GO samples, it is seen that a silver coating adheres onto this vascular graft, remaining fairly similar after the washing test, meaning that the release of a small aggregate into the washing solution is not significant for the overall stability of the coating. However, topography after coating with carbon and PEDOT:PSS inks is closer to the uncoated samples, from which can be inferred that a very thin layer stays on the sample but does not completely change topography. It is important to note that pHEMA/Go vascular graft is characterized as non-fouling [65], which represents an adversity for any long-term coating stability.

Finally, from the observation of the outer surface of artery samples, it can be concluded that the electrode coatings are present on the arteries, as the characteristic collagen fibers are covered.

Concerning the infiltration of the inks into the luminal surface of the solid-phases, it was observed that the inner surfaces of the ePTFE coated samples maintain their profile, showing that it does not occur. For the pHEMA/GO and artery solid-phases, there seems to have been a slight alternation of the topography after coating with carbon and PEDOT:PSS inks, alerting for the possibility of ink penetration having occurred (Figure A2 Annexes).

4.2. Electrical outputs of Flu-TENG

Following the assemble of the electrodes on the solid-phases, these samples were connected to the peristaltic pump set up to be perfused with different fluids to achieve the proposed Flu-TENGs. Flu-TENGs' triboelectric performance was studied varying different parameters associated with the fluid-phase, the electrode and the solid-phase, to understand how they can individually influence the generated energy. Regarding the fluid-phase, it was evaluated different types and flow rates. As for the electrode, it was studied the influence of its type, length and design variation. Lastly, concerning the solid material, it was also varied its type, as well as respective wall thickness and inner diameter.

4.2.1. Influence of fluid-phase

4.2.1.1. Fluid type

To study the influence of different fluids characteristics/composition on the generated electric energy, the voltage and current outputs acquired using PBS, plasma and blood as the fluid-phases (Figure 23) were compared, varying external resistor and capacitors (Figure 24). For all these tests, flow rate was maintained at 161 mL/min (60 rpm) and it was used ePTFE as solid-phase (1.5 mm ID and 100 µm WT) coated with a silver electrode (2 cm length).

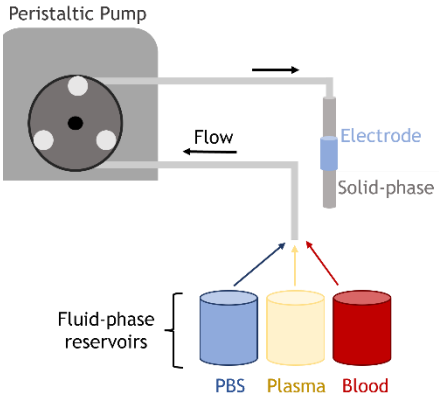

Figure 23. Representation of the set-up varying the type of fluid-phase (PBS, plasma and blood).

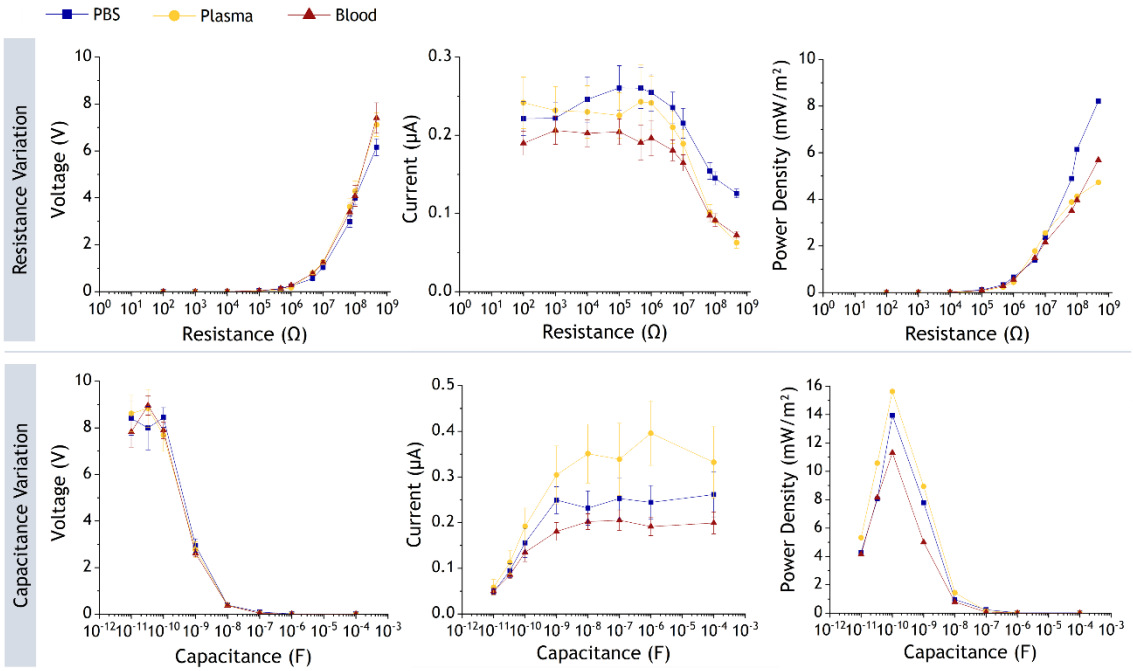

Figure 24. Triboelectric outputs, in voltage, current and resulting power density, for resistor and capacitor's variation, for assessing the influence of the fluid-phase type. Comparison between PBS, plasma and blood. Flow rate used was 161 mL/min (60 rpm) and solid-phase consisted of ePTFE (1.5 mm ID and 100 μm WT) with 2 cm length silver electrode.

By definition, for low load resistance, where the output is closer to the short circuit conditions, voltage tends to zero while there is maximum transfer charge and the current exhibits the maximum value (I_{sc}). For high load resistance, where the output is closer to the open circuit condition, voltage tends to saturate (V_{oc}) and current goes to zero. In between these, voltage increases while current drops [71]. The opposite behavior is expected when varying the external capacitance of the system.

Figure 24 shows that for our set-up it is not verified a saturation of the voltage output, reaching a maximum value in which it settles (V_{oc}), when using the highest resistors or smallest capacitors. From this, it is assumed that the circuit of the set-up, namely the range of resistors and capacitors available, does not allow to evaluate the maximum triboelectric output that is able to be generated with the proposed Flu-TENG, from which is concluded that these outputs could be even higher.

Moreover, there is not a consistent relation between the outputs obtained from resistor and capacitor's variation as, for example, in resistance variation, there is a tendency of higher power density when using PBS whereas in the case of capacitance variation, overall outputs are higher with plasma.

As it is not possible to keep increasing resistance to try and reach saturation, since there will be the limitation of the equipment's internal resistance, it was developed a measuring method for further evaluation of the Flu-TENG's electric performance, to enable accurate conclusions regarding the influence of the different parameters in the obtained outputs. This new measuring method consists of capacitators charging. While charging,

capacitors reach a maximum voltage, meaning that they are saturated and so that there is an equilibrium between the energy being generated (instantaneous energy output) and the energy that is being accumulated. Therefore, it was hypothesized that the maximum voltage reached by the capacitor is equal to the voltage supplied by the source. To test this, AC signals of 1 Hz frequency, 1 mV offset, 1% duty cycle and with voltage of 1, 2.5, 5 and 10 V were generated, resorting to a BK Precision® function generator, to mimic the frequency of the alternated current obtained with Flu-TENG. Then, the signal was rectified (AC/DC conversion), with a bridge rectifier, and 100 nF, 1μF and 10 μF capacitors charged. The generated signals as well as resulting capacitors charging were measured with the electrometer (Figure A3 Annexes). This part of the study was performed with Carolina Silva (Master student in Physics) from IFIMUP.

In Table 3 is represented the peak voltage of the generated signals as well as capacitor saturation, along with the corresponding difference between these.

Table 3. Outputs regarding capacitor charging with generated signals.

Generated signal (V)	Generated signal rectified (V)	Capacitor saturation (V)	Difference between generated signal and capacitor saturation (%)
1	0.98	0.73	27.2
2.5	2.43	2.14	14.3
5	4.81	4.53	9.4
10	9.81	9.47	5.3

From the obtained results, it is possible to observe that when the generated signals pass through the bridge rectifier for the AC/DC conversion, there is a characteristic voltage drop that slightly reduces the peak voltage of the resulting signal, which is then used to charge the capacitor. Despite, Table 3 shows that the peak of the original generated signal is similar to the voltage obtained when the capacitors are saturated. The highest difference (27.2%) is observed when the lowest peak voltage signal is generated (1 V), being around 5% for the highest tested signal (10 V). Hence, this associated error notoriously decreases as the output voltage value increases. Furthermore, it is important to note that the voltage at capacitor saturation is always lower than the generated signal, used to charge it through the bridge rectifier, which means that even though by using this measuring set-up we are closer to the output generated by Flu-TENG (V_{out}), we will still underestimate it.

Therefore, for all tested parameters, apart from the conventional resistor and capacitor's variation measuring method, different capacitors were charged for 10 minutes to conclude on the maximum voltage outputs generated by the Flu-TENG. The first method provides information on instantaneous electric outputs that can be acquired resorting to a specific external resistor or capacitor, while the second allows for the assessment of the energy that can be accumulated in the capacitors.

The capacitor charging curves obtained for the three fluid-phase variations are represented in Figure 25.

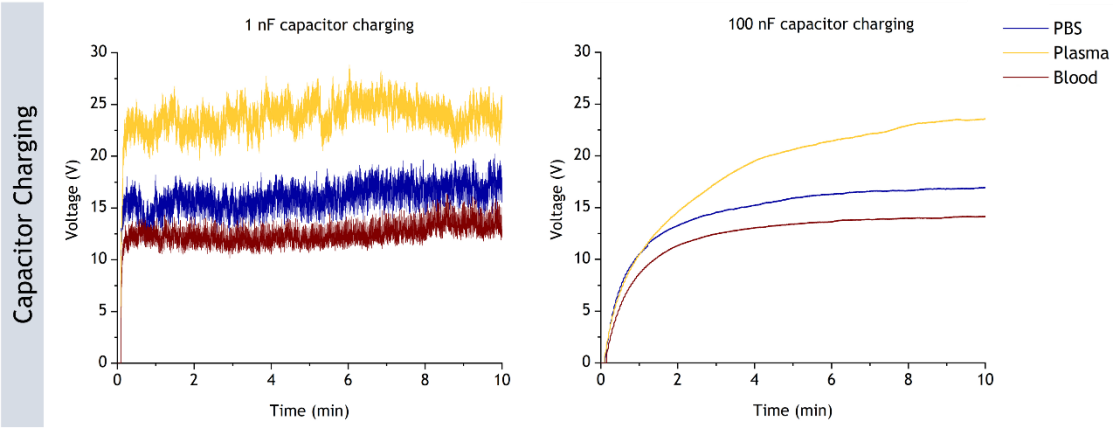

Figure 25. Capacitor charging comparison for PBS, plasma and blood as the fluid-phase.

From the saturation of capacitors, it is possible to observe that V_{out} is higher when using plasma as fluid-phase, being achieved 23.6 V, followed by PBS, 17.3 V, and blood, 14.2 V. These results show that fluid's properties and its composition will have a significant impact on the triboelectric output of a Flu-TENG, since highest voltage outputs were achieved using plasma and lowest with blood, even though plasma represents 50% of blood's total volume [72]. These differences in the outputs could be explained by the presence of blood cells or by their distinctive rheological properties, behaving differently in streaming flow.

Considering the real application of herein studied Flu-TENG, the fluid-phase will always be human blood. However, due to the scarcity of blood donors and the associated ethical concerns, PBS was used as a reference fluid for the further experiments, since its electric output is closer to the obtained using blood.

4.2.1.2. Fluid flow rate

The influence of two fluid flow rates, 161 mL/min and 268 mL/min, was assessed by comparing the triboelectric outputs acquired using ePTFE as solid-phase (6 mm ID and 152 µm WT), coated with silver electrode (2 cm length), and PBS as fluid-phase. The flow rates correspond to angular velocity of 60 and 100 rpm, respectively, which matches to the number of pulses per minute of the fluid. These were chosen accordingly to the limits of the heart rate range of normal resting phase of an adult (60 to 100 beats per minute, defined by the American Heart Association [73]). The obtained results are summarized in Figure 26.

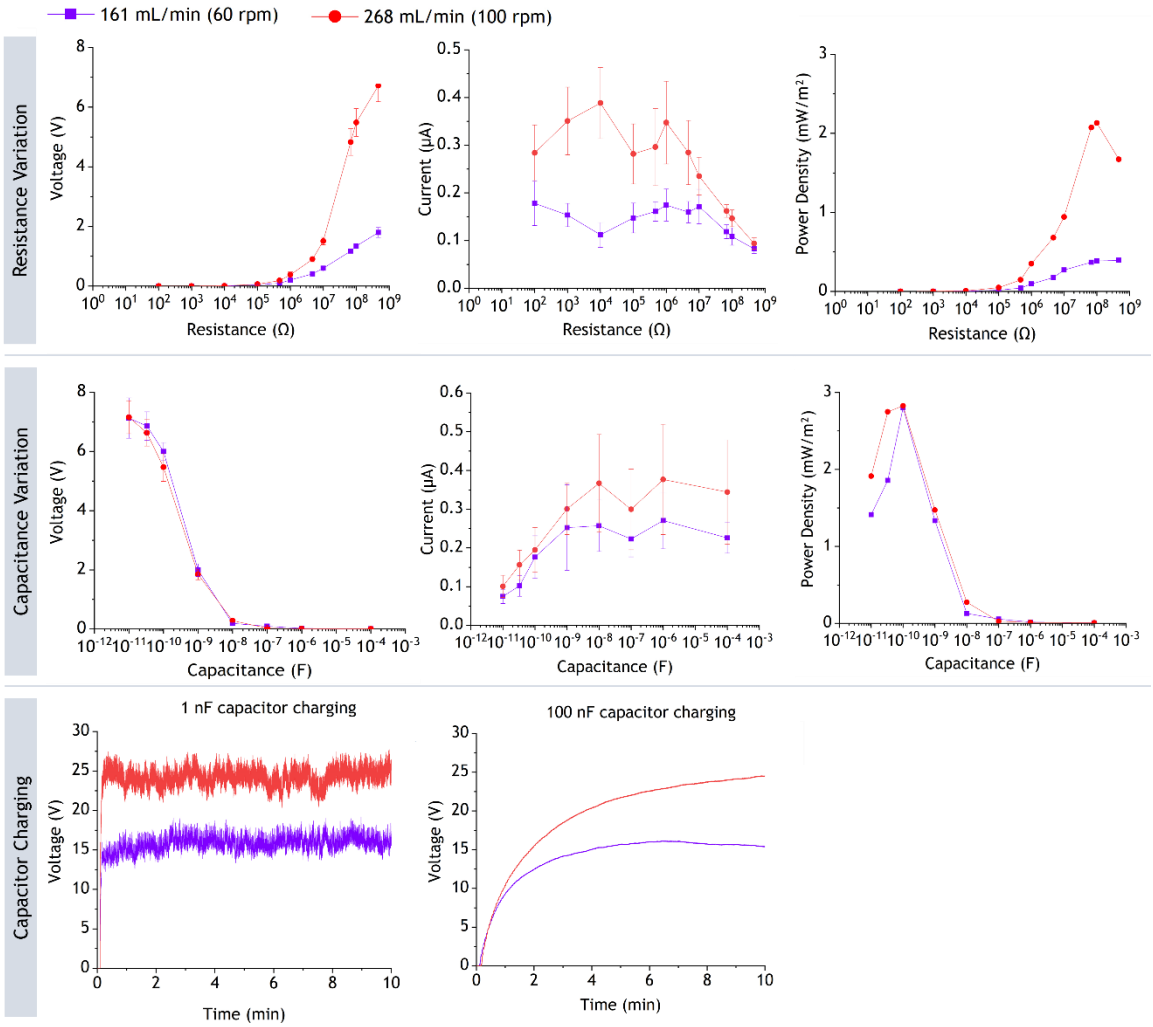

Figure 26. Triboelectric outputs, in voltage, current and resulting power density, for resistor and capacitor's variation, and capacitor charging curves, for assessing the influence of the fluid-phase's flow rate. Comparison between PBS with 161 and 268 mL/min flow rate (60 and 100 rpm, respectively). Solid-phase consisted of ePTFE (6 mm ID and 152 μm WT) with 2 cm length silver electrode.

Figure 26 shows that for all measuring set-ups, it is possible to observe a clear increase in the achieved outputs, both in terms of voltage and current, with the increase of the flow rate. For an external resistance of 100 MΩ it was obtained the maximum power density of 2.1 mW/m^2. Evaluating the saturation of the capacitor, it is verified that an increase in flow rate of just about 100 mL/min (from 161 to 268 mL/min) leads to a V_{out} approximately 10 V higher, being possible to achieve 25 V.

Briefly, blood flow rate is highly dependent on the type of vessel and its location on the body, since it varies directly with difference in pressure (ΔP) and inversely to vasculature resistance (R), which consists of a resistance that must be overcome so as to force the flow of blood along the circulatory system. Relating these variables, flow rate (Q) can be defined by the *Hagen-Poiseuille* equation, that can be further applied for other types of fluids, as $Q = \frac{\Delta P}{R} = \frac{\pi \Delta P r^4}{8\eta\lambda}$, where r is radius of the vessel, η the blood's viscosity and λ the vessels length. [74]. The same can be applied for an implanted vascular graft. Considering that Flu-TENG is sensible to flow rate variations, it will vary with location and also, pathological conditions

that affect it, such as blood pressure and viscosity alterations, could affect the obtained triboelectric outputs. As such, these factors should be considered during the Flu-TENG's design, envisioning its final application.

4.2.2. Influence of electrode

4.2.2.1. Electrode length

To study the influence of electrode's length on the triboelectric outputs, silver electrodes with different lengths of 0.5, 1, 2, 4, 6, 8 and 10 cm were painted in ePTFE (1.5 mm ID and 100 µm WT) from the support Venflon™ end down (Figure 27). PBS with a flow rate of 161 mL/min (60 rpm) was used as fluid-phase.

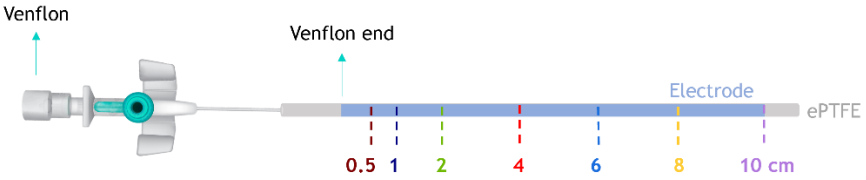

Figure 27. Representation of ePTFE solid-phase (grey) with silver electrode (blue) varying in lengths from 0.5 to 10 cm.

In Figure 28 are represented the obtained triboelectric outputs in voltage, current and resulting power density. In Figure A4 (Annexes) are represented these results normalized by the electrodes area.

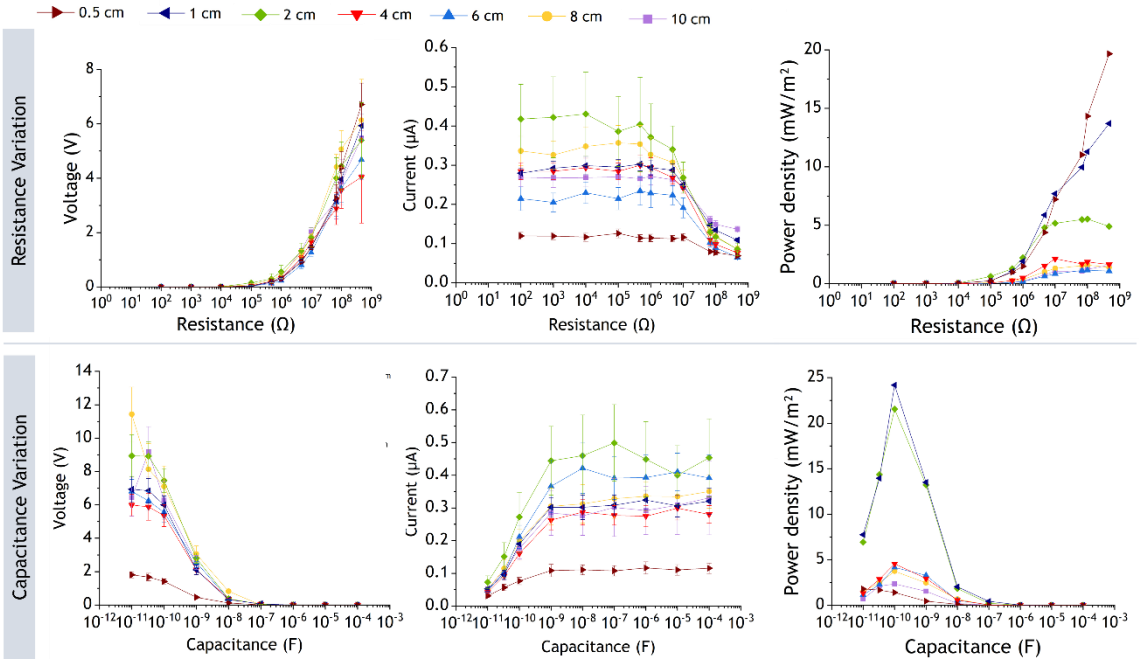

Figure 28. Triboelectric outputs, in voltage, current and resulting power density, for resistor and capacitor's variation for assessing the influence of electrode's length. Comparison between silver conductive ink electrode of 0.5, 1, 2, 4, 6, 8 and 10 cm length. Flu-TENG consisted of ePTFE solid-phase (1.5 mm ID and 100 µm WT) with PBS fluid-phase (161 mL/min, 60 rpm).

Similarly to the results obtained for previous tests, for the range of resistors and capacitors tested, there is not a consistent trend in the behavior of the Flu-TENG using the different electrode lengths. Considering these results, it seems that the electric output is independent of the electrodes length. Normalizing by the electrode's area (Figure A4 Annexes), higher outputs, in terms of voltage and current and, consequently, in power density, per area unit (cm^2) are achieved with the smaller length electrodes. When varying external resistance, the highest power density, 19.7 mW/cm^2, was observed when using the highest resistor of 470 MΩ with the 0.5 cm length electrode, for which it was obtained the corresponding outputs in voltage and current of 28.5 V/cm^2 and 0.29 $\mu A/cm^2$, respectively. Varying capacitance, and resorting to the 100 pF capacitor, 12.7 V/cm^2, 0.29 $\mu A/cm^2$ and 24.2 mW/cm^2 are achieved, but with the electrode having a length of 1 cm.

However, analyzing the charging curves obtained for the 1 nF capacitor, it is possible to observe that V_{out} of Flu-TENG varies from 6.7 V to 47.6 V when passing from a 0.5 cm to 10 cm electrode length. This represents an increase in efficacy of around 85%. Moreover, it is noted a linear relation between electrode length and generated voltage outputs, as shown in Figure 29.

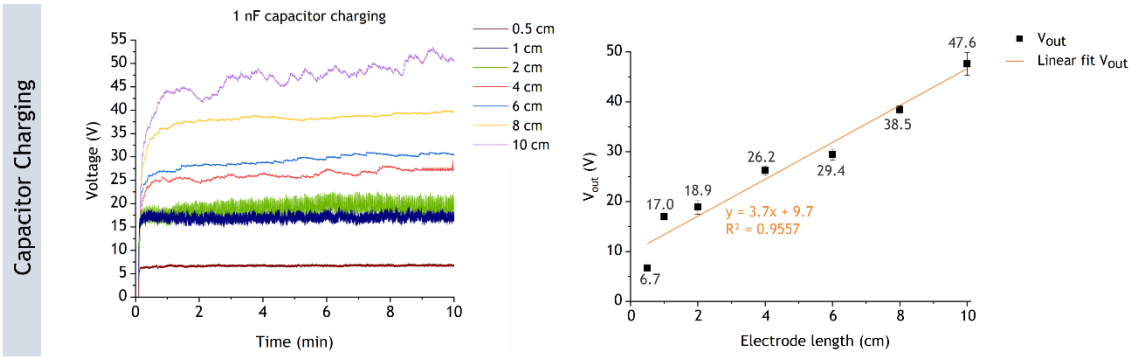

Figure 29. Capacitor charging with the electric energy acquired with silver electrode length variation from 0.5 to 10 cm. Representation of charging curves for 1 nF capacitor as well as of the relation between average output generated by the Flu-TENG (V_{out}), obtained by the saturation of the same 1 nF capacitor, and electrode's length, with its linear fit. Flu-TENG consisted of ePTFE solid-phase (1.5 mm ID and 100 µm WT) with PBS fluid-phase (161 mL/min, 60 rpm).

For practical applications, higher value capacitors tend to be more interesting for their capability to store more usable energy. However, these take longer to charge and also go through a self-discharge, meaning that it is not achieved saturation. Nevertheless, by allowing a 100 µF capacitor to charge for 2 hours, using the same 10 cm length silver electrode, it was possible to accumulate approximately 1.5 V of energy (Figure 30).

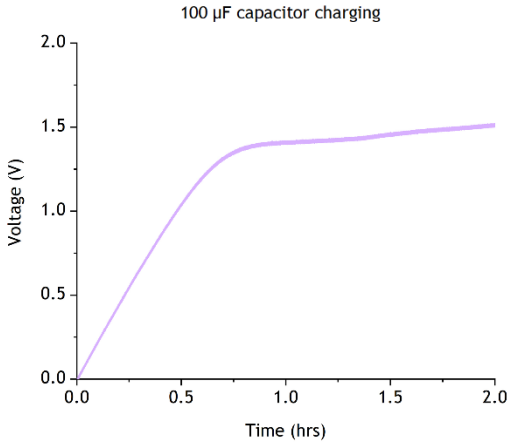

Figure 30. Charging of 100 µF capacitor for 2 hours, using a 10 cm length silver electrode. Flu-TENG consisted of ePTFE solid-phase (1.5 mm ID and 100 µm WT) with PBS fluid-phase (161 mL/min, 60 rpm).

Here, it is emphasized that, as seen above in section 4.2.1.1., the outputs acquired by varying resistance and capacitance within the available range are not representative of the behavior of the Flu-TENG, as it might still be far from the saturation point and subjected to fluctuations.

4.2.2.2. Electrode type

Silver, carbon and PEDOT:PSS conductive ink electrodes were compared, under the same conditions, namely 2 cm length and use on a Flu-TENG consisting of ePTFE solid-phase (1.5 mm ID and 100 µm WT) (Figure 31) with PBS fluid-phase (161 mL/min, 60 rpm). Voltage and current outputs, as well as capacitor charging results are represented in Figure 32.

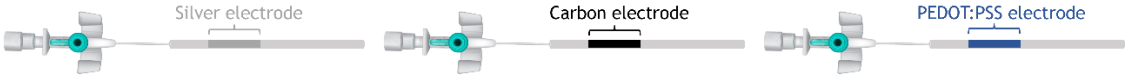

Figure 31. Representation of ePTFE solid-phase (grey) with varying electrode type (silver, carbon and PEDOT:PSS conductive inks).

All electrodes allow the acquisition of the generated charge. Nonetheless, from the charging comparison curves, it is depicted that silver is more conductive, because of a quicker capacitor charging and corresponding saturation voltage. For the conditions tested, and accordingly to the saturation of the capacitors, V_{out} with silver is of approximately 17.3 V, with carbon 12.9 V and using PEDOT:PSS it is 10.4 V. When comparing to the output achieved with the silver electrode, a decrease in energy acquisition efficacy can be determined as 25% for carbon and 40% for PEDOT:PSS.

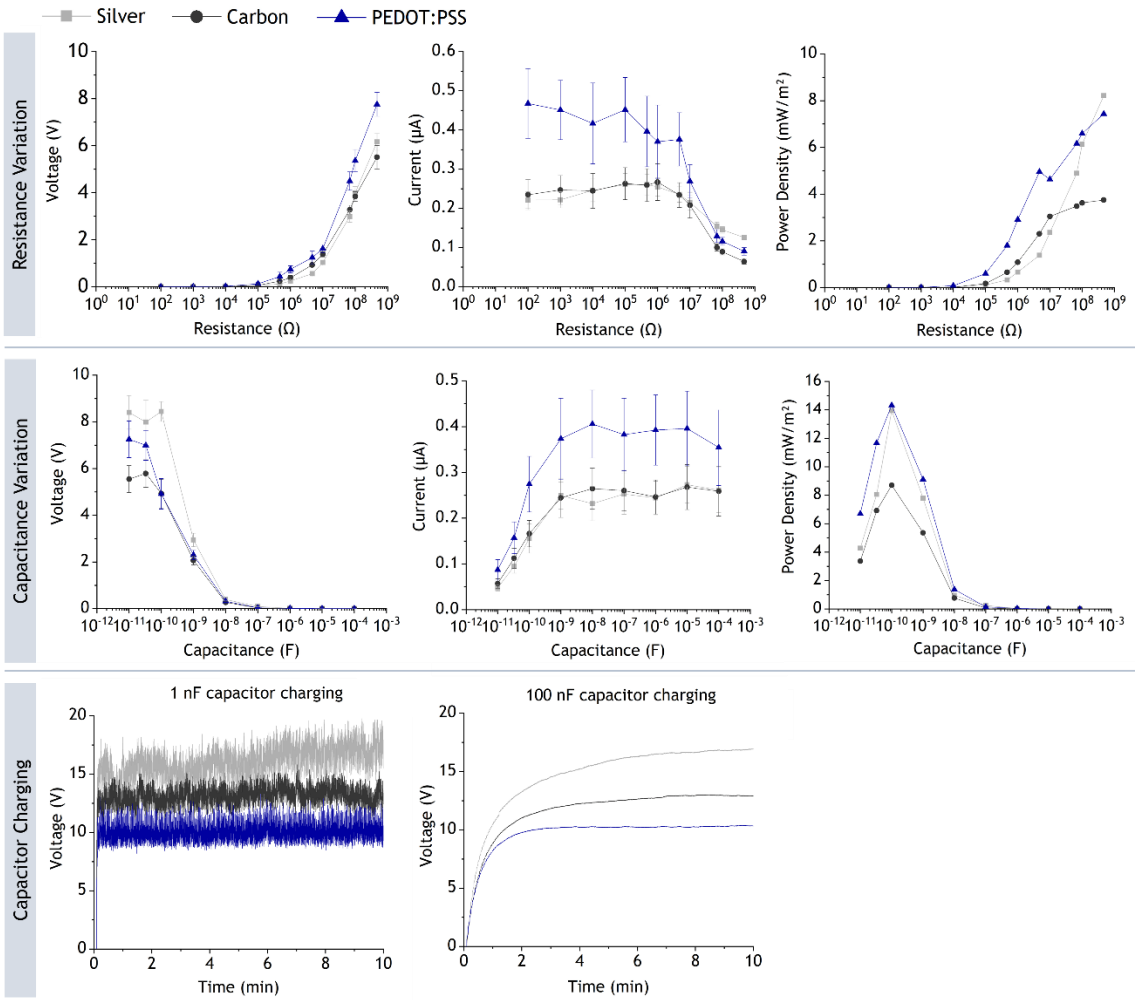

Figure 32. Triboelectric outputs, in voltage, current and resulting power density, for resistor and capacitor's variation, and capacitor charging curves, for assessing the influence of the electrode type. Comparison between silver, carbon and PEDOT:PSS 2 cm length electrodes. Flu-TENG consisted of ePTFE solid-phase (1.5 mm ID and 100 μm WT) with PBS fluid-phase (161 mL/min, 60 rpm).

These results show that the electrode used has a high impact on the outcome of the whole Flu-TENG, and so its choice is an important step when assembling a device for a specific application. However, it must be emphasized that this efficiency results from the combination of many factors, namely conductive properties as well as electrode's interaction with the specific solid-phase, as assessed previously through its stability. In section 4.1. it was shown that all electrodes are stable when assembled onto ePTFE solid-phase.

4.2.2.3. Design

Results described in the previous sections have been obtained using ePTFE samples in which the electrodes are painted from its proximal end (closer to the support) down, as represented in Figure 33 (A). To evaluate the influence of the electrode's position on the solid-phase, namely its proximity to the beginning of the solid-phase, on the energy acquired from the Flu-TENG, the same electrode was painted 3.5 cm away from the proximal end (Figure 33 (B)). For testing of both configurations, the non-varying parameters of Flu-TENG

consisted of ePTFE solid-phase (1.5 mm ID and 100 µm WT) with PBS fluid-phase (161 mL/min, 60 rpm) and 2 cm length silver electrode. The configurations output comparison curves are represented in Figure 34.

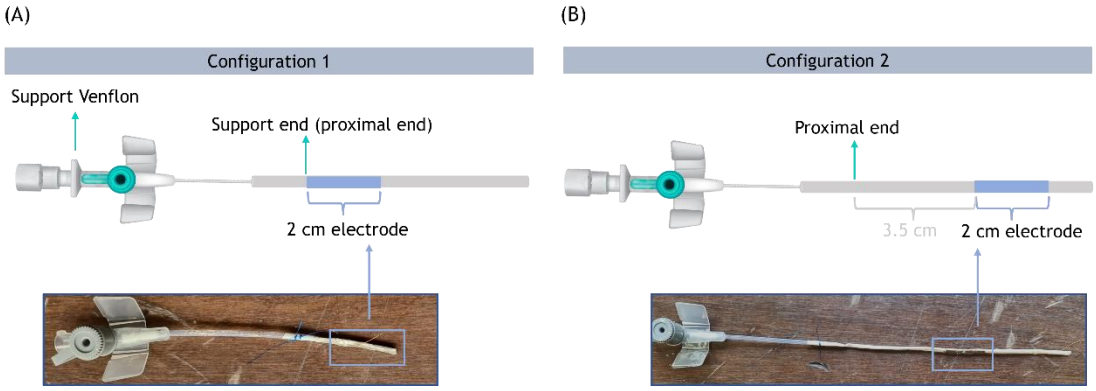

Figure 33. Representation of the different configurations tested, regarding the position of the electrode (blue) on the solid-phase (grey), in relation to the support end. (A) Configuration 1 – electrode placed by the proximal end of the sample; (B) Configuration 2 – electrode placed 3.5 cm away from the proximal end.

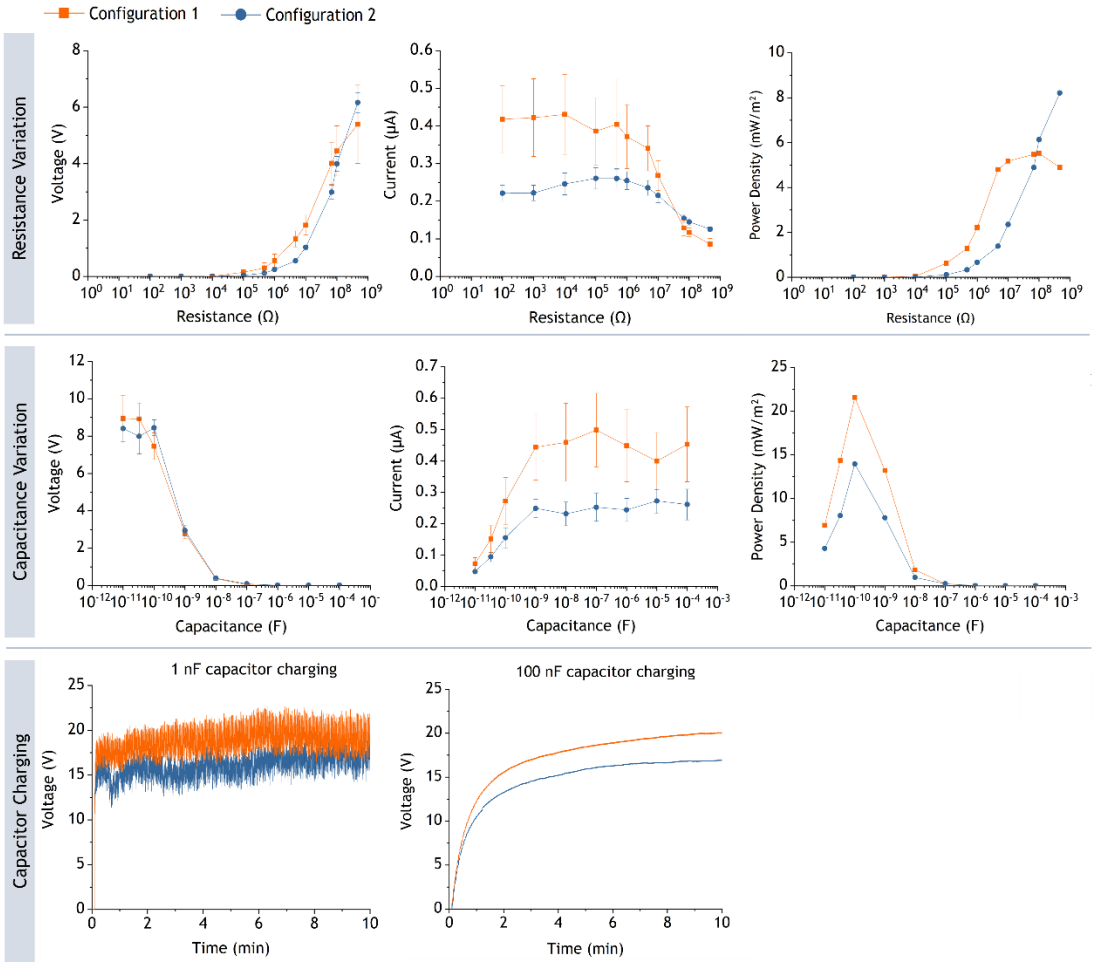

Figure 34. Triboelectric outputs, in voltage, current and resulting power density, for resistor and capacitor's variation, and capacitor charging curves, for comparison of two possible configurations, regarding the electrode positioning on the solid phase. For both configurations tested, Flu-TENG consisted of ePTFE solid-phase (1.5 mm ID and 100 µm WT) with PBS fluid-phase (161 mL/min, 60 rpm) and 2 cm length silver electrode.

Overall, configuration 1, where the electrode is near to the proximal end, leads to higher electric outputs. From the saturation of capacitors, it is obtained a difference in V_{out} of 3.3 V when going from configuration 1 (20.3 V_{out}) to 2 (17.0 V_{out}). This means that ePTFE is a resistive biomaterial and so there is an added electron resistance in configuration 2, as a result of the fluid flowing across a larger ePTFE area before reaching the electrode coated portion that slightly reduces the output that can be generated at that point. Thus, it seems that the output decreases as the electrode's distance to the solid-phase's proximal end increases. Therefore, in order to generate and acquire the utmost energy, the electrode should be assembled onto the solid-phase closer to its proximal end, to avoid material resistance issues as much as possible.

To try and increase the output in current, another variation of the design was tested, which combines more than one segment of electrodes in parallel. By combining the outputs of each electrode in this configuration, it would be expected for the voltage provided to the load to be equal to the voltage generated by just one of the sources, while the load current would be the result of the sum of each supply output current. The equivalent circuit of this configuration is represented in Figure 35, in which each energy source represents an electrode segment (*n*) and V_n and i_n its corresponding voltage and current outputs, respectively.

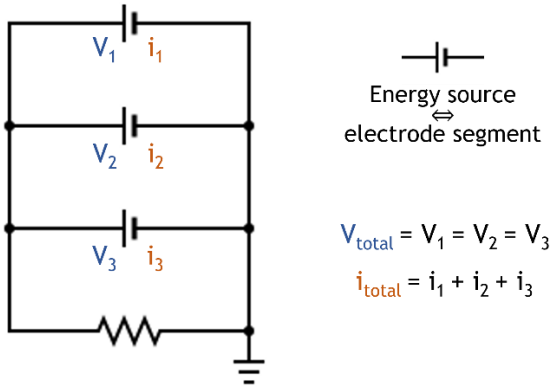

Figure 35. Equivalent circuit of three energy sources in parallel.

For the assembly of Flu-TENG, 2 cm segments of silver electrode were painted onto an ePTFE solid-phase (6 mm ID and 152 µm WT), with equal spacing of 1.3 cm between them, from the proximal end down (Figure 36). Conductive copper wires were connected to each electrode segment and then joined at the other extremity to get the common terminal in which it is obtained the result of the combination of the electrodes in parallel, and so that is connected to the acquisition system. The triboelectric output resulting from using 2 and 3 segments in parallel was acquired and then compared to the obtained with the standard configuration of only 1 electrode. All tests were done resorting to the PBS reference fluid-phase (161 mL/min, 60 rpm).

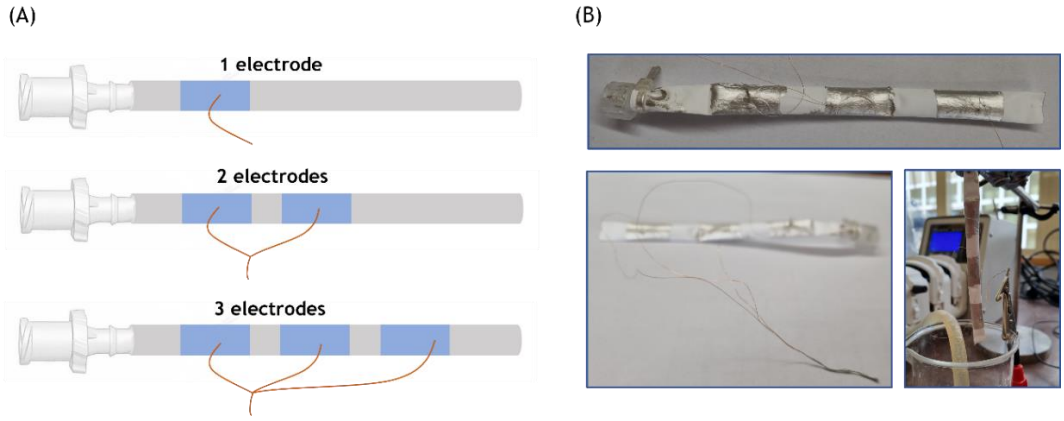

Figure 36. Representation of electrodes assembled in parallel. (A) Representation of the solid-phase (grey) with the electrodes (blue) in parallel for assessment of the influence of the number of electrodes; (B) Exemplificative sample used, consisting of an ePTFE solid-phase with 3 electrode segments in parallel.

The comparison curves of the triboelectric outputs using just 1 electrode or 2 or 3 electrodes in parallel are represented in Figure 37.

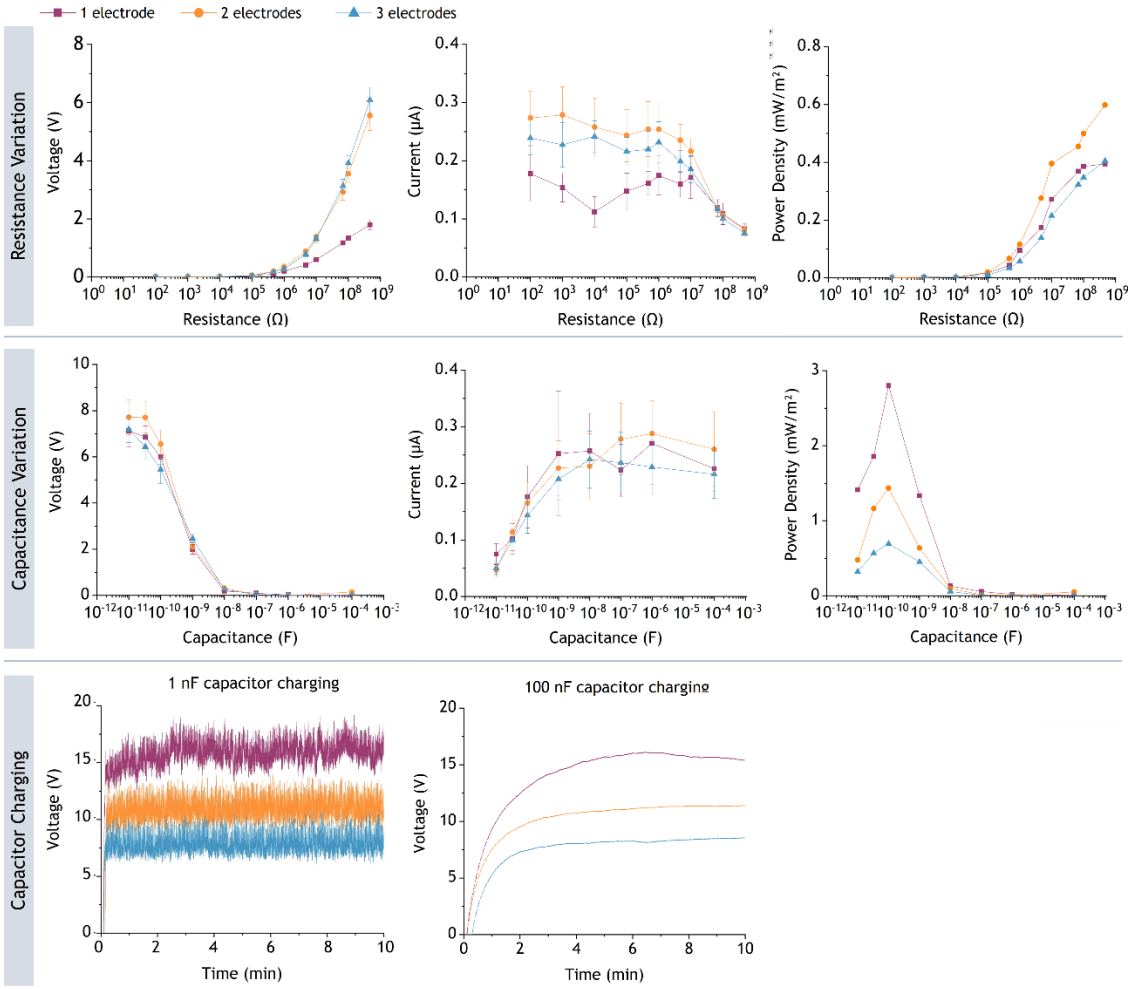

Figure 37. Triboelectric outputs, in voltage, current and resulting power density, for resistor and capacitor's variation, and capacitor charging curves, for comparison of 1 electrode and 2 and 3 electrodes in parallel. Flu-TENG consisted of ePTFE solid-phase (6 mm ID and 152 μm WT) with PBS fluid-phase (161 mL/min, 60 rpm) and 2 cm length silver electrode segments with 1.3 cm spacing.

Analyzing the saturation of the capacitors, it is observed that a V_{out} of 15.3 V is obtained when using just 1 electrode and that the output is reduced when 2 electrodes are combined (11.5 V). Adding a third electrode in parallel, the output is further decreased (8.7 V). Besides, a quicker charging of the capacitors can be observed when using only 1 electrode when compared to having 2 and 3 electrodes in parallel, meaning that there is a reduction in the current supply when the electrodes are combined.

As mentioned above, by placing energy sources in parallel, it would be expected to increase the total current supply. However, if the sources are not well matched, meaning that the different sources provide different voltage value outputs, the resulting circuit may not increase the power supply. As previously seen from the study on the influence of the electrode positioning on the solid-phase, it is expected that the first electrode provides the highest output and that it progressively decreases to the second and then to the third electrode due to an increased distance to the solid-phase's proximal end. Therefore, the different individual sources are providing different voltage outputs and, in that case, when combined in parallel, the current supply should be mainly done by the source with the highest voltage, which is always the first electrode. Nevertheless, as a negative effect on the total output is observed when the second and third electrodes are combined to the first in parallel, it can be inferred that the effect of their position is impairing the overall performance of the first one. To further explore this influence, the electrodes were combined in parallel in pairs, as schematized in Figure 38.

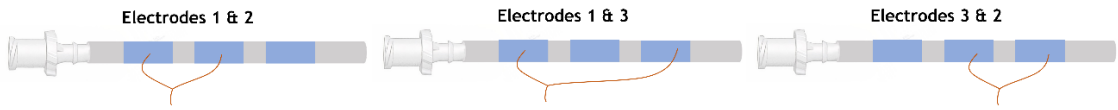

Figure 38. Representation of the solid-phase (grey) with two electrodes (blue) in parallel for the assessment of the influence of the electrodes position on the solid-phase on the outcome of this design.

The comparison curves of the triboelectric outputs using electrode pairs in parallel, varying their combination in terms of their positioning along the solid-phase, are represented in Figure 39.

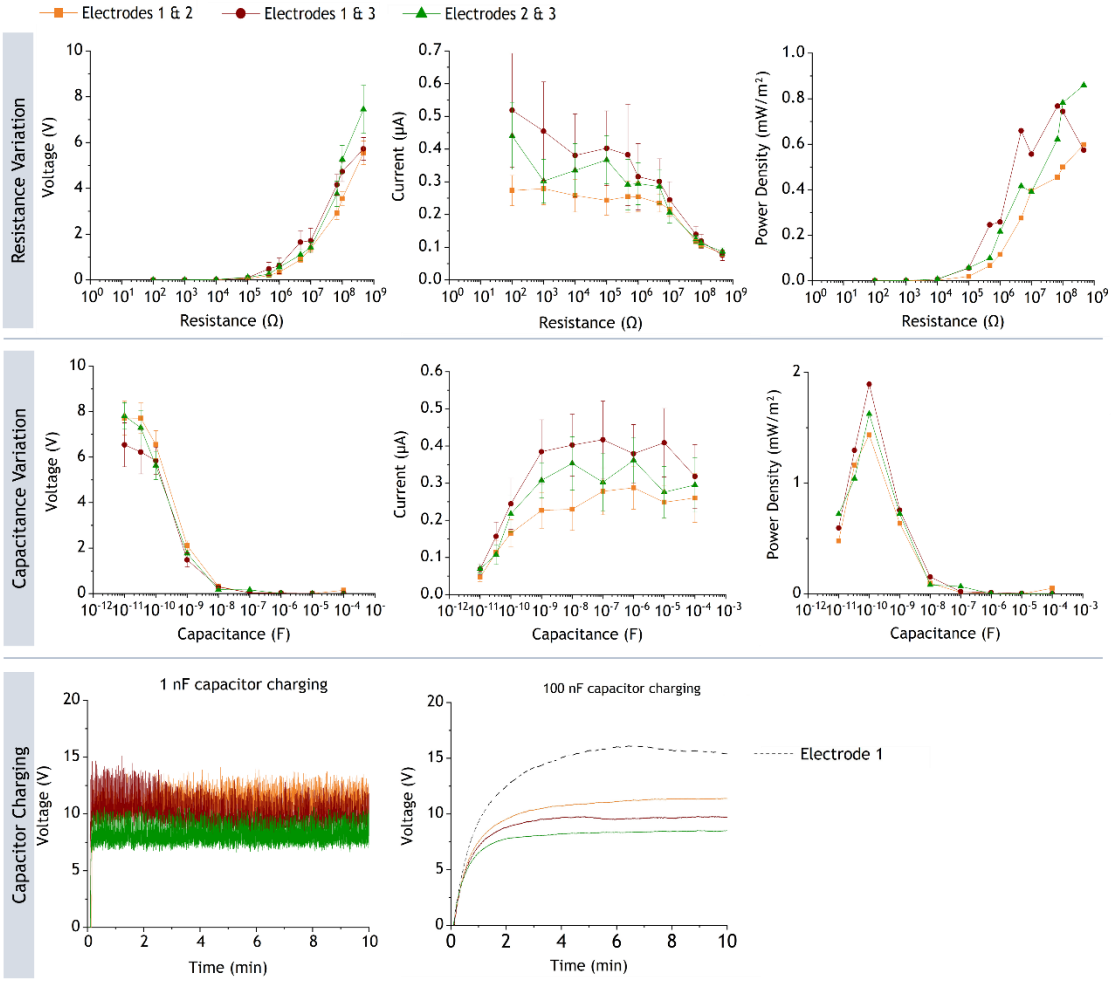

Figure 39. Triboelectric outputs, in voltage, current and resulting power density, for resistor and capacitor's variation, and capacitor charging curves, for comparison of the influence of the position of two electrodes in parallel on the solid-phase. Flu-TENG consisted of ePTFE solid-phase (6 mm ID and 152 μm WT) with PBS fluid-phase (161 mL/min, 60 rpm) and 2 cm length silver electrode segments with 1.3 cm spacing.

It can be seen that V_{out} is different with the variation in combination of the two electrodes in the different positions. Therefore, it is confirmed that the positions on the solid-phase have an effect on the general performance of the Flu-TENG when the electrode segments are in parallel.

The output is higher when electrode 1 is combined with 2 (1 & 2) or with 3 (1 & 3) since electrode 1 allows for the acquisition of the higher V_{out} of the Flu-TENG. However, there is a reduction in V_{out} when compared to the obtained using just electrode 1 alone (15.3 V comparing with 11.5 V (electrodes 1 & 2) and 9.6 V (electrodes 1 & 3)). This effect can be explained because there is a flow of electrons from electrode 1 to the following, to which it is combined, to compensate for the output difference, to reach an equilibrium between the sources. This leads to a reduction in the original outputs of electrode 1, which is more significant when it is combined with electrode 3 (more distant from proximal end). Electrode 3 provides the lowest individual V_{out}, requiring a higher flow of the electrons to reach an equilibrium and, consequently, the overall achieved output is lower. The lowest output is

achieved when combined electrodes 2 & 3 (8.5 V) since both electrodes have already a lower individual V_{out} due to their position further from the solid-phase's proximal end.

Overall, solid-phase resistance leads to a decrease in the obtained output throughout its length. Due to this effect, the combination of electrode segments in parallel is not effective to increase either voltage or current outputs of Flu-TENG.

4.2.3. Influence of solid-phase

4.2.3.1. Wall thickness

ePTFE vascular grafts with different wall thickness (75 and 500 µm, with IDs 4.5 and 4 mm, respectively) were used to assess the influence of this parameter in the generated outputs (Figure 40). For reference, PBS fluid-phase (161 mL/min, 60 rpm) and a 2 cm length silver electrode were used for both Flu-TENGs assemble.

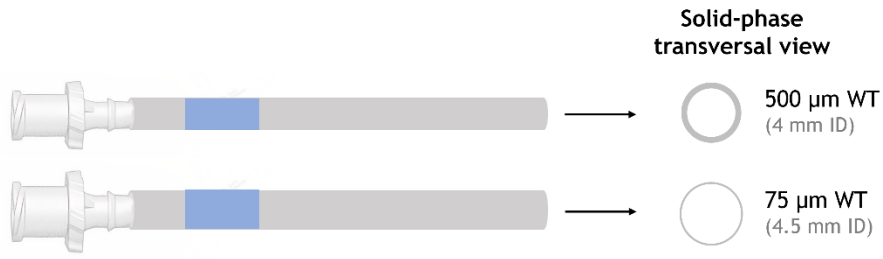

Figure 40. Representation of ePTFE solid-phase (grey) with varying wall thickness of 500 and 75 µm.

Triboelectric output results are represented in Figure 41.

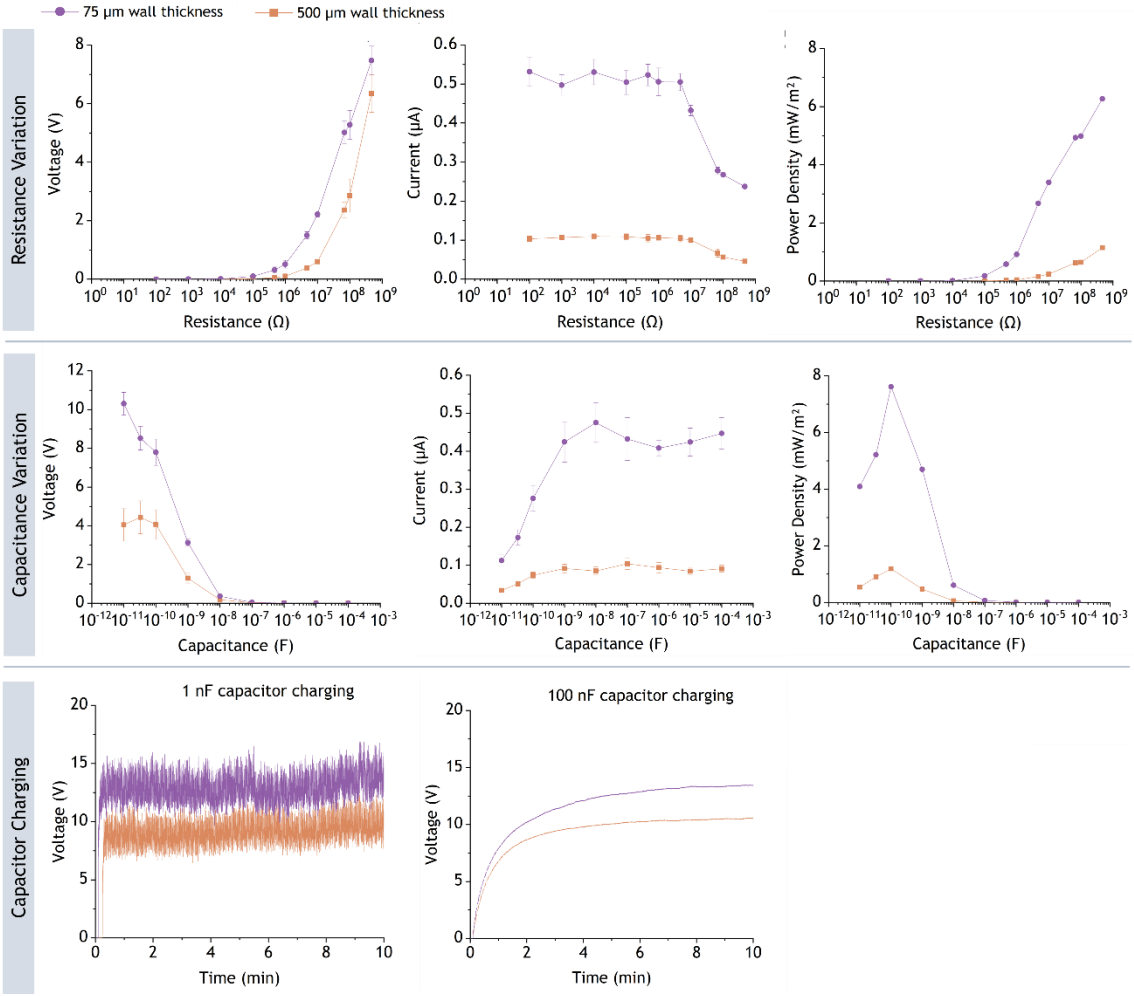

Figure 41. Triboelectric outputs, in voltage, current and resulting power density, for resistor and capacitor's variation, and capacitor charging curves, for assessing the influence of the solid-phase's wall thickness. Comparison between 75 µm and 500 µm WT. Flu-TENG consisted of ePTFE solid-phase (75 µm WT and 4.5 mm ID; 500 µm WT and 4 mm ID) with PBS fluid-phase (161 mL/min, 60 rpm) and 2 cm length silver electrode.

From the observation of results, it is clear that higher outputs are achieved when solid-phase's wall thickness is reduced. Analyzing the capacitor charging curves, it is determined a V_{out} of 13.5 V when using a 75 µm WT solid-phase and 10.5 V for the 500 µm WT one, representing a decrease in efficiency of approximately 22%.

Reduction in output with increase of solid-phase's wall thickness can be explained by the fact that there is an increase in induction distance, through which the charges, generated at the inner surface of the solid-phase, need to travel in order to reach the electrode, placed around the outer surface, as previously observed in the literature [75-77]. The reduction in thickness of a triboelectric layer leads to an improvement of TENG's relative capacitance, hence improving its performance [78].

4.2.3.2. Inner diameter

To study the effect of inner diameter variation, measurements were done using ePTFE solid-phase of 6 mm ID (152 µm WT) and compared to the acquired with ePTFE of 1.5

mm ID (100 µm WT) (Figure 42). For reference, PBS fluid-phase (161 mL/min, 60 rpm) and a 2 cm length silver electrode were used for both Flu-TENGs assemble.

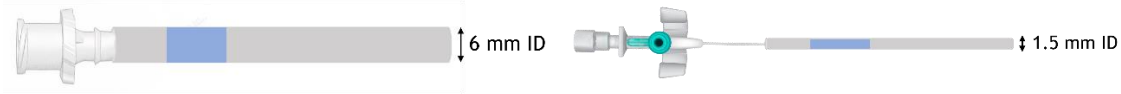

Figure 42. Representation of ePTFE solid-phase (grey) with varying inner diameter of 6 and 1.5 mm.

Figure 43 shows that ePTFE with a larger diameter originates smaller triboelectric outputs (V_{out} of 15.3 V versus the 20.3 V with the smaller diameter ePTFE). This difference in output can be explained by the fact that ePTFE with larger ID also presents a 52 µm thicker wall, which, as shown in section 4.2.3.1., reduces the output. Moreover, as the ID increased while the flow rate was kept the same (161 mL/min), the pressure inside the vascular graft decreased, leading to a weaker contact between fluid and inner surface of the solid-phase, which could have a negative impact in the Flu-TENG performance.

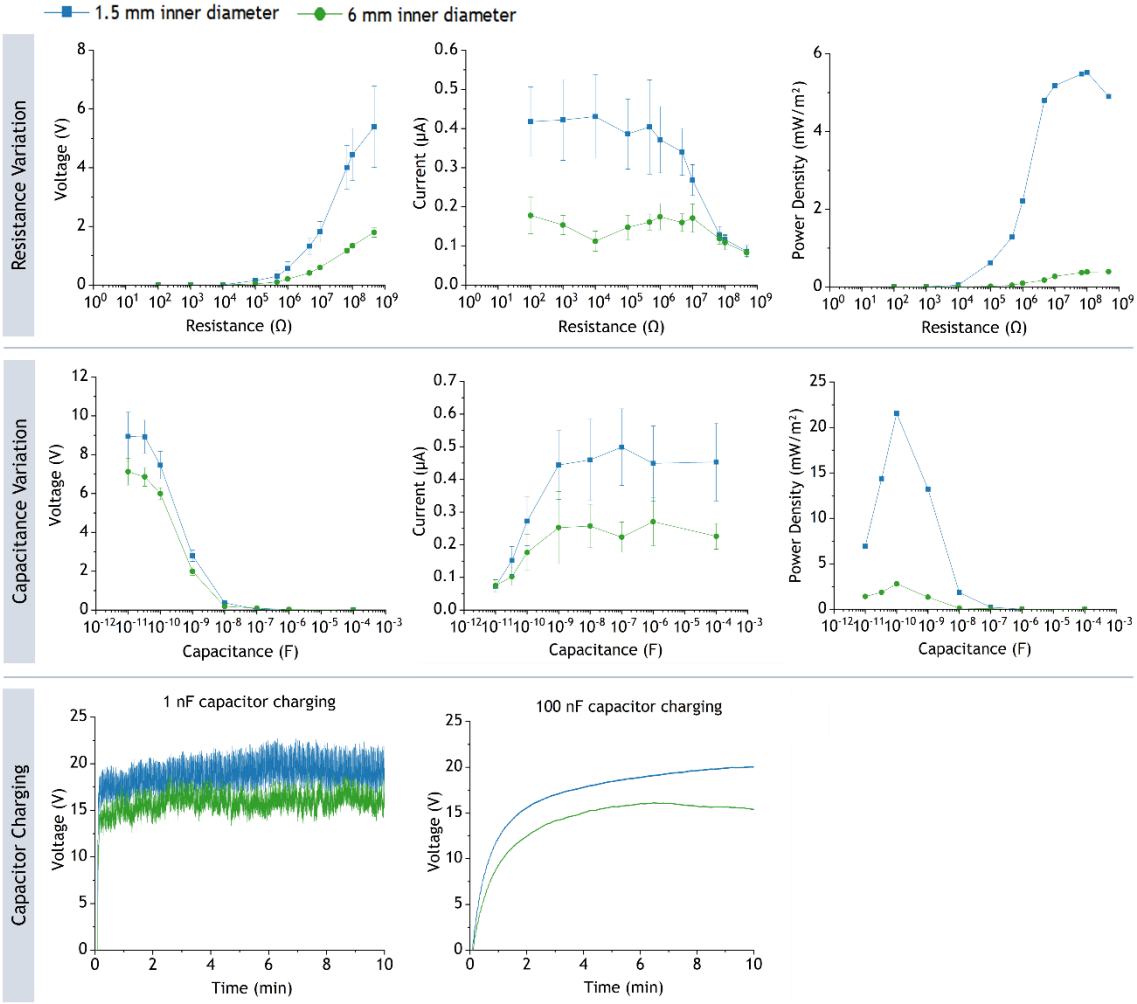

Figure 43. Triboelectric outputs, in voltage, current and resulting power density, for resistor and capacitor's variation, and capacitor charging curves, for assessing the influence of the solid-phase's inner diameter. Comparison between 1.5 and 6 mm ID. Flu-TENG consisted of ePTFE solid-phase (1.5 mm ID and 100 µm WT; 6 mm ID and 152 µm WT) with PBS fluid-phase (161 mL/min, 60 rpm) and 2 cm length silver electrode.

4.2.3.3. Solid type

Lastly, to assess the influence of the solid-phase material, the triboelectric properties of ePTFE and pHEMA/GO synthetic vascular grafts and umbilical cord arteries as the solid-phases were evaluated. For the three solid-phases, a 2 cm length silver electrode was used with PBS as the fluid-phase. For synthetic vascular grafts was used a flow rate of 161 mL/min (60 rpm), but in the case of the arteries, the flow rate was decreased (134 mL/min, 50 rpm) to avoid additional noise on the acquired electrical signal due to the external movement of the whole Flu-TENG, as a consequence of the high pressure inside the vessel.

The results obtained for ePTFE (4 mm ID and 500 µm WT), pHEMA/GO solid-phase (4 mm ID and 1 mm WT) and artery (umbilical cord) solid-phases are represented in Figure 44.

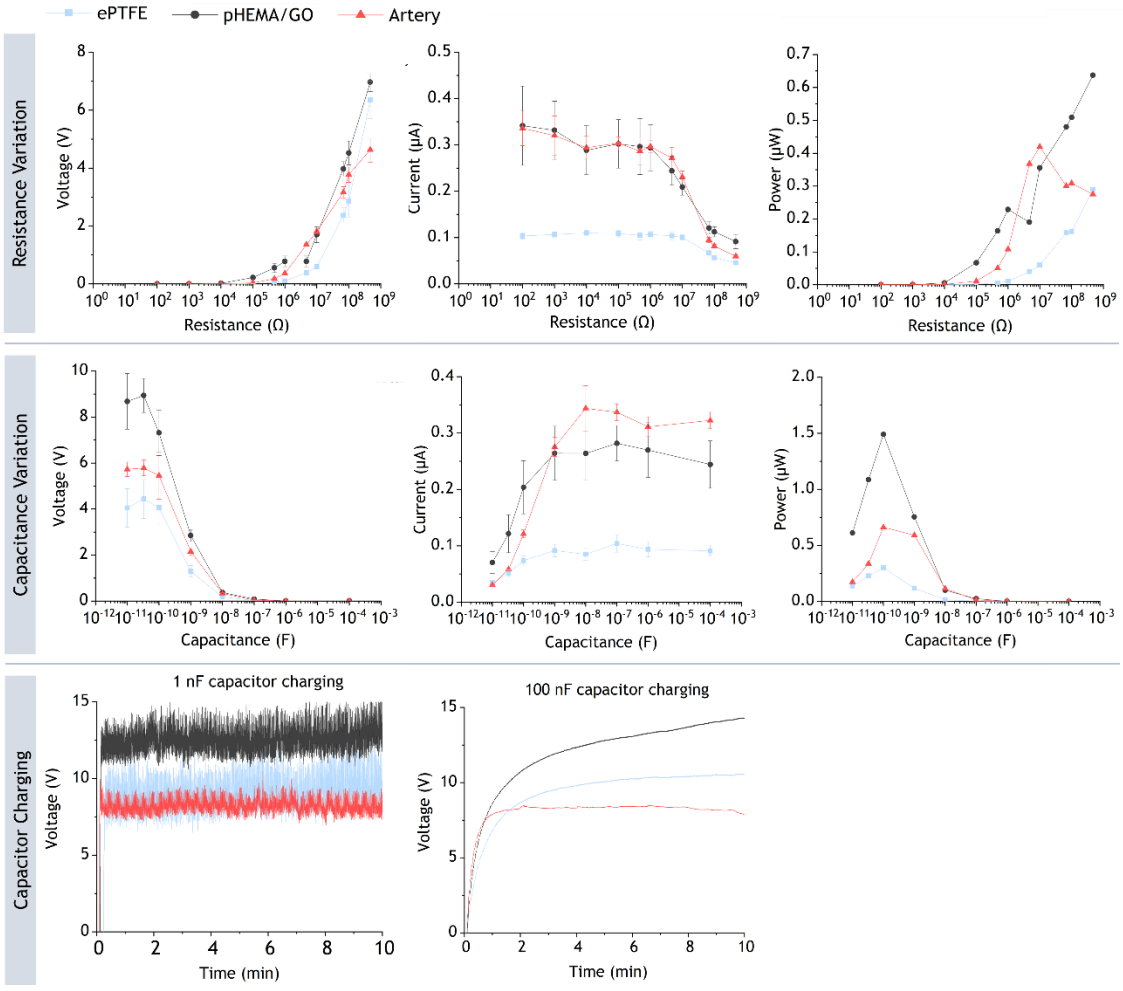

Figure 44. Triboelectric outputs, in voltage, current and resulting power, for resistor and capacitor's variation, and capacitor charging curves, for assessing the influence of the solid-phase's type. Comparison between ePTFE (4 mm ID and 500 µm WT), pHEMA/GO solid-phase (4 mm ID and 1 mm WT) and artery (umbilical cord). Flu-TENGs consisted of each solid-phase with PBS fluid-phase (161 mL/min, 60 rpm) and 2 cm length silver electrode.

From the analysis of the capacitor charging curves of Figure 44, it was observed a V_{out} of 14.5 V for pHEMA/GO and 10.5 V for ePTFE. Both vascular grafts have the same inner diameter, but pHEMA/GO has two times ePTFE's wall thickness (1 mm and 500 µm, respectively). Considering that thicker solid-phases result in decreased triboelectric outputs, as seen in section 4.2.3.1, it would be expected for ePTFE solid-phase to overperform pHEMA/GO. However, that is not the case, and so it can be inferred that pHEMA/GO's triboelectric properties make it a more efficient solid-phase when using PBS as the fluid-phase. This better performance implies that there is a higher difference in tribopolarity between pHEMA/GO and PBS than between ePTFE and PBS. Previously in the lab, it was shown that pHEMA/GO is more tribopositive than PTFE, which means that PBS should be a more tribonegative liquid. Considering the scarcity of information regarding triboelectric series of liquid materials, further studies should be performed to establish it. Moreover, pHEMA/GO results from the incorporation of GO into the already explored FDA-approved hemo- and bio-compatible hydrogel, pHEMA. Electric properties of GO have been explored for many biomedical applications, including the development of TENG, due to its capability of storing the charges generated by triboelectrification while preserving low interface resistance due to its good mechanical, electrical, and thermal properties [79]. Additionally, GO has been reported as an additive capable of scavenging the charges generated at the surface, and storing and transporting them deeper into the solid-phase material [19], and so closer to the electrode, compensating the negative effect of increased wall thickness. Thus, it can be inferred that the incorporation of GO into pHEMA leads to an augmented Flu-TENG performance.

Biomaterials, in particular used for the production of vascular grafts, can be used as the solid-phase of a Flu-TENG to harvest energy from the human body, and with the possibility of introduction of modifications for an enhanced performance.

The Flu-TENG consisting of the artery solid-phase can generate approximately 8 V of energy, as observed from the charging saturation of the tested capacitors. It is relevant to highlight that for this case the silver ink electrode could not be dried at 130 ºC, as the vessel would dry out and become unusable, but this is a very important step for the drying of the inks and improvement of their conductivity and, consequently, the efficiency of electrical output acquisition. Nevertheless, from these results, it is confirmed the potential of using native vessels as the solid-phase of a Flu-TENG to harvest energy from the human body, having the possibility to further optimize the energy generated, as previously mentioned.

The operating voltage of most CEDs is within the 2-3 V range [13], for instance, pacemaker battery requirements are of 2.8 V of open circuit voltage and 10 µA of control circuit current drain [80]. From the Flu-TENG performance results presented so far, it can be observed that voltage outputs are higher than the required for most applications, having the possibility of being optimized through the different parameters variation. However, current

outputs should be further increased. Hence, a development of the external power management circuit is needed so as to maximize the energy that is acquired from the Flu-TENG.

Overall, many variables associated with each component of the Flu-TENG device need to be taken into consideration for its influence on the output. In Table 4 is summarized the Flu-TENG's studied parameters with respective triboelectric output (V_{out}) results and corresponding energy density, calculated as $U = \frac{1}{2}CV^2$, considering the charging of the 1 nF capacitor, as well as short circuit current (I_{sc}), considering an external resistance of 100 Ω. To note that a direct comparison of these outputs is only possible within the same parameter as between parameters there is an influence of the variation of other Flu-TENG components characteristics.

Table 4. Summary of the triboelectric outputs for the Flu-TENG's studied parameters and corresponding energy density for 1 nF capacitor charging. The best achieved energy density outputs, for each parameter, are highlighted in green.

Flu-TENG component	Parameter	Parameter specification	V_{out} (V)	Energy density (nJ)	I_{sc} (μA)
Fluid	Type	PBS	17.3	149.6	0.23
		Plasma	23.6	278.5	0.24
		Blood	14.2	100.8	0.19
	Flow-rate	60 rpm	15.3	117.0	0.18
		100 rpm	24.6	302.6	0.28
Electrode	Type	Silver	17.3	149.6	0.22
		Carbon	12.9	83.2	0.23
		PEDOT:PSS	10.4	54.1	0.47
	Length	0.5 cm	6.7	22.4	0.12
		1 cm	17.0	144.5	0.28
		2 cm	18.9	178.6	0.42
		4 cm	26.2	343.2	0.28
		6 cm	29.4	432.2	0.21
		8 cm	38.5	741.1	0.34
		10 cm	47.6	1132.9	0.27
Solid	Type	ePTFE vascular graft	10.5	55.1	0.10
		pHEMA/GO vascular graft	14.5	105.1	0.34
		Umbilical cord artery	8.0	32.0	0.34
	Wall thickness	75 μm	13.5	91.1	0.53
		500 μm	10.5	55.1	0.10
	Diameter	1.5 mm	20.3	206.0	0.42
		6 mm	15.3	117.0	0.18

4.2.4. Flu-TENG as a narrowing sensor

Triboelectric measurements performed until this point have been focused on the study of the parameters that affect the electric output and how they do so, to conclude on

how the Flu-TENG can be optimized regarding the amount of energy that it will generate. However, Flu-TENGs can be used as a sensor themselves, if the acquired electrical signal changes with the occurrence of a biological event.

Vascular grafts fail due to thrombosis and infection occurrence, which is very harmful for the patient. Therefore, it is of great importance to detect these problems at an early stage. The narrowing/blockage of the solid-phase can affect Flu-TENG's outputs in different ways, one of which is a localized reduction of diameter that leads to a perturbation of the fluid-phase's flow, and this could affect the electrical output being acquired (Figure 45).

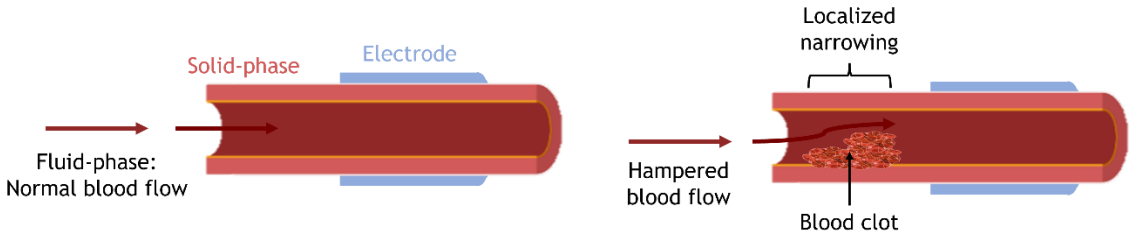

Figure 45. Representation of the perturbation of blood flow caused by narrowing of the solid-phase as a consequence of, for example, blood clot formation, and how it can affect Flu-TENG's performance. Longitudinal view of the solid-phase.

To test this hypothesis, firstly the triboelectric output was acquired using the Flu-TENG set up, with an ePTFE vascular graft as solid-phase (4 mm ID and 500 µm WT) with a silver electrode (2 cm length) and PBS as fluid-phase (161 mL/min), without any perturbation of the flow (Figure 46 (A)). Then, it was compared to the output acquired with the same Flu-TENG but with an induced perturbation. To mimic the localized reduction of the ePTFE's diameter and consequent flow perturbation, a plastic clamp was placed around the solid-phase, as represented in Figure 46 (B), inducing a 30% narrowing.

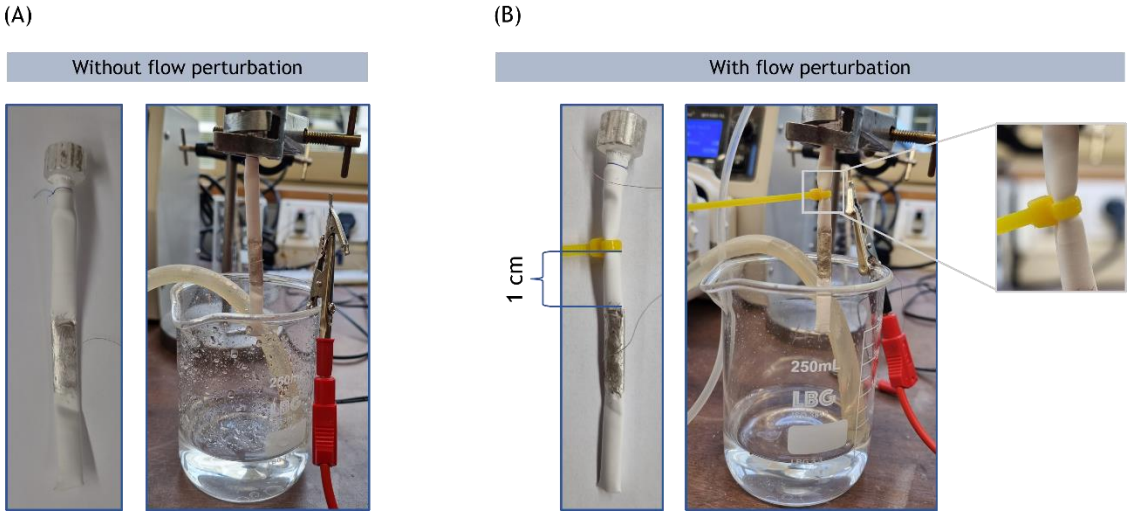

Figure 46. Set up assembled for the testing of Flu-TENG as a narrowing sensor. (A) Flu-TENG without induced narrowing; (B) Flu-TENG with 30% narrowing induced using a clamp.

The comparison results of triboelectric outputs with and without flow perturbation are represented in Figure 47.

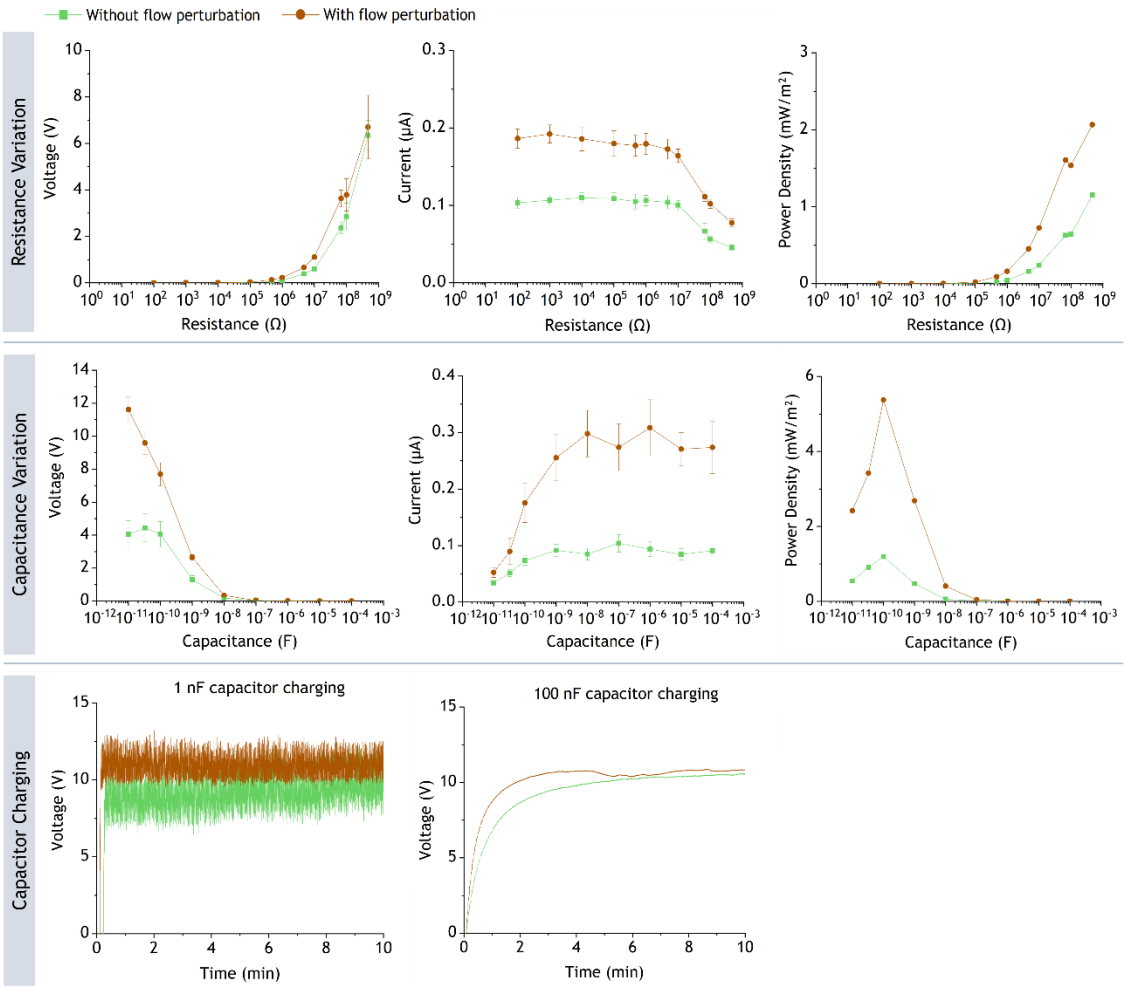

Figure 47. Triboelectric outputs, in voltage, current and resulting power density, for resistor and capacitor's variation, and capacitor charging curves, for assessing the difference in output as a result of narrowing of the solid-phase and consequent flow perturbation. Flu-TENG consisted of ePTFE solid-phase (4 mm ID and 500 μm WT) with PBS fluid-phase (161 mL/min, 60 rpm) and 2 cm length silver electrode.

By comparing the acquired electrical signals, it is possible to observe an increase in current outputs for all tested resistances and capacitances, upon 30% narrowing of the solid-phase. Moreover, voltage outputs are also increased, being observed a more significant difference for the case of capacitance variation. For both cases, this results in an increase of power density. For instance, resorting to an external 100 pF capacitor, for a narrowing of just 30%, at least a 3.6 V, 0.1 μA and 4.2 mW/m^2 output difference can be detected. With a 10 pF capacitor, the maximum increase in voltage output with the induced flow perturbation is obtained and is of 7.6 V. Therefore, this Flu-TENG set up can be used to detect the narrowing of the vascular graft, as there is a significant change in the energy generated. Further studies should be done with varying narrowing levels for the establishment of a relation between the degree of occlusion and the corresponding electrical signal obtained. For a more reproducible testing, tubing segments of well-defined diameter could be assembled onto the inner space of the vascular graft to mimic real biological conditions.

Here, it was focused on the evaluation of the effect of narrowing in the flow as a result of localized solid-phase diameter change, however, occlusion can be associated with other Flu-TENG parameters change. For instance, when a thrombus or atherosclerosis plaque forms on the luminal surface of the vascular graft, the solid-phase itself changes, as instead of having the fluid flow against the biomaterial, it will be momentarily flowing across a portion of tissue, therefore the liquid-solid contact changes and that will have an impact on charges generated, *i.e.* on the outcome of the Flu-TENG. Additionally, wall thickness will also increase, which is known to decrease the electrical output.

4.3. *In vitro* cytocompatibility assessment

For biomedical applications, Flu-TENGs should be biocompatible. For the case of the end goal application of the herein presented work, as fluid-phases consist of biofluids and solid-phases of either native vessels, already present on the body, or biomaterials, safely usable *in vivo*, the electrode is the only component of the Flu-TENG that must be introduced in the biological environment and could be toxic. Therefore, the cytocompatibility of the studied electrodes was assessed. Moreover, electrodes will be located in the outer wall of solid-phases, meaning that it will not be in direct contact with blood. Electrodes biocompatibility is especially relevant for the case of assembly on a native vessel solid-phase, as it will be in direct contact with the cells of the vascular wall (fibroblasts).

4.3.1. Extracts assay

In the extracts assay, fibroblast cells, present in the outer wall of native vessels, were put in contact with the extracts of ePTFE coated with the studied electrodes (silver, carbon and PEDOT:PSS conductive inks and copper tape). Figure 48 (A) shows the morphology of adhered cells after the contact with the different extracts. To further analyze these results, the metabolic activity of HFF-1, after extracts assay, was assessed by resazurin assay. Resazurin is a fluorescent dye which will be reduced during aerobic respiration of metabolically active cells, leading to optical changes that will allow for the detection of the presence of viable cells. In this assay, cells were seeded in the tissue culture plates before contact with the extracts. Thus, only the ones that remained alive after this contact were able to metabolize the resazurin. Fluorescence results of a 24 hour incubation time-point are represented in Figure 48 (B).

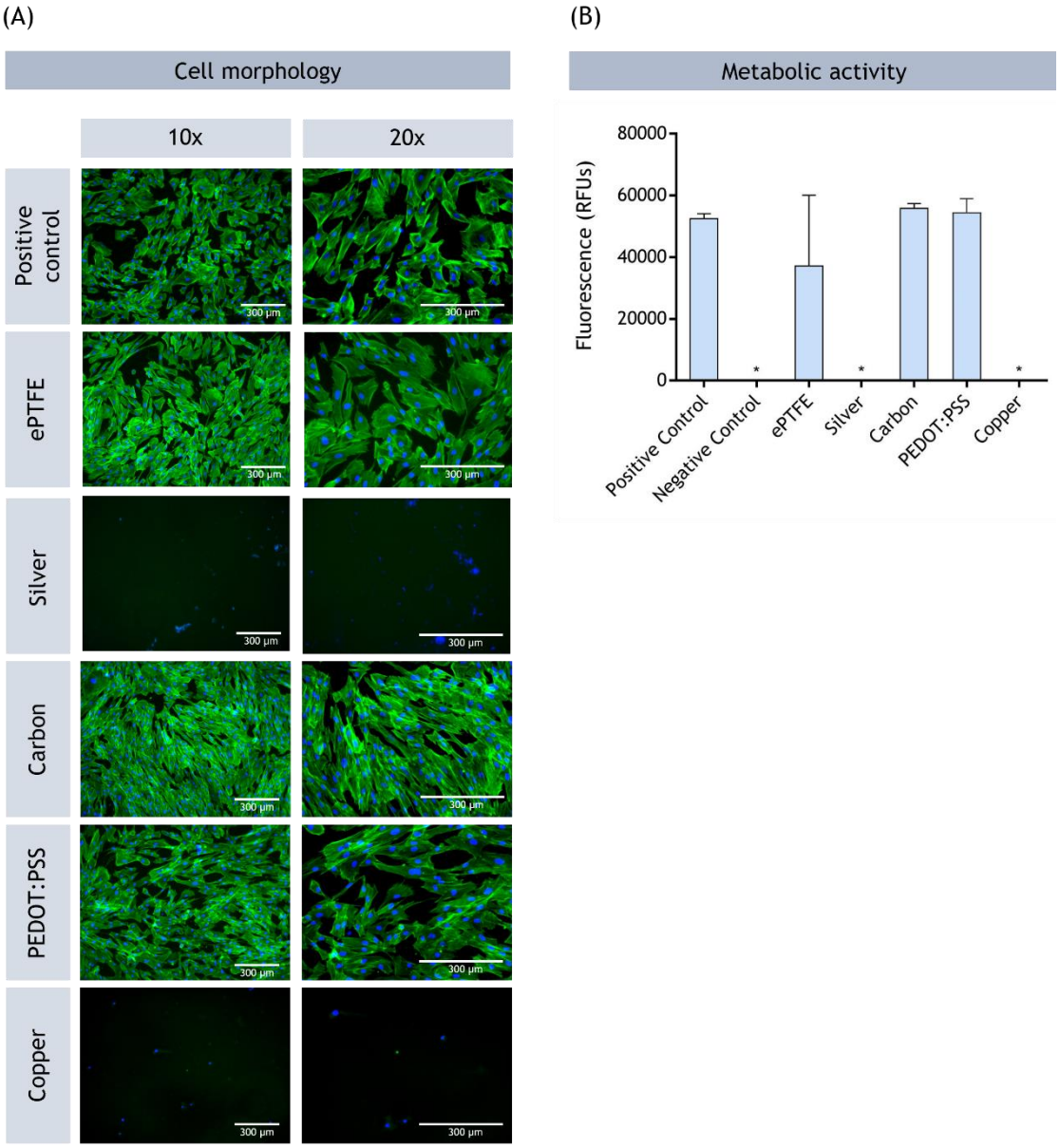

Figure 48. HFF-1 morphology and metabolic activity after incubation with electrode coated ePTFE extracts for 24 hours. Positive control consists of cells after contact with TC-PET extracts. ePTFE results consist of the cells after contact with uncoated ePTFE extract. (A) Microscopy images. Cells stained with DAPI (nuclei) and Alexa Fluor 488 (cytoplasm). Magnification 10x and 20x. Scale bar: 300 µm; (B) Fluorescence, measured in relative fluorescence units (RFUs), after HFF-1 incubation with resazurin. Statistical analysis performed with one-way ANOVA Dunnett's multiple comparison tests. * Statistically significant difference ($p<0.05$) from positive control.

It is possible to see a confluent layer of fibroblast cells with spread morphology, for the cells that were in contact with carbon and PEDOT:PSS coated ePTFE and ePTFE extracts, similar to positive control. Oppositely, it was not possible to see cells after the contact with extracts resulting from leaching of silver and copper, which means that these are cytotoxic.

Comparing the fluorescence measured for the positive control to the measured for the cells in contact with the electrode coated ePTFE extracts, it is clear that the fibroblast cells survived in the presence of extracts of ePTFE coated with carbon and PEDOT:PSS, but died in contact with the ones resulting from silver and copper coatings, as indicated by the

non-metabolization of resazurin (statistically different from the positive control). This is in accordance with the microscopy images, in which is not possible to see any cells in the wells where they were put in contact with silver and copper coated ePTFE extracts. Besides, cell growth when in contact with uncoated ePTFE extracts was approximately the same as in the positive control, as depicted from close RFUs values, confirming that ePTFE is biocompatible. Thus, it can be said that cell death after contact with the silver and copper coated ePTFE extracts is not related to the release of some toxic component from the biomaterial but from the electrode coatings themselves.

Overall, our findings show that the used silver conductive ink and copper tape electrodes are cytotoxic, whilst carbon and PEDOT:PSS conductive inks are cytocompatible, therefore could potentially be used for a biological application.

Silver conductive ink and copper tape electrodes' toxicity is a consequence of the particles releasing from the coatings into the cell culture medium, which does not allow for cells to survive. However, the use of silver has been reported for biological applications without biocompatibility issues [81-83], for example, there are vascular grafts commercially available which are coated with silver for its antimicrobial properties [84, 85]. Therefore, it can be hypothesized that the properties of silver ink coatings could be tuned to try and achieve biocompatibility. The amount of silver ink on the coating layer assembled onto the solid-phase, namely its mass and homogeneity, is not controlled, as it is manually brush painted in the sample. Hence, the amount of silver on the coating should be well defined for further testing of a possible influence of the variation of this concentration on cytotoxicity, so as to determine a coating concentration limit.

4.3.2. Direct contact assay

In the direct contact assay, fibroblast cells were seeded onto coverslips previously coated with the different electrodes, with incubation time points of 24 hours and 7 days. To assess cell adherence to the coatings and their morphology, the samples were observed under microscopy (Figure 49 (A)). Similarly to the extracts assay, metabolic activity of the adhered fibroblast cells was assessed by measuring the fluorescence of the suspension resulting from the incubation of the samples with resazurin (Figure 49 (B)).

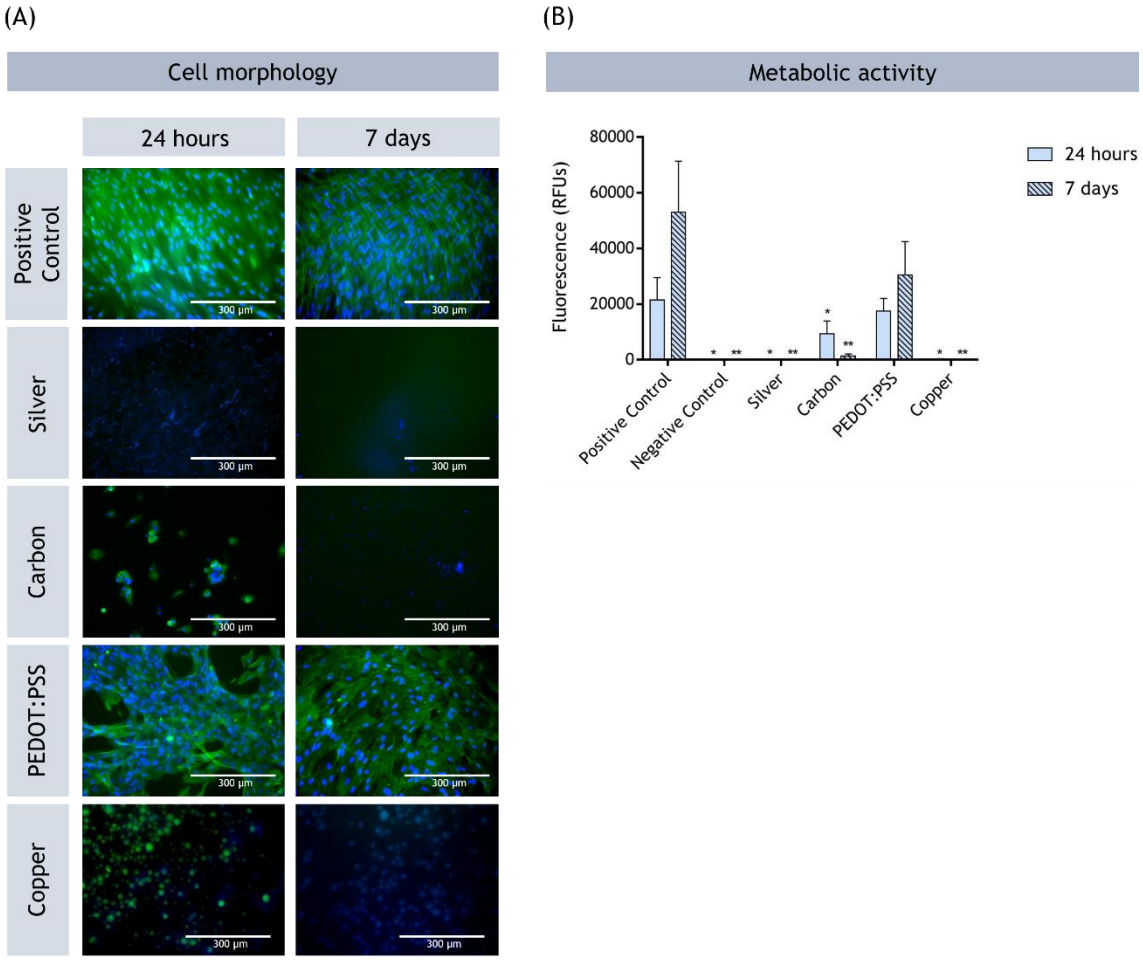

Figure 49. HFF-1 morphology and metabolic activity after incubation with electrode coated coverslips for 24 hours and 7 days. Positive control consists of cells adhered to TC-PET coverslips. (A) Microscopy images. Cells stained with DAPI (nuclei) and Alexa Fluor 488 (cytoplasm). Magnification 20x. Scale bar: 300 µm; (B) Fluorescence, measured in relative fluorescence units (RFUs), after HFF-1 incubation with resazurin. Statistical analysis performed with one-way ANOVA Dunnett's multiple comparison tests. * Statistically significant difference ($p<0.05$) from 24h positive control, ** Statistically significant difference ($p<0.05$) from 7 days positive control.

In the microscopy images, both for the 24 hours and 7 days time-points, a confluent layer of cells spread across the whole coverslip area, and in a similar morphology as in the positive control, can be seen in the PEDOT:PSS coated coverslips. However, less fibroblast cells can be observed in the carbon coated samples, presenting a slightly different aspect at the 24 hour time-point and being absent after 7 days. For the case of silver and copper, no cells seem to be present from the first day on.

Regarding the 24 hour time-point, comparing the fluorescence measured for the positive control to the measured for the testing samples, it is possible to see that carbon and PEDOT:PSS electrodes allow the presence of a higher number of metabolically active fibroblast cells, whereas for silver and copper, no cells are available to noticeably reduce the resazurin, as indicated by a significantly higher difference in RFUs from the positive control, and close to the obtained for the negative control. Statistically significant differences ($p<0.05$) are found between the positive control and the samples resulting from the contact with silver, carbon and copper. The quantitative results corroborate the microscopy images,

where a greater amount of adhered cells can be seen in the PEDOT:PSS coated coverslips but slightly different for carbon samples, for which it was obtained a smaller RFU value.

As for the 7 day time-point, the main difference is attributed to the carbon samples, as the metabolic activity detected reduces notoriously, oppositely to the PEDOT:PSS samples, in which it increases as it does in the positive control.

These results are in accordance with extracts assay, which revealed that silver and copper are cytotoxic. Additionally, as carbon was found to be cytocompatible, the absence of cells can be justified by this electrode leading to a non-fouling surface, in which case the majority of cells do not adhere to the coated coverslips.

Chapter 5: Conclusions and Future Work

5.1. Conclusions

Three different electrodes (silver, carbon and PEDOT:PSS conductive inks) were assembled by brush painting in the three solid-phase conduits (ePTFE, pHEMA/GO and native vessels). The stability of these electrodes depends on the used solid-phase. For ePTFE, it was possible to achieve a stable assemble of all the tested electrodes, oppositely to pHEMA/GO and the artery solid-phases, where some coating detachment and ink infiltration to the luminal surface were verified. Overall, silver conductive ink was the most stable electrode for ePTFE and pHEMA/GO. Despite being observed some instability for vessels, silver electrodes seem to infiltrate less to the lumen than the others.

Regarding the triboelectric outputs, all the Flu-TENGs tested in this study generated electric outputs, confirming the potential of using biofluids flow through different materials to harvest energy from the human body. However, for these Flu-TENGs, it was not verified a saturation of the output voltage for the range of resistors and capacitors used for acquisition, which means that with the conventional triboelectric measuring set-up it was not possible to obtain the maximum Flu-TENG output (V_{out}). Thus, it was developed a new measuring method which consists in capacitators charging. It was concluded that V_{out} is approximate to the saturation voltage of capacitors charged with that output, therefore this method was adopted throughout this study to compare the performance of the different Flu-TENGs.

Comparing the three fluid-phases tested, higher outputs could be achieved with plasma (23.6 V), with PBS (17.3 V) providing a closer output to blood (14.2 V). From this, it can be concluded that fluids characteristics have an impact on general performance of the Flu-TENG. Besides, these fluids' flow rate also impacts the triboelectric outputs, being higher for higher flow rates.

Considering the solid-phases, higher outputs were achieved resorting to the synthetic solid-phases, especially with pHEMA/GO (14.5 V), comparing with ePTFE (10.5 V) and native vessels (8 V). Moreover, it was concluded that the increase in wall thickness and inner diameter of the solid-phases led to a reduction in the voltage output.

Silver electrode was the most efficient (17.3 V), followed by carbon (12.9 V) and lastly PEDOT:PSS (10.4 V), for which there was a reduction in efficiency of 25% and 40%,

respectively, when compared to silver. Testing length variation of silver electrodes, it was verified that triboelectric outputs increase linearly with the electrode's length. Besides, the position of the electrode in the solid-phase influences the achieved output, namely, it was seen a decrease in the output with the distance of the electrode to the proximal end of the ePTFE vascular graft. As a consequence of this phenomenon, a combination of electrode segments, placed along the solid-phase in parallel, does not improve the current output, as it would be expected.

Lastly, some preliminary tests were done for the use of the Flu-TENG as a self-powered sensor of vascular grafts narrowing/blockage, from which it was concluded that the Flu-TENG is sensitive to induced flow perturbations as a consequence of 30% narrowing.

Cytocompatibility assays reveled that silver and copper electrodes tested in this study are cytotoxic whereas carbon and PEDOT:PSS are cytocompatible towards human fibroblasts.

Triboelectric performance of the proposed Flu-TENGs depends on the fluid-phase and its flow rate, the solid-phase and respective wall thickness and inner diameter, and on the electrode, as well as its length and design.

Overall, this work showed the potential of using a new energy source, which consists in the flow of blood through native vessels and/or vascular grafts, to power electronic medical devices. Moreover, it was demonstrated the possibility of use of this technology to be a self-powered sensor of vascular grafts narrowing/blockage to early detect their failure.

5.2. Future work

The study developed in this thesis was pioneer in proposing the use of biofluids flow through vessels and vascular grafts to harvest energy, answering many questions related to the factors that most affect the Flu-TENG output and the possible applications of the generated energy. However, this vast topic can be further explored opening several questions to address in future work.

Firstly, a more in-depth study on the influence of fluids on the triboelectric output could be done in order to define a liquids triboelectric series, as information on this is still lacking on the literature. By combining this study with a variation of solid-phase materials, whose tribopolarity is already well defined, it would be possible to establish a relation between the tribopolarity of different fluids and solids in a series, allowing to decide on the best material combination for the production of the most efficient Flu-TENG. Moreover, for the specific study of the triboelectric properties of blood, the study and comparison of the outcome using buffy coats (white blood cells and platelets) as the fluid-phase to the already studied plasma and blood would provide a further insight on the components of the whole blood that most affect its tribopolarity.

Regarding the solid-phase variation, more biomaterials currently used for the production of devices in which biofluids flow in the body should be tested, such as vascular

grafts, *e.g.* polyethylene terephthalate (PET) and polyurethane, and catheters, *e.g.* polyvinyl chloride (PVC).

The choice of electrode alone is crucial when designing a Flu-TENG and so other electrode options should be addressed so as to optimize not only the electric properties but also its implementation in a medical setting, namely the stability on the solid-phase and biocompatibility. Electrode composites and varying fabrication techniques can be explored so as to maximize the efficacy of the Flu-TENG device as a whole, taking into the consideration the requirements of a specific application, such as flexibility and stretchability [86]. This study also implies the optimization of the coating assemble, both for new electrodes and for the already tested (silver, carbon and PEDOT:PSS inks), to study a possible influence of the number of layers and concentration of the coating on the stability and biocompatibility of the electrode. In particular, silver was found to be cytotoxic, however, there are reported biological applications and even commercially available vascular grafts coated with silver. Additionally, these vascular grafts [84, 85] could also be tested as possible Flu-TENG's solid-phases of enhanced electrical properties.

The possibilities of use of the generated energy have already been discussed. However further optimization of the Flu-TENGs characteristics should be done, combining the knowledge acquired, to achieve the utmost energy for the desired application. Collaborators at the University of Navarra have evaluated the order of magnitude of the energy outputs obtained so far, hypothesizing that, with the proposed Flu-TENGs, it will be possible to increase a pacemaker's longevity in approximately 10% and to use it as a sensor for narrowing/blockage, capable of sending a wireless signal once a day. However, for both cases, this involves the optimization of the external circuitry, namely the power management unit associated, to maximize the energy acquired from the Flu-TENG's output, convert it into a DC signal and store for further use. In that regard, a simple way to try and accumulate a higher amount of energy through the optimization of the external circuitry whilst still resorting to the segmentation of electrodes on the Flu-TENG, would be to charge different capacitors with the different electrode segments so as to accumulate in each the energy that can be generated across the solid-phase, at those corresponding points. In Figure 50 is schematized the Flu-TENG sample as well as the external circuit needed for these tests.

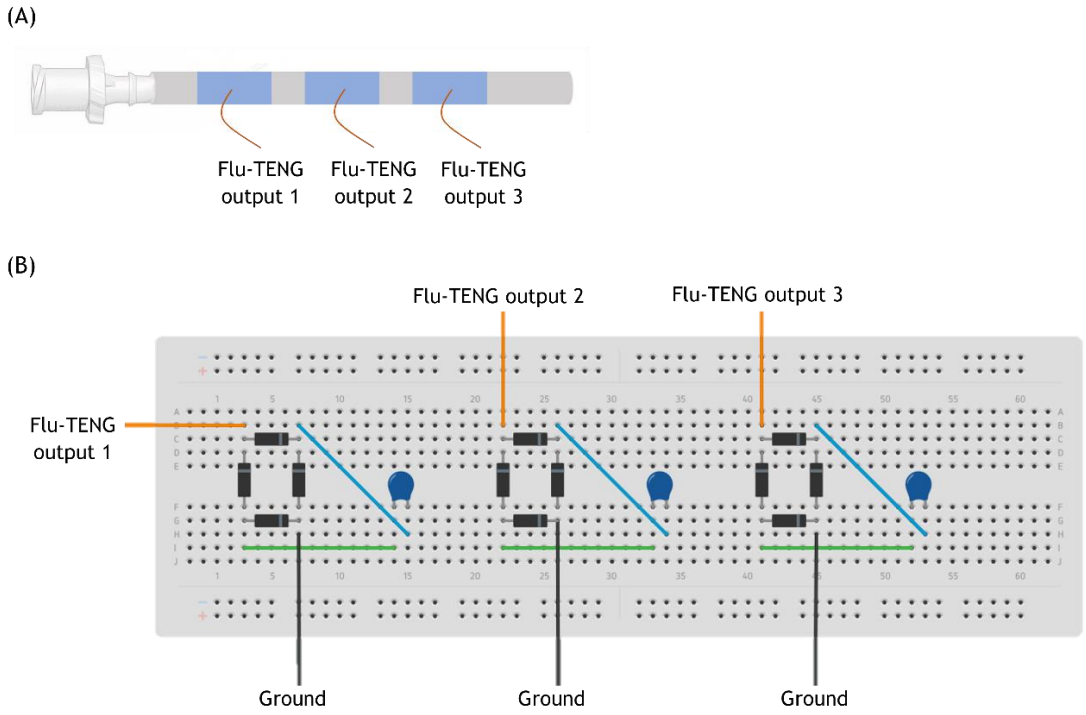

Figure 50. Set up for three capacitors charging with the outputs of Flu-TENG (A) Schematic representation of solid-phase (grey) with the segmented electrodes (blue); (B) Circuit composed of three bridge rectifiers for charging of three capacitors with the output of each electrode segment.

Regarding sensing applications, in particular the use of the proposed Flu-TENG for the detection of narrowing/blockage, which was also one of the focus on this work, tests should be continued to define its efficacy and to extend for other applications. As previously discussed, these events can be detected resorting to the Flu-TENG and through variations of different related aspects. Therefore, for the study of the combined effect of localized change in the solid-phase's diameter and composition, coagulation could be induced and an atherosclerosis plaque bioengineered to evaluate the changes in electrical output in the presence of these occurrences. Furthermore, to evaluate the effect of vessel/graft blockage, blocking methods could be applied, such as to inflate a balloon in the interior of the solid-phase to cause pressure perturbations of the flow in motion [57].

Lastly, once established the most effective Flu-TENG, *in vivo* tests of the herein presented applications could be done. For native vessels as the solid-phase, electrodes should be assembled into different vessels of small and large scale animals. Concerning vascular graft generators, Flu-TENG performance could be evaluated through an arteriovenous-shunt model [65].

Figure 51 schematizes the Flu-TENG of the herein presented work for future applications in medical settings.

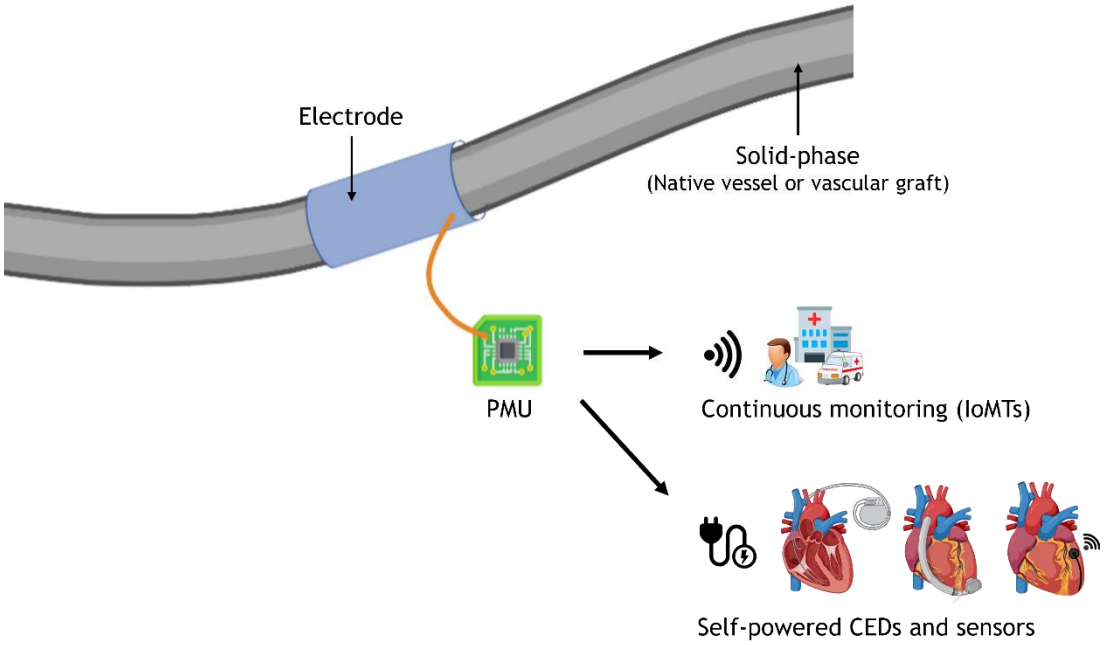

Figure 51. Future directions of the herein presented Flu-TENG for medical settings.

References

[1] W. H. Organization. "Cardiovascular diseases." https://www.who.int/health-topics/cardiovascular-diseases (accessed Apr 10, 2022).

[2] G. A. Roth *et al.*, "Global Burden of Cardiovascular Diseases and Risk Factors, 1990-2019: Update From the GBD 2019 Study," *Journal of the American College of Cardiology,* vol. 76, no. 25, pp. 2982-3021, 2020.

[3] R. Beaglehole, R. Saracci, and S. Panico, "Cardiovascular diseases: causes, surveillance and prevention," *International Journal of Epidemiology,* vol. 30, no. suppl 1, pp. S1-4, 2001.

[4] F. Zanon *et al.*, "Device Longevity in a Contemporary Cohort of ICD/CRT-D Patients Undergoing Device Replacement," *Journal of Cardiovascular Electrophysiology,* vol. 27, no. 7, pp. 840-845, 2016.

[5] G. Boriani, J. Merino, D. J. Wright, F. Gadler, B. Schaer, and M. Landolina, "Battery longevity of implantable cardioverter-defibrillators and cardiac resynchronization therapy defibrillators: technical, clinical and economic aspects. An expert review paper from EHRA," *EP Europace,* vol. 20, no. 12, pp. 1882-1897, 2018.

[6] J. S. Sammons and J. S. Gerber, "Clinical Syndromes of Device-Associated Infections," in *Principles and Practice of Pediatric Infectious Diseases (Fifth Edition)*, 2018, pp. 600-612.

[7] J. E. Poole *et al.*, "Complication Rates Associated With Pacemaker or Implantable Cardioverter-Defibrillator Generator Replacements and Upgrade Procedures," *Circulation,* vol. 122, no. 16, pp. 1553-1561, 2010.

[8] J. K. Schmier, E. C. Lau, J. D. Patel, J. A. Klenk, and A. J. Greenspon, "Effect of battery longevity on costs and health outcomes associated with cardiac implantable electronic devices: a Markov model-based Monte Carlo simulation," *Journal of Interventional Cardiac Electrophysiology,* vol. 50, no. 2, pp. 149-158, 2017.

[9] G. Boriani, F. Braunschweig, J. C. Deharo, F. Leyva, A. Lubinski, and C. Lazzaro, "Impact of extending device longevity on the long-term costs of implantable cardioverter-defibrillator therapy: a modelling study with a 15-year time horizon," *Europace,* vol. 15, no. 10, pp. 1453-62, 2013.

[10] J. Li *et al.*, "Triboelectric nanogenerators enabled internet of things: A survey," *Intelligent and Converged Networks,* vol. 1, no. 2, pp. 115-141, 2020.

[11] "Internet of Medical Things (IoMT) Market Size, Share & Covid-19 Impact Analysis," in "Market Research Report," Fortune Business Insight, 2020. [Online]. Available: https://www.fortunebusinessinsights.com/industry-reports/internet-of-medical-things-iomt-market-101844

[12] S. Wang, L. Lin, and Z. L. Wang, "Triboelectric nanogenerators as self-powered active sensors," *Nano Energy,* vol. 11, pp. 436-462, 2015.

[13] Q. Zheng, Q. Tang, Z. L. Wang, and Z. Li, "Self-powered cardiovascular electronic devices and systems," *Nature Reviews Cardiology,* vol. 18, no. 1, pp. 7-21, 2021.

[14] G. Khandelwal, N. P. Maria Joseph Raj, and S.-J. Kim, "Triboelectric nanogenerator for healthcare and biomedical applications," *Nano Today,* vol. 33, p. 100882, 2020.

[15] A. Amar, A. Kouki, and H. Cao, "Power Approaches for Implantable Medical Devices," *Sensors,* vol. 15, no. 11, pp. 28889-28914, 2015.
[16] S. Khalid, I. Raouf, A. Khan, N. Kim, and H. S. Kim, "A Review of Human-Powered Energy Harvesting for Smart Electronics: Recent Progress and Challenges," *International Journal of Precision Engineering and Manufacturing-Green Technology,* vol. 6, pp. 821–851, 2019.
[17] X. Li, C. Jiang, Y. Ying, and J. Ping, "Biotriboelectric Nanogenerators: Materials, Structures, and Applications," *Advanced Energy Materials,* vol. 10, no. 44, p. 2002001, 2020.
[18] M. E. Kiziroglou and E. M. Yeatman, "Materials and techniques for energy harvesting," in *Functional Materials for Sustainable Energy Applications*, 2012, pp. 541-572.
[19] F. F. Hatta, M. A. S. Mohammad Haniff, and M. A. Mohamed, "A review on applications of graphene in triboelectric nanogenerators," *International Journal of Energy Research,* vol. 46, no. 2, pp. 544-576, 2022.
[20] H. Ryu and S.-W. Kim, "Emerging Pyroelectric Nanogenerators to Convert Thermal Energy into Electrical Energy," *Small,* vol. 17, no. 9, p. 1903469, 2021.
[21] W. Wang *et al.*, "Applications of nanogenerators for biomedical engineering and healthcare systems," *InfoMat,* vol. 4, no. 2, p. e12262, 2022.
[22] Y. Yang, "Pyroelectric and Thermoelectric Nanogenerators," in *Hybridized and Coupled Nanogenerators*, 2020, pp. 219-257.
[23] D. Zhang, Y. Wang, and Y. Yang, "Design, Performance, and Application of Thermoelectric Nanogenerators," *Small,* vol. 15, p. 1805241, 2019.
[24] A. Thakre, A. Kumar, H. C. Song, D. Y. Jeong, and J. Ryu, "Pyroelectric Energy Conversion and Its Applications-Flexible Energy Harvesters and Sensors," *Sensors,* vol. 19, no. 9, p. 2170, 2019.
[25] S. Sahoo, S. Ratha, C. Rout, and S. Nayak, "Self-charging supercapacitors for smart electronic devices: a concise review on the recent trends and future sustainability," *Journal of Materials Science,* vol. 57, pp. 4399–4440, 2022.
[26] S. Korkmaz and a. Kariper, "Pyroelectric nanogenerators (PyNGs) in converting thermal energy into electrical energy: Fundamentals and current status," *Nano Energy,* vol. 84, p. 105888, 2021.
[27] A. Ben Amar, A. B. Kouki, and H. Cao, "Power Approaches for Implantable Medical Devices," *Sensors,* vol. 15, no. 11, pp. 28889-28914, 2015.
[28] A. Sharma, G. Singh, and S. K. Arya, "Biofuel cell nanodevices," *International Journal of Hydrogen Energy,* vol. 46, no. 4, pp. 3270-3288, 2021.
[29] A. Ahmed *et al.*, "Triboelectric Nanogenerator versus Piezoelectric Generator at Low Frequency (<4 Hz): A Quantitative Comparison," *iScience,* vol. 23, no. 7, p. 101286, 2020.
[30] M. Pan, C. Yuan, X. Liang, J. Zou, Y. Zhang, and C. Bowen, "Triboelectric and Piezoelectric Nanogenerators for Future Soft Robots and Machines," *iScience,* vol. 23, no. 11, p. 101682, 2020.
[31] T. Zhang, T. Yang, M. Zhang, C. Bowen, and Y. Yang, "Recent Progress in Hybridized Nanogenerators for Energy Scavenging," *iScience,* vol. 23, p. 101689, 2020.
[32] Q.-T. Nguyen and K.-K. K. Ahn, "Fluid-Based Triboelectric Nanogenerators: A Review of Current Status and Applications," *International Journal of Precision Engineering and Manufacturing-Green Technology,* vol. 8, no. 3, pp. 1043-1060, 2021.
[33] S. Chatterjee *et al.*, "Recent advancements in solid–liquid triboelectric nanogenerators for energy harvesting and self-powered applications," *Nanoscale,* vol. 12, no. 34, pp. 17663-17697, 2020.
[34] Y. Zi and Z. L. Wang, "Nanogenerators: An emerging technology towards nanoenergy," *APL Materials,* vol. 5, no. 7, p. 074103, 2017.
[35] X. An, C. Wang, R. Shao, and S. Sun, "Advances and prospects of triboelectric nanogenerator for self-powered system," *International Journal of Smart and Nano Materials,* vol. 12, no. 3, pp. 233-255, 2021.
[36] H. Zou *et al.*, "Quantifying the triboelectric series," *Nature Communications,* vol. 10, no. 1, p. 1427, 2019.

[37] Y. Hu, Y. Shi, X. Cao, Y. Liu, S. Guo, and J. Shen, "Enhanced output and wearable performances of triboelectric nanogenerator based on ePTFE microporous membranes for motion monitoring," *Nano Energy,* vol. 86, p. 106103, 2021.
[38] F.-R. Fan, Z.-Q. Tian, and Z. Lin Wang, "Flexible triboelectric generator," *Nano Energy,* vol. 1, no. 2, pp. 328-334, 2012.
[39] Q. Zheng *et al.*, "In Vivo Powering of Pacemaker by Breathing-Driven Implanted Triboelectric Nanogenerator," *Advanced Materials,* vol. 26, no. 33, pp. 5851-5856, 2014.
[40] S. K. Mulpuru, M. Madhavan, C. J. McLeod, Y.-M. Cha, and P. A. Friedman, "Cardiac Pacemakers: Function, Troubleshooting, and Management: Part 1 of a 2-Part Series," *Journal of the American College of Cardiology,* vol. 69, no. 2, pp. 189-210, 2017.
[41] H. Ouyang *et al.*, "Symbiotic cardiac pacemaker," *Nature Communications,* vol. 10, no. 1, p. 1821, 2019.
[42] Y. Ma *et al.*, "Self-Powered, One-Stop, and Multifunctional Implantable Triboelectric Active Sensor for Real-Time Biomedical Monitoring," *Nano Letters,* vol. 16, no. 10, pp. 6042-6051, 2016.
[43] K. Sim *et al.*, "An epicardial bioelectronic patch made from soft rubbery materials and capable of spatiotemporal mapping of electrophysiological activity," *Nature Electronics,* vol. 3, no. 12, pp. 775-784, 2020.
[44] Z. Lin *et al.*, "Triboelectric Nanogenerator Enabled Body Sensor Network for Self-Powered Human Heart-Rate Monitoring," *ACS Nano,* vol. 11, no. 9, pp. 8830-8837, 2017.
[45] H. Ouyang *et al.*, "Self-Powered Pulse Sensor for Antidiastole of Cardiovascular Disease," *Advanced Materials,* vol. 29, no. 40, p. 1703456, 2017.
[46] X. Xia, Q. Liu, Y. Zhu, and Y. Zi, "Recent advances of triboelectric nanogenerator based applications in biomedical systems," *EcoMat,* vol. 2, no. 4, p. e12049, 2020.
[47] S. Lin, L. Xu, A. Chi Wang, and Z. L. Wang, "Quantifying electron-transfer in liquid-solid contact electrification and the formation of electric double-layer," *Nature Communications,* vol. 11, no. 1, p. 399 2020.
[48] Z. L. Wang and A. C. Wang, "On the origin of contact-electrification," *Materials Today,* vol. 30, pp. 34-51, 2019.
[49] S. Hu *et al.*, "Superhydrophobic Liquid–Solid Contact Triboelectric Nanogenerator as a Droplet Sensor for Biomedical Applications," *ACS Applied Materials & Interfaces,* vol. 12, no. 36, pp. 40021-40030, 2020.
[50] G. H. Nam, J. H. Ahn, G. H. Lee, C. P. Vo, and K. K. Ahn, "A New Pathway for Liquid–Solid Triboelectric Nanogenerator Using Streaming Flow by a Novel Direct Charge Transfer," *Advanced Energy and Sustainability Research,* vol. 1, no. 1, p. 2000031, 2020.
[51] Y. Su *et al.*, "Hybrid triboelectric nanogenerator for harvesting water wave energy and as a self-powered distress signal emitter," *Nano Energy,* vol. 9, pp. 186-195, 2014.
[52] R. K. Cheedarala, M. Shahriar, J. H. Ahn, J. Y. Hwang, and K. K. Ahn, "Harvesting liquid stream energy from unsteady peristaltic flow induced pulsatile Flow-TENG (PF-TENG) using slipping polymeric surface inside elastomeric tubing," *Nano Energy,* vol. 65, p. 104017, 2019.
[53] X. Cui, H. Zhang, S. Cao, Z. Yuan, J. Ding, and S. Sang, "Tube-based triboelectric nanogenerator for self-powered detecting blockage and monitoring air pressure," *Nano Energy,* vol. 52, pp. 71-77, 2018.
[54] J. H. Ahn, J. Y. Hwang, C. G. Kim, G. H. Nam, and K. K. Ahn, "Unsteady streaming flow based TENG using hydrophobic film tube with different charge affinity," *Nano Energy,* vol. 67, p. 104269, 2020.
[55] J. Nie *et al.*, "Probing Contact-Electrification-Induced Electron and Ion Transfers at a Liquid–Solid Interface," *Advanced Materials,* vol. 32, p. 1905696, 2020.
[56] H. Cho *et al.*, "Toward sustainable output generation of liquid–solid contact triboelectric nanogenerators: The role of hierarchical structures," *Nano Energy,* vol. 56, pp. 56-64, 2018.
[57] H. Ouyang *et al.*, "A Bioresorbable Dynamic Pressure Sensor for Cardiovascular Postoperative Care," *Advanced Materials,* vol. 33, no. 39, p. 2102302, 2021.

[58] H. Minasyan, "Oxycytosis and the role of triboelectricity and oxidation in bacteria clearing from the bloodstream," *European Journal of Microbiology and Immunology,* vol. 11, no. 2, pp. 23-28, 2021.
[59] Y.-I. Cho and D. J. Cho, "Hemorheology and microvascular disorders," *Korean Circ J,* vol. 41, no. 6, pp. 287-295, 2011.
[60] M. Brust *et al.*, "Rheology of human blood plasma: viscoelastic versus Newtonian behavior," *Physical Review Letters,* vol. 110, no. 7, p. 078305, 2013.
[61] S. Varchanis, Y. Dimakopoulos, C. Wagner, and J. Tsamopoulos, "How viscoelastic is human blood plasma?," *Soft Matter,* vol. 14, no. 21, pp. 4238-4251, 2018.
[62] H. L. Bush, "Mechanisms of graft failure," *Journal of Vascular Surgery,* vol. 9, no. 2, pp. 392-394, 1989.
[63] K.-M. Park, Y. J. Park, S.-S. Yang, D.-I. Kim, and Y.-W. Kim, "Treatment of failing vein grafts in patients who underwent lower extremity arterial bypass," *J Korean Surg Soc,* vol. 83, no. 5, pp. 307-315, 2012.
[64] R. F. Neville, S. K. Gupta, and D. J. Kuraguntla, "Initial in vitro and in vivo evaluation of a self-monitoring prosthetic bypass graft," *Journal of Vascular Surgery,* vol. 65, no. 6, pp. 1793-1801, 2017.
[65] A. T. Pereira *et al.*, "Graphene-based materials: the key for the successful application of pHEMA as a blood-contacting device," *Biomaterials Science,* vol. 9, no. 9, pp. 3362-3377, 2021, doi: 10.1039/d0bm01699c.
[66] A. T. Pereira *et al.*, "Graphene Oxide Coating Improves the Mechanical and Biological Properties of Decellularized Umbilical Cord Arteries," *ACS Applied Materials & Interfaces,* vol. 13, no. 28, pp. 32662-32672, 2021.
[67] Y. Wang and G. J. Weng, "Electrical Conductivity of Carbon Nanotube- and Graphene-Based Nanocomposites," in *Micromechanics and Nanomechanics of Composite Solids*, 2018, pp. 123-156.
[68] Z. Yu, Y. Xia, D. Du, and J. Ouyang, "PEDOT:PSS Films with Metallic Conductivity through a Treatment with Common Organic Solutions of Organic Salts and Their Application as a Transparent Electrode of Polymer Solar Cells," *ACS Applied Materials & Interfaces,* vol. 8, no. 18, pp. 11629-11638, 2016.
[69] A. R. N. L. Gomes, "Antimicrobial silicones for use as dialysis catheters," 2017. [Online]. Available: https://hdl.handle.net/10216/106736
[70] C. Rodrigues *et al.*, "Integrated study of triboelectric nanogenerator for ocean wave energy harvesting: Performance assessment in realistic sea conditions," *Nano Energy,* vol. 84, p. 105890, 2021.
[71] M. F. Robbins, "Open Circuit and Short Circuit," *Ultimate Electronics: Practical Circuit Design and Analysis*: CircuitLab, Inc., 2021.
[72] C. G. Atkins, K. Buckley, M. W. Blades, and R. F. B. Turner, "Raman Spectroscopy of Blood and Blood Components," *Applied Spectroscopy,* vol. 71, no. 5, pp. 767-793, 2017.
[73] J. W. Mason, D. J. Ramseth, D. O. Chanter, T. E. Moon, D. B. Goodman, and B. Mendzelevski, "Electrocardiographic reference ranges derived from 79,743 ambulatory subjects," *Journal of Electrocardiology,* vol. 40, no. 3, pp. 228-234.e8, 2007.
[74] R. Chaudhry, J. H. Miao, and A. Rehman, "Physiology, Cardiovascular," in *StatPearls*, 2021.
[75] W. Tang *et al.*, "Liquid-Metal Electrode for High-Performance Triboelectric Nanogenerator at an Instantaneous Energy Conversion Efficiency of 70.6%," *Advanced Functional Materials,* vol. 25, pp. 3718–3725, 2015.
[76] X. Li, J. Tao, X. Wang, J. Zhu, C. Pan, and Z. L. Wang, "Networks of High Performance Triboelectric Nanogenerators Based on Liquid–Solid Interface Contact Electrification for Harvesting Low-Frequency Blue Energy," *Advanced Energy Materials,* vol. 8, no. 21, p. 1800705, 2018.
[77] G. Zhu *et al.*, "A shape-adaptive thin-film-based approach for 50% high-efficiency energy generation through micro-grating sliding electrification," *Advanced Materials,* vol. 26, no. 23, pp. 3788-3796, 2014.

[78] Y. M. Shabana *et al.*, "Thin Films in Triboelectric Nanogenerators for Blue Energy Harvesting: Fabrication, Characterization, and Modeling," *Key Engineering Materials,* vol. 835, pp. 335-346, 2020.
[79] I. Shabbir *et al.*, "A graphene nanoplatelets-based high-performance, durable triboelectric nanogenerator for harvesting the energy of human motion," *Energy Reports,* vol. 8, pp. 1026-1033, 2022.
[80] V. S. Mallela, V. Ilankumaran, and N. S. Rao, "Trends in cardiac pacemaker batteries," *Indian Pacing Electrophysiol J,* vol. 4, no. 4, pp. 201-212, 2004.
[81] J.-B. Ricco and O. Assadian, "Antimicrobial Silver Grafts for Prevention and Treatment of Vascular Graft Infection," *Seminars in Vascular Surgery*, vol. 24, no. 4, pp. 234-241, 2011.
[82] C. M. Tîlmaciu *et al.*, "In vitro and in vivo characterization of antibacterial activity and biocompatibility: a study on silver-containing phosphonate monolayers on titanium," *Acta Biomaterialia,* vol. 15, pp. 266-277, 2015.
[83] M. Zegelman *et al.*, "Results from the International Silver Graft Registry for high-risk patients treated with a metallic-silver impregnated vascular graft," *Vascular,* vol. 21, no. 3, pp. 137-147, 2013.
[84] B. Braun. "Silver Graft." https://www.bbraun-asiapacific.com/en/products/b/silver-graft.html (accessed March 22, 2022).
[85] M. G. Group. "Intergard Silver." https://www.getinge.com/int/products/intergard-silver/ (accessed March 22, 2022).
[86] I. Aazem *et al.*, "Electrode materials for stretchable triboelectric nanogenerator in wearable electronics," *RSC Advances,* vol. 12, no. 17, pp. 10545-10572, 2022.

Annexes

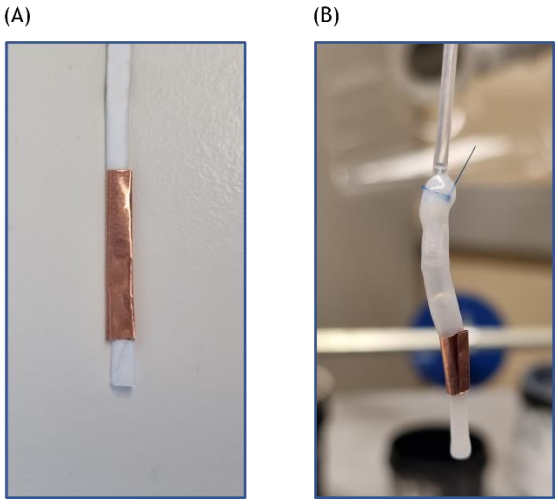

Figure A1. Copper tape electrode assembled onto (A) ePTFE vascular graft and (B) umbilical cord artery solid-phases. Wrapping of the tape around the solid-phases leads to their strangling, hampering the normal flow of the fluid inside, when assembled the whole Flu-TENG.

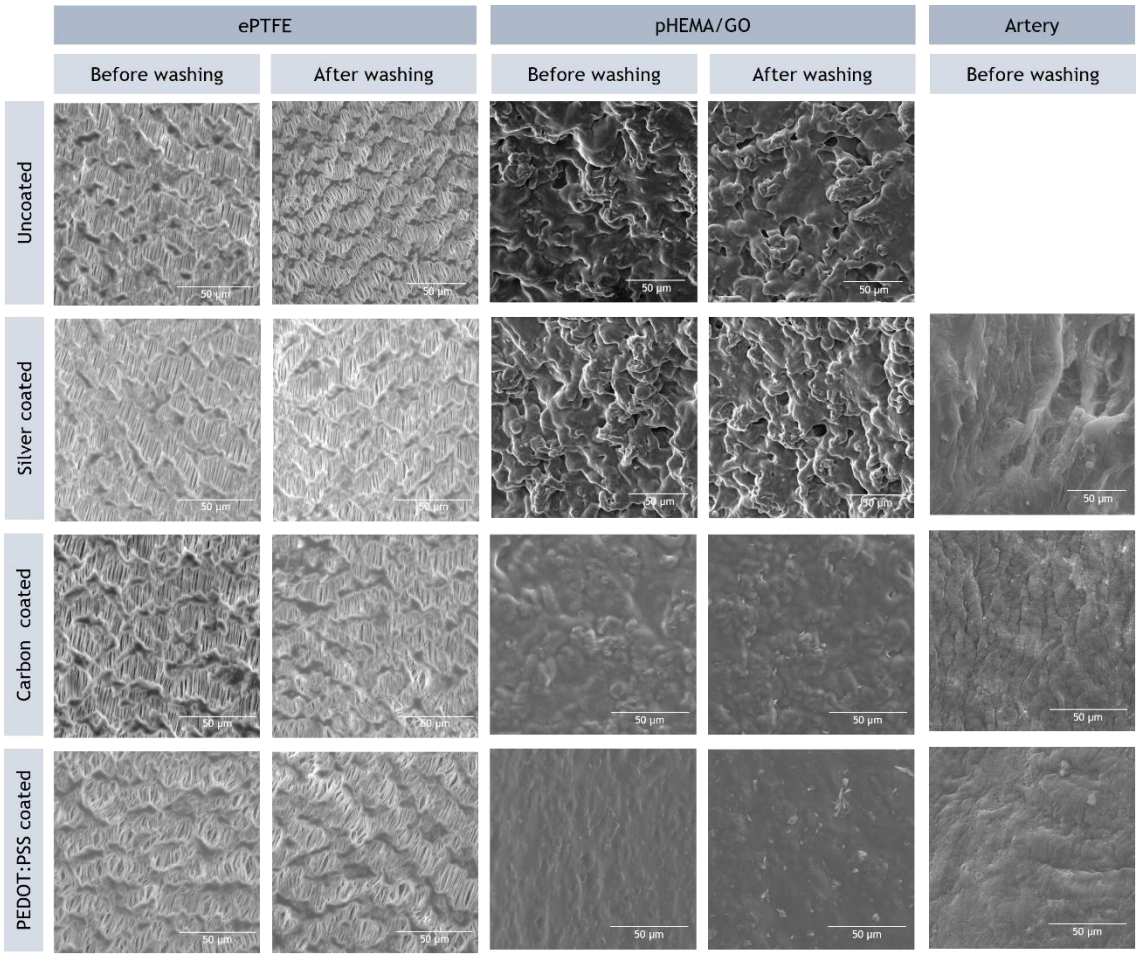

Figure A2. SEM analysis of the inner surfaces of the coated and uncoated ePTFE and pHEMA/GO vascular grafts samples before and after the washing tests, and of coated artery samples before washing tests. Each row represents a different conductive ink coating. Scale bar: 50 µm. Magnification 2000x.

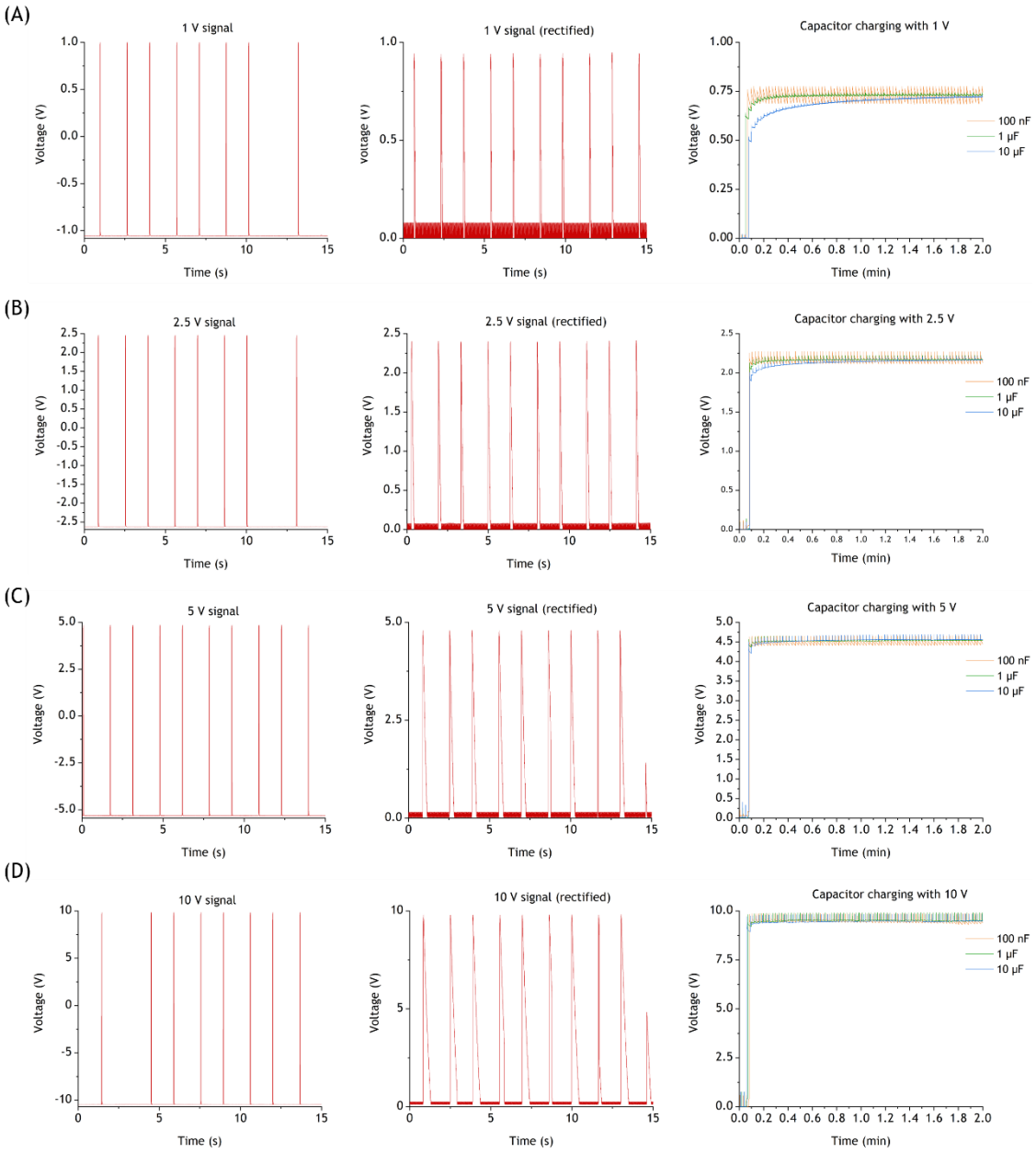

Figure A3. 100 nF, 1 µF and 10 µF capacitor charging, resorting to a bridge rectifier, with generated signals varying in peak voltage. (A) Results for 1 V signal; (B) Results for 2.5 V signal; (C) Results for 5 V signal; (D) Results for 10 V signal.

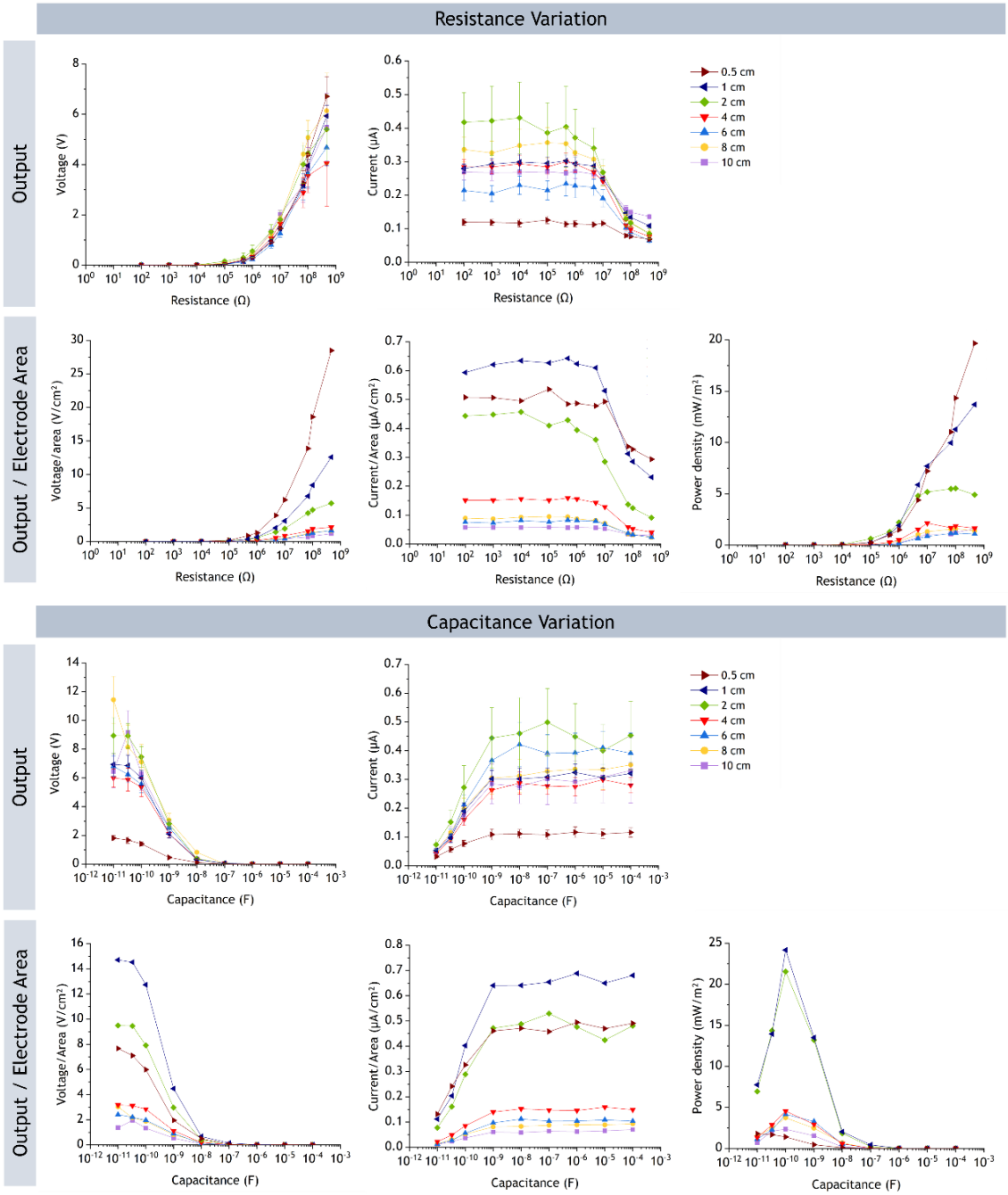

Figure A4. Triboelectric outputs, in voltage and current, both not and normalized by the electrodes area, and resulting power density, for resistor and capacitor's variation, for assessing of the influence of selectrode length. Comparison between silver conductive ink electrode of 0.5, 1, 2, 4, 6, 8 and 10 cm length. Flu-TENG consisted of ePTFE solid-phase (1.5 mm ID and 100 μm WT) with PBS fluid-phase (161 mL/min, 60 rpm).